To the Graduate Council:

I am submitting herewith a thesis written by Michael Scott Hileman entitled "A UV-B Radiometer for Making Field Measurements of UV-B (280 to 320 nanometers) Irradiance from Solar Sunlight and a UV-B Lamp Source." I have examined this thesis for form and content and recommend that it be accepted for partial fulfillment of the requirements for the degree of Master of Science, with a major in Electrical Engineering.

T. V. Blalock, Major Professor

We have read this thesis
and recommend its acceptance:

J. M. Googe

M. J. Roberts

Accepted for the Council:

Vice Provost
and Dean of The Graduate School

STATEMENT OF PERMISSION TO USE

In presenting this thesis in partial fulfillment of the requirements for a Master's degree at The University of Tennessee, Knoxville, I agree that the Library shall make it available to borrowers under rules of the Library. Brief quotations from this thesis are allowable without special permission, provided that accurate acknowledgment of the source is made.

Permission for extensive quotation from or reproduction of this thesis may be granted by my major professor, or in his absence, by the Head of Interlibrary Services when, in the opinion of either, the proposed use of the material is for scholarly purposes. Any copying or use of the material in this thesis for financial gain shall not be allowed without my written permission.

Signature Michael S. Heleman

Date 7/23/91

A UV-B RADIOMETER FOR MAKING FIELD MEASUREMENTS OF UV-B (280 TO 320 NANOMETERS) IRRADIANCE FROM SOLAR SUNLIGHT AND A UV-B LAMP SOURCE

A Thesis

Presented for the

Master of Science

Degree

The University of Tennessee, Knoxville

Michael S. Hileman

August 1991

DEDICATION

I dedicate this thesis to the memory of my father, who greatly influenced me; to my mother, for all she has done for me; and to my wife, for the daily joy she brings to my life.

ACKNOWLEDGMENTS

I thank Dr. T. V. Blalock for serving as my Major Professor and especially for providing his time, advice, and encouragement. I am also grateful to Dr. J. M. Googe and Dr. M. J. Roberts for serving on my thesis committee.

I am grateful to Martin Marietta Energy Systems, Inc., for providing equipment and supplies for this thesis and to the Instrumentation and Controls Division of Oak Ridge National Laboratory (ORNL) for much-needed encouragement. My graditude goes also to J. O. Hylton, Lou Thacker, Curt Maxey, and Marc Simpson for spending time in consultation in areas of their expertise. The group leaders under whom I served during this thesis work, Sam Gould, Jim McEvers, George Miller, and Raymond Tucker, Jr., provided advice and encouragement for which I am grateful. I thank Lori Stinnett, who created most of the figures used in this thesis. My graditude is extended to Nelson Edwards of the Environmental Sciences Division at ORNL for providing the funding for the radiometer printed circuit board and for the use of the ORNL Outdoor UV-B Exposure Facility to obtain test data.

I am especially grateful to my wife, without whose support this thesis would not have been possible. Finally and most important, I thank my Heavenly Father and Holy Spirit for guiding me through this endeavor and my entire life.

This research was performed at Oak Ridge National Laboratory, managed by Martin Marietta Energy Systems, Inc., for the U.S. Department of Energy under contract DE-AC05-84OR21400.

ABSTRACT

A UV-B radiometer was developed for field use in measuring solar ultraviolet-B (UV-B) irradiance from 280 to 320 nm and UV-B irradiance from a UV-B lamp source. The steps taken in the analysis and design, implementation, and testing of this device are presented. The radiometer was designed for an operating temperature of −10 to 60°C and a supply voltage of 30 V dc.

The circuit was designed to be a three-wire field instrument, with the output being a 4- to 20-mA signal contained in the power supply loop used to bias the circuit. The circuit signal bandpass was designed to be 1.6 Hz, and this was measured and verified. The output noise of the circuit was calculated to be 88 μV and was measured to be 92 μV (less than 1 count of the analog-to-digital converter this signal interfaced with).

The output of this radiometer was compared with an off-the-shelf radiometer, and correction factors for both meters were calculated to correct their outputs for measuring only the UV-B irradiance of 280 to 320 nm. After taking into consideration the differences in the design of the sensors, difference errors in their readings were calculated to be ~15%.

The worst-case circuit drift was calculated to be less than −0.25% of full scale over the temperature operating range of the instrument when the temperature-compensating resistor is used in the feedback path of the transimpedance amplifier. The output zero current error was measured to be approximately ±0.2% for a temperature span of 0 to 50°C.

TABLE OF CONTENTS

SECTION PAGE

1. INTRODUCTION 1

2. INITIAL DESIGN 5

   2.1 Selection of the Photodetector Element 5
   2.2 Selection of the Bandpass Optical Filter 6
   2.3 Design of the Transimpedance Amplifier 10
   2.4 Selection of the Transconductance Amplifier 18

3. FINAL DESIGN 22

   3.1 Transimpedance Amplifier Frequency Stability Analysis 22
   3.2 Radiometer Noise Analysis 26
   3.3 Radiometer Error Budget Analysis 41

4. CALIBRATION 47

   4.1 Correction Factor Derivation 47
   4.2 Ambient Sunlight Source 52
   4.3 UVB-313 Lamp Source 54

5. CIRCUIT CONSTRUCTION 56

   5.1 Thesis UV-B Radiometer Construction 56
   5.2 UVX Sensor 58

6. EXPERIMENTAL TECHNIQUES AND RESULTS 60

   6.1 Frequency Response and Gain Linearity 60
   6.2 Offset and Drift 64
   6.3 Output Noise Voltage 66
   6.4 Radiometer Performance Comparisons 66

7. SUMMARY AND CONCLUSIONS 86

LIST OF REFERENCES AND BIBLIOGRAPHY 87

APPENDIX. MATHCAD PROGRAMS 90

VITA 146

LIST OF TABLES

TABLE PAGE

2.1. Hamamatsu G1127-02 Photodiode Performance Specifications 8

2.2. AD707C Performance Specifications 13

2.3. AD693 Performance Specifications 20

3.1. Noise Calculation Ideal Closed-Loop Gain Terms 34

3.2. Resistor and Capacitor Values Used in Ideal Closed-Loop Gain Terms 35

3.3. Noise Source Ideal Closed-Loop Transfer Functions 36

3.4. Output Noise Power of Current Noise Sources 37

3.5. Output Noise Power of Voltage Noise Sources 38

3.6. Calculated Output Noise Power 39

3.7. Summary of Error Budget Analysis 46

6.1. Pinhole Test Data on UV-B Sensors 77

LIST OF FIGURES

FIGURE PAGE

2.1. Hamamatsu G1127-02 Photodiode Spectral Response 7

2.2. Schott UG-11 Spectral Transmittance 9

2.3. Transimpedance Amplifier Model 11

2.4. Solar Spectral Irradiance Data 15

2.5. Schematic Diagram of Radiometer Circuit 21

3.1. Amplifier Loop Transmission Model 23

3.2. Amplifier Loop Transmission Gain 27

3.3. Amplifier Loop Transmission Phase 28

3.4. Radiometer Noise Model 30

4.1. UVX Meter Absolute Response 48

4.2. Thesis Meter Absolute Response 50

4.3. Summer Sunlight 53

4.4. UVB-313 Spectral Power Distribution 55

5.1. Thesis UV-B Sensor Enclosure Construction 57

5.2. UVX Sensor Construction 59

6.1. Radiometer Test Setup 61

6.2. Radiometer Gain Linearity 63

6.3. Radiometer Frequency Response 65

6.4. Temperature Drift Results of Thesis Radiometer 67

6.5. Percentage of Drift Error for 4-mA Zero Current 68

LIST OF FIGURES (continued)

FIGURE PAGE

6.6. Sensor Field of View Illustration 70

6.7. Sensor Cosine Response Illustration 71

6.8. Cosine Response of Sensors 73

6.9. Initial Comparison Testing with UVB-313 Lamps 74

6.10. Pinhole Testing Configuration 76

6.11. Sensor Testing at Lamp Distance of 41 Inches 79

6.12. Sensor Testing at Lamp Distance of 68 Inches 80

6.13. Sunlight Testing on Horizontal Surface 82

6.14. Ratio of Sensors in Sunlight - Horizontal 83

6.15 Sunlight Testing - Sun Tracker 84

6.16 Ratio of Sensors - Sun Tracker 85

1. INTRODUCTION

In response to concerns relating to depletion of the earth's stratospheric ozone layer, there is a need to forecast potential effects on terrestrial life as a result of increased levels of solar ultraviolet-B (UV-B) radiation. Most previous experiments to study these effects have peen performed in the laboratory by exposing plants to accelerated levels of purely artificial UV-B radiation. Plants can exhibit photo-repair mechanisms in the presence of naturally occurring levels of solar radiation that lie outside the UV-B spectrum (280 to 320 nm). Therefore, a more realistic approach is to carry out such studies outdoors where the plants can be exposed to natural sunlight as well as artificial UV-B radiation to increase the total exposure of the test plants to UV-B.

To perform such studies, an automated outdoor exposure facility for supplementing ambient solar UV-B was developed by the Instrumentation and Controls (I&C) Division of Oak Ridge National Laboratory (ORNL). The system includes many components such as UV-B lamps, lamp filter materials, lamp power supplies, and a data acquisition and control system. This thesis will focus on the heart of the system, which is the integrating UV-B sensors.

These sensors are used in a closed-loop feedback control system to maintain UV-B irradiance exposure at some control percentage above ambient. The closed-loop feedback control is obtained by using two UV-B radiometers. One radiometer is placed away from the facility to measure only ambient solar UV-B radiation, and the other is placed beneath the exposure facility lamps to measure ambient plus artificial UV-B radiation. A proportional-integral-derivative (PID) controller is used to adjust the UV-B lamp plasma voltage to keep the total UV-B radiation at the facility at some selectable percentage above the ambient UV-B radiation.

The ideal radiometer would respond exactly the same to all wavelengths of radiation in the range of interest and have zero response to all other wavelengths (ideal bandpass filter). For this project, the range of interest is from 280 to 320 nm, which is known as the UV-B region of ultraviolet (UV) light. Unfortunately, real radiometers have a response that peaks at some wavelength and rolls off toward zero away from this peak. Therefore, the response is not uniform across this region. However, by knowing the relative spectral distribution of the light sources that need to be measured and the absolute spectral response of the radiometer, it is possible to calculate correction factors that will allow accurate, absolute UV-B irradiance measurements. The correction factor is the percentage of the radiometer response that is due to only those wavelengths of interest. Derivation of this correction factor will be presented in Section 4. Commercially available radiometers that might meet these requirements were investigated. Unfortunately, radiometers that came even close to performing this function were designed for laboratory use only.

The goal of the work reported in this thesis was to design a UV-B radiometer that performs this function. The instrument will have a 4- to 20-mA output proportional from 0 irradiance (W/m^2) to some upper design level to be determined later. This upper design level will be determined from the maximum ambient UV-B expected plus some percentage that will cover the elevated exposure ranges required by the UV-B facility.

A UV-B radiometer will be designed using commercially available components. The instrument will be designed to be a three-wire loop powered from an external dc power supply ranging from 24 to 40 V. The photosensing element will utilize a Hamamatsu GaAsP photodiode (Hamamatsu, 1988) whose spectral response includes the UV region of light. Specifically, a Hamamatsu GaAsP Model G1127-02 will be used as the diode

(with traceable calibration spectral data) in this project. The optical filter material chosen to reject other wavelengths of light outside the UV-B region will be a Schott UG-11 bandpass filter whose peak transmission occurs near the UV-B region.

A transimpedance amplifier will be designed utilizing an operational amplifier in which the photocurrent flows through the feedback impedance to develop a voltage (millivolt range). This amplifier will be chosen to minimize errors due to input bias currents and input offset voltage. If obtainable, the feedback resistor will have a positive temperature coefficient of the same order of magnitude as the negative temperature coefficient of the short-circuit diode current to minimize errors caused by thermal drift. An error analysis that includes temperature effects, op-amp offset voltage, and so forth will be performed to determine the worst-case error of the entire circuit. A low-pass filter load will be driven by the transimpedance amplifier stage to minimize the noise bandwidth of the circuit.

An Analog Devices Model AD693 loop-powered 4- to 20-mA sensor transmitter will be used to convert the millivolt output of the op-amp stage to a 4- to 20-mA output signal to be used by an external data acquisition device. An external NPN power transistor will be used to supply the 4- to 20-mA output current to minimize self-heating of the AD693 and improve its thermal drift characteristics. A noise analysis of the thesis radiometer circuit will be performed to determine the minimum detectable photodiode current, thereby specifying the noise floor of the radiometer output.

The UV-B radiometer will be essentially precalibrated because the photodiode absolute spectral response is known [from calibration data traceable to the National Institute of Standards and Technology (NIST)] and the feedback resistance and optical filter transmission characteristics are well known. Because the radiometer response is not

"ideal," correction factors will be calculated for ambient sunlight and the UV-B lamps. The calibration and correction factors will be checked by comparing the performance of the thesis UV-B sensor with an Ultraviolet Products, Inc. (UVP), (Model UVX digital radiometer with a UVP Model UVX-31 sensor. This sensor is calibrated by the manufacturer with traceability to NIST. Because the optical bandpass of the UVX radiometer is also not "ideal," correction factors will be calculated for ambient sunlight and the UV-B lamps to determine the portion of its output that is due to only the UV-B irradiance. Performance data will be collected comparing the output of both meters to ambient sunlight and at least one UV-B lamp source.

The remainder of this thesis is divided into six sections. Section 2 contains the initial design philosophy for the radiometer considering its intended application. Section 3 deals with stability, noise analysis, and error budget analysis of the radiometer. Section 4 develops the necessary correction factors for obtaining the percentage of the radiometer response that is due to only UV-B irradiance. Section 5 describes the construction of the UV-B sensor and how it varies from the UVX design. Section 6 attempts to verify the results obtained in the other sections by testing and experimentation. Finally, Section 7 summarizes this effort and gives suggestions for improvements and further research.

2. INITIAL DESIGN

The purpose of this section is to select the individual components of the radiometer based on its intended application and to justify each selection. Minor changes may be made if the analysis in Section 3 warrants changes.

2.1 Selection of the Photodetector Element

Initial investigation into the type of photodetector to use on this project led the author to consider thermal detectors, photocathodes, and solid state junction photodetectors. Some of the important parameters that were considered in designing this radiometer were photon sensitivity, signal-to-noise ratio, spectral response, filtering requirements, signal linearity, stability, and size. Upon considering the various factors, it appeared GaAsP that junction photodetectors would be the most logical choice for several reasons. They are physically small and lend themselves to field instrumentation because they require small bias voltage, whereas photomultiplier-type photodetectors require high-voltage power supplies. In comparison with thermal-type detectors, photodiodes have much higher sensitivities in the UV region as compared to the GaAsP photodioder and, with appropriate filtering, reject any out-of-band radiation. This is especially important in making solar UV measurements because the out-of-band solar radiation is many orders of magnitude higher than the UV-B radiation. Silicon photodiodes were also considered, but their radiant sensitivities are not as great in the UV region as compared to the GaAsP photodiodes and, in addition, their radiant sensitivities extend to the red region of light, thus making the filter requirements more stringent for making the detector solar blind. Also, work by Wilson and Lyall (1986a) concluded that GaAsP Schottky barrier photodiodes are superior to silicon in both noise performance and high current linearity.

Furthermore, GaAsP photodiodes can be used at higher irradiance levels where the silicon photodiode cannot be recommended for high UV exposure because it shows severe reductions in quantum efficiency on exposure to UV (Wilson and Lyall, 1986b). This would be unacceptable because it would cause continuous decalibration of the radiometer.

As mentioned earlier, a Hamamatsu Model G1127-02 GaAsP photodiode with calibration data traceable to NIST was available for use in this project. The calibrated spectral response of this diode is shown in Figure 2.1, and the important performance specifications are given in Table 2.1.

2.2 Selection of the Bandpass Optical Filter

The ideal optical bandpass filter/photodiode response would be flat in the region of interest (280 to 320 nm) and have zero response outside this region. Because a flat response and perfect cutoff is not realizable, a filter material that is centered near the region of interest and has a sharp roll-off on both sides would be the most practical choice.

Several types of UV filters were considered for this project. All-dielectric interference filters (ADIF), metal-dielectric interference filters (MDIF), and glass absorption filters (GAF) were considered. ADIF filters were eliminated because they are UV unstable (Wilson and Lyall, 1986b). A decision was made to use GAF types because they were somewhat less expensive when compared to the custom-designed MDIFs, and they allow a greater transmittance in the desired bandpass region. Specifically, the Schott UG-11 bandpass filter was chosen. Figure 2.2 shows the spectral transmittance (ratio of the transmitted spectral radiant flux to the incident radiation flux) of this filter vs

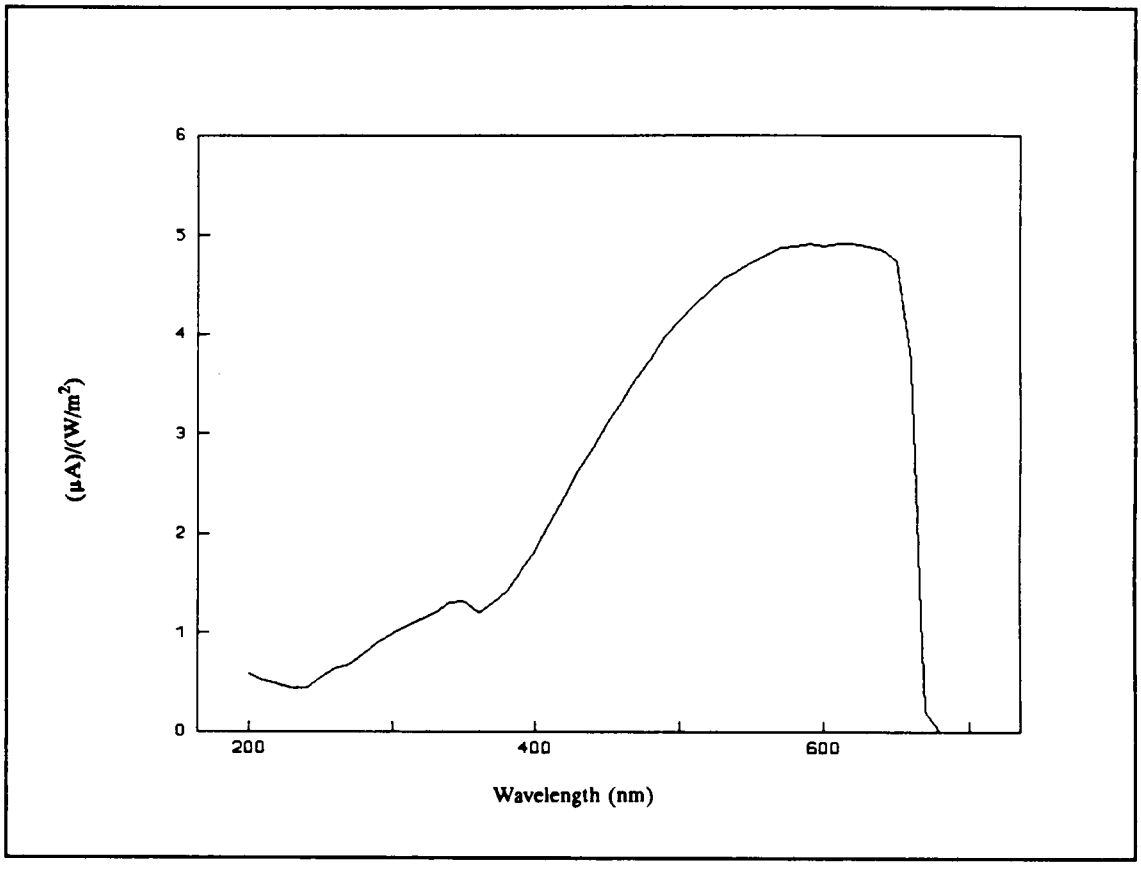

Figure 2.1. Hamamatsu G1127-02 Photodiode Spectral Response.

Table 2.1. Hamamatsu G1127-02 Photodiode Performance Specification

Parameter	Specification
Radiant sensitivity at peak wavelength	0.18 A/W typical
Radiant sensitivity in UV-B region	0.04 A/W typical
Photosensitive surface area	21.16 mm^2
Junction capacitance	7000 pF typical[a]
Shunt resistance	1 GΩ minimum[b]
Photodiode current noise spectral density	3.5 fA/RTHz
Spectral response range	190 to 680 nm
Dark current	10^{-10} A maximum[b]
I_L temperature coefficient	−0.1%/°C typical
Operating temperature range	−10 to 60°C

[a]Reverse voltage equals zero voltage; measurement taken at room temperature of 25°C.

[b]Includes −10 to 60°C temperature range.

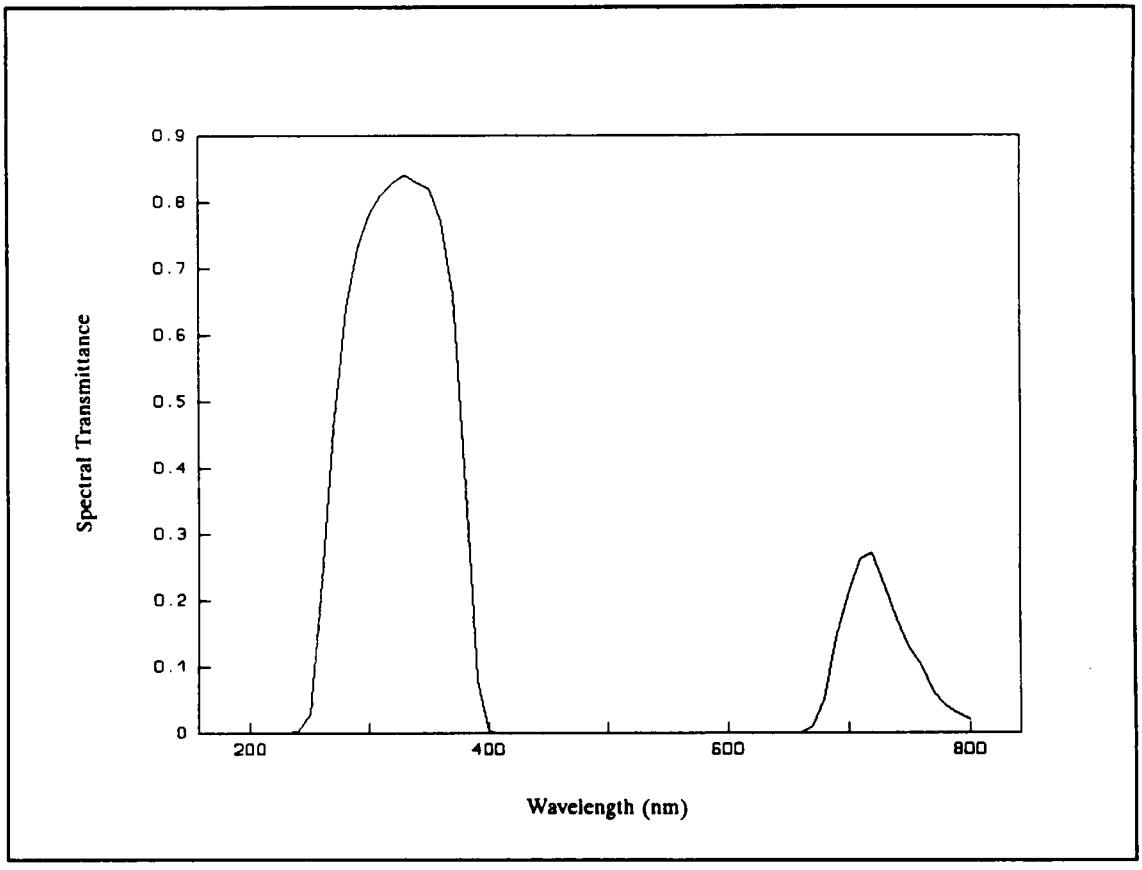

Figure 2.2. Schott UG-11 Spectral Transmittance.

wavelength. The peak transmittance of this filter occurs at ~330 nm, which is close to the required region of interest (280 to 320 nm). The filter does contain some unwanted response above 680 nm, but this is where the sensitivity of the G1127-02 photodiode approaches zero. Thus, the product of the filter transmittance with the photodiode spectral response approaches zero in this region.

2.3 Design of the Transimpedance Amplifier

Figure 2.3 shows a general model of the photodiode (components labeled subscript "d") and the transimpedance amplifier circuit that contains enough features to examine the most important circuit characteristics, namely frequency response and stability. The main element within the transimpedance amplifier circuit is an operational amplifier (op-amp). Careful consideration was given to selecting this component. In this application, the most important parameters are that the op-amp have very low drift, low bias currents, and good noise performance characteristics. Consideration of several op-amps led to a final selection of the Analog Devices Model AD707 (bipolar input stage). Field-effect transistor input stage op-amps were considered (especially the Analog Devices Model AD549 monolithic electrometer operational amplifier) because of their low-input bias currents and, more important, their low-input offset currents. However, because the feedback resistor on this radiometer circuit is of low magnitude (750 Ω) as compared to most applications where the feedback resistance is in the neighborhood of megaohms, the input offset current contributes almost no error. It will be shown in Section 3.2 that the op-amp contributes very little noise to the total output noise power. Thus, the AD707 was selected because of its outstanding drift characteristics (the radiometer will be used mainly in the field and not in a laboratory setting).

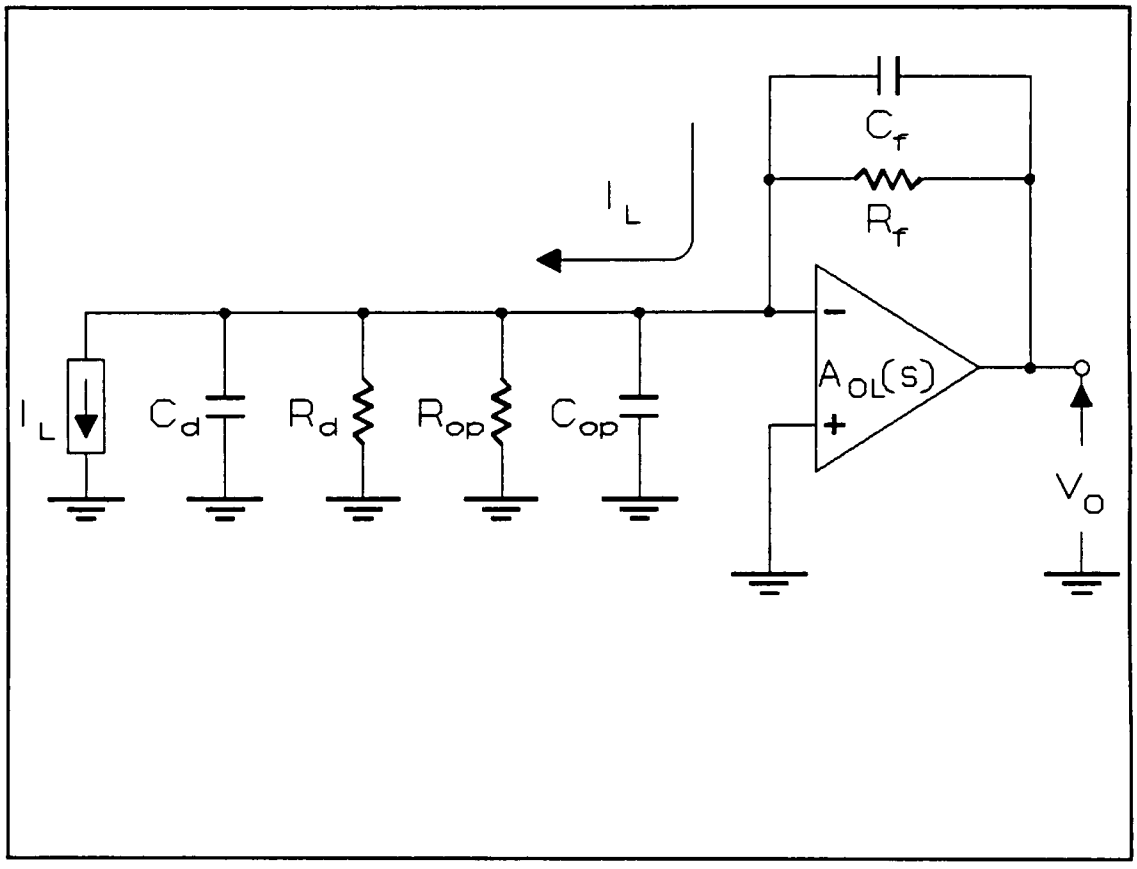

Figure 2.3. Transimpedance Amplifier Model.

Table 2.2 contains specifications for the AD707 obtained from the data sheets (Analog Devices, 1988). These specifications are worst-case values and assume an operating temperature of 25°C and a supply voltage of ±15 V unless otherwise specified.

The photodiode current I_L (current generated by incident UV-B irradiance) is shown in Figure 2.3 in the position to cause a rise in the output voltage for increase in current. Using the concept of the ideal op-amp model (infinite gain, infinite input impedance, and zero output impedance), the ideal closed-loop gain is found by noting that because the inverting input is a virtual ground, the total signal current I_L flows through the feedback impedance Z_f (R_f in parallel with C_f) of the amplifier and is given by Eq. (2.1). The minus 3-dB corner frequency, f_{3dB}, for the ideal closed-loop response is given by Eq. (2.2).

$$\frac{V_o}{I_L} = Z_f = \frac{R_f}{1 + jf/f_{3_{dB}}} \quad . \tag{2.1}$$

$$f_{3_{dB}} = \frac{1}{2\,\pi\,R_f\,C_f} \quad . \tag{2.2}$$

The dc gain of the amplifier is chosen by R_f and is selected by determining the maximum amount of photodiode current. This maximum is determined by the diode photodiode spectral response, the spectral transmittance of the optical filter, and the spectral irradiance of the source of light to be measured. More specifically, the photodiode current is defined by

$$I_L = \int_{\lambda_{Lo}}^{\lambda_{Hi}} S(\lambda)D(\lambda)F(\lambda)d\lambda \quad , \tag{2.3}$$

Table 2.2. AD707C Performance Specifications

Parameter	Specification
Input offset voltage	15 μV[a] maximum
Input offset voltage drift	0.1 μV/°C[a]
Input bias current	2 nA[a] maximum
Input offset current	1.5 nA[a]
Input offset and bias current drift	25 pA/°C[a]
Low-frequency input voltage noise (0.1 to 10 Hz)	0.35 μV (p-p)[b]
Input voltage noise spectral density (10 Hz)	13 nV/RTHz
Low-frequency input current noise (0.1 to 10 Hz)	30 pA (p-p)[b]
Input current noise spectral density (10 Hz)	0.8 pA/RTHz
Operating supply voltage	±3 to ±18 V
Operating temperature range	−40 to 85°C
Power supply rejection ratio	120 dB[a,c]
Differential input resistance	60 MΩ
Open-loop output resistance	60 Ω
Open-loop voltage gain	8 V/μV[a,d] minimum 13 V/μV typical

[a]Includes −40 to 85°C temperature range.

[b]Voltage noise corner frequency is 0.7 Hz. No corner frequency given for current noise.

[c]Includes supply voltage variation of ±3 to ±18 V.

[d]Includes supply voltage variation of 3 to 24 V. Typical value is 13 V/μV. Dominant pole estimated to be at 0.08 Hz.

where

$S(\lambda)$ = solar spectral irradiance,

$D(\lambda)$ = diode spectral radiant sensitivity,

$F(\lambda)$ = optical filter spectral transmittance,

λ_{Hi} = upper wavelength limit where product of $S(\lambda)F(\lambda)D(\lambda)$ approaches zero,

λ_{Lo} = lower wavelength limit where product of $S(\lambda)F(\lambda)D(\lambda)$ approaches zero.

For this calculation, $S(\lambda)$ in Eq. (2.3) is the ambient solar spectral irradiance at the surface of the earth. Because the radiometer is to be used in a UV-B exposure facility that will expose plants to an elevated UV-B level some percentage above ambient, the radiometer must be designed to see more than just the ambient spectral irradiance.

Initially, the author selected a value of 50% above ambient UV-B irradiance. If in fact this value needs to be increased, the feedback resistor can be decreased accordingly. Typical postulated increases in UV-B for the future (10 to 15 years), at the present rate of stratospheric ozone level depletions, correspond to roughly 30% increases in present-day ambient UV-B. This is based on predictions of a global ozone reduction of 7 to 16% in that period (National Academy of Sciences, 1982). Thus, the full-scale radiometer output must be designed to correspond to 50% above ambient UV-B irradiances.

The upper and lower limits of integration in Eq. (2.3) are 400 and 280 nm, respectively, because the optical filter spectral transmission is effectively zero outside this range. The optical filter has spectral transmittance from about 680 to 800 nm, but the photodiode spectral response is practically zero at wavelengths > 680 nm. Figure 2.4 shows two plots of the solar spectral irradiance at the surface of the earth. The data for the first plot were obtained from actual summer sunlight data taken in Cleveland, Ohio, by

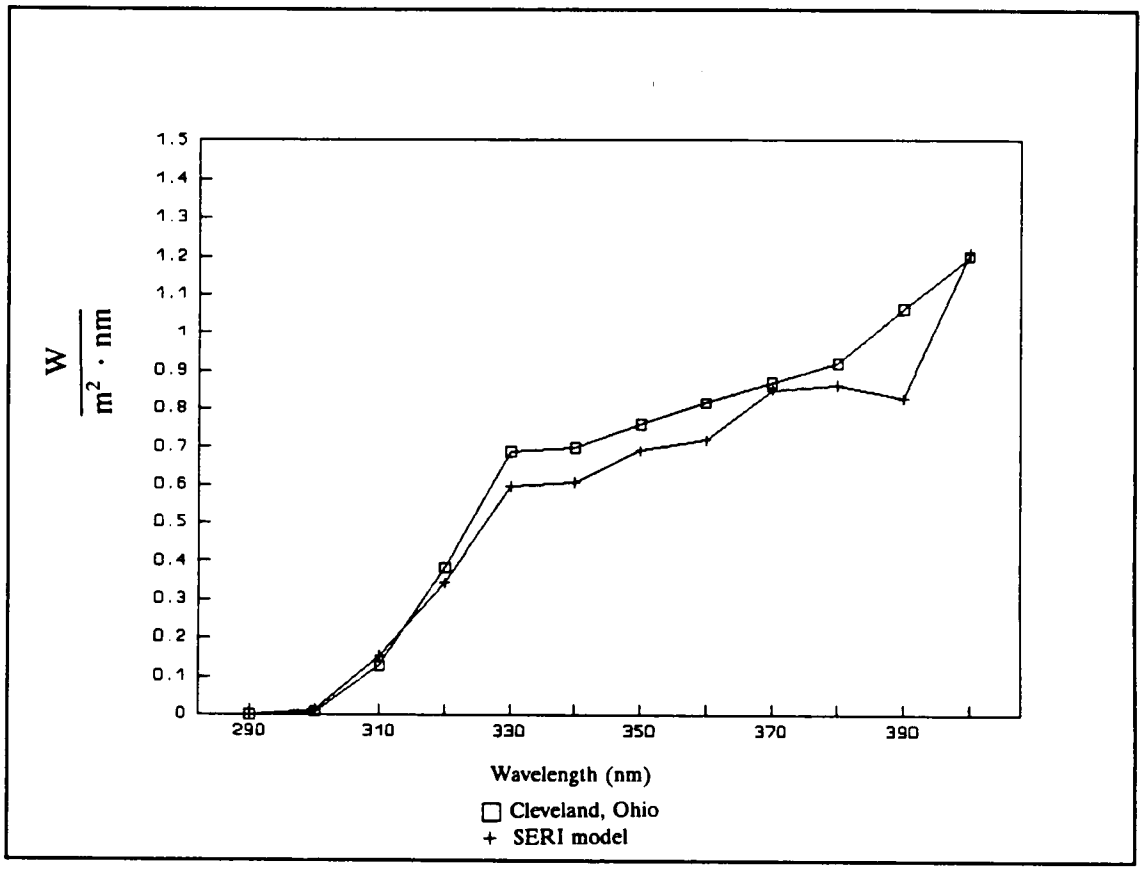

Figure 2.4. Solar Spectral Irradiance Data.

the Q-Panel Company (Brennan, 1989). The second plot was made from data produced by the Solar Energy Research Institute's (SERI's) solar irradiance at the surface of the earth FORTRAN model, SPECTRL2 (Solar Energy Research Institute, 1990). As can be seen from Figure 2.4., the absolute magnitudes of both curves are roughly the same but, more important, the shapes of both curves are almost identical.

Using a personal computer- (PC-) based math package called MathCad, the author performed these integrations using the Trapezoidal Rule. The MathCad programs are labeled ZFBGAIN0 (uses the SERI solar spectral irradiance model data as the light source) and ZFBGAIN1 (uses the actual ground-level summer solar spectral data taken in Cleveland, Ohio) and are contained in the appendix.

The maximum output voltage of the transimpedance amplifier is designed to be 60 mV. This is determined by the maximum full-scale input signal applied to the next stage of the radiometer—the transconductance amplifier, whose full-scale input is designed to be 60 mV. This amplifier will be discussed in Section 2.4. As previously stated, the author will assume the total current to be 50% greater than the photodiode current calculated for the ambient solar response to allow for the additional maximum contributions of the UV-B light sources. Thus, R_f is determined by

$$R_f = \frac{60\,mV}{1.5 \int_{\lambda_{Lo}}^{\lambda_{Hi}} D(\lambda)S(\lambda)F(\lambda)d\lambda} \quad . \tag{2.4}$$

From the results of the MathCad programs, this value is calculated to be 775 Ω (MathCad Program ZFBGAIN1) and 897 Ω (ZFBGAIN0). A conservative value of 750 Ω will be chosen initially and will be reevaluated if testing warrants change.

The frequency response required by the radiometer will be determined by the desired output response due to changes in the radiometer input. It will be desirable to limit the bandwidth of the system as much as possible to minimize the radiometer output due to circuit noise sources. Because the radiometer is designed to measure outdoor ambient UV-B, the fastest changes in UV-B irradiance at the surface of the earth will occur when clouds are passing overhead. The time associated with a cloud passing in front of the sun from full sunlight to total cloud shading is on the order of seconds. Thus, a low-pass filter frequency response of ~1 Hz will be chosen initially. This low-pass filtering could be performed at the feedback impedance of the transimpedance amplifier as seen in Eq. (2.2); however, this would require a large capacitance on the order of hundreds of microfarads with a 750-Ω feedback resistor. More important, it will be shown in Section 3.1 that this feedback capacitor will be chosen to provide a zero in the loop transmission to cancel a pole due to the high input capacitance from the photodiode. This feedback compensation is required to provide an adequate phase margin to ensure stability.

Thus, the closed-loop response of the radiometer will be provided by an additional low-pass filter resistor and capacitor network at the output of the transimpedance amplifier stage (this will not lower the noise bandwidth of the next stage, the transconductance amplifier, but it will be shown that the total circuit noise is negligible). The value of the low-pass filter resistor should be large enough to minimize the output current of the transimpedance operational amplifier, but it should not be so large as to

cause loss of signal with voltage division with the input impedance of the next stage, which is the transconductance amplifier. More important, the input bias current of the transconductance amplifier must flow through these filter resistors; thus, the resistors should be kept to fairly low values to minimize errors due to input offset currents of the transconductance amplifier. The author selected resistance in the kilohm range and capacitance in the microfarad range by choosing standard values of 47 μF and 2151 Ω to provide a −3-dB low-pass corner frequency at 1.6 Hz.

2.4 Selection of the Transconductance Amplifier

The author has used an Analog Devices Model AD693 loop-powered 4- to 20-mA sensor transmitter in other circuit projects and has been pleased with its excellent span and offset errors. Thus, the AD693 was chosen to be the transconductance amplifier for the radiometer.

The AD693 is a monolithic signal-conditioning circuit that accepts low-level voltage inputs to control a standard 4- to 20-mA current-loop output. Precalibrated input spans of 30 and 60 mV are set by pin strapping. Output span and zero are also determined by pin strapping, and this includes the standard 4- to 20-mA output. The precalibrated input and output spans are performed by laser-wafer trimming. Under a typical set of conditions, the total unadjusted error of this device is guaranteed to be <0.75% of full scale, over the industrial temperature range of −40°C to +85°C. Most of this error can be reduced significantly (typically to <0.1%) by trimming the zero current. The remaining unadjusted error sources are (1) variations of the transconductance with signal level and (2) transconductance nonlinearity.

A monitored output is provided to drive an external pass transistor; the author has chosen an NSE180 NPN medium-power transistor for this purpose. This feature will be used in the radiometer design because it off-loads power dissipation from the AD693 to extend the temperature range of operation, improve reliability, and minimize self-heating errors (Analog Devices, 1990). Input filtering to the AD693 is provided by the low-pass filter; Section 2.3 mentioned that the input filter resistors are to be kept fairly low to minimize errors due to the AD693 input bias current offset.

Table 2.3 contains specifications of the AD693 obtained from the data sheets (Analog Devices, 1990). These specifications assume an initial operating temperature of 25°C, a 24-V supply voltage, an input span of 30 or 60 mV, an output span of 4 to 20 mA, a load of 250 Ω, and the use of an external pass transistor. Figure 2.5 is a schematic diagram of the initial design of the UV-B radiometer circuit.

Table 2.3. AD693 Performance Specifications

Parameter	Specification
Total unadjusted error	±0.75% Full Scale[a,b]
Zero current error	±80 μA
Zero current error drift	±1.5 μA/°C[c]
Input offset current	±3.0 nA
Input bias current	+20 nA Maximum[d]
Nominal transconductance	0.2666 A/V
Nonlinearity	±0.07 % of Span
Temperature range	−40 to 80°C
3-dB bandwidth	500 Hz
Input voltage noise spectral density	50 nV/RTHz[e]
Input current noise spectral density	40 fA/RTHz[f]
Operating range	−40 to 85°C

[a]Includes −40 to +85 °C temperature range.

[b]Total error can be reduced significantly (typically to less than 0.1%) by trimming the zero current. The remaining unadjusted error sources are transconductance and nolinearity.

[c]Tested with an external pass transistor.

[d]Bias currents are not symmetrical with input signal level and flow out of the input pins. The input bias current of the noninverting input increases with input signal voltage to cause a maximum differential input current of 1.8 times the input bias current maximum (at 60 mV input).

[e]Voltage noise corner frequency ~ 10 Hz.

[f]Current noise corner frequency ~ 80 Hz.

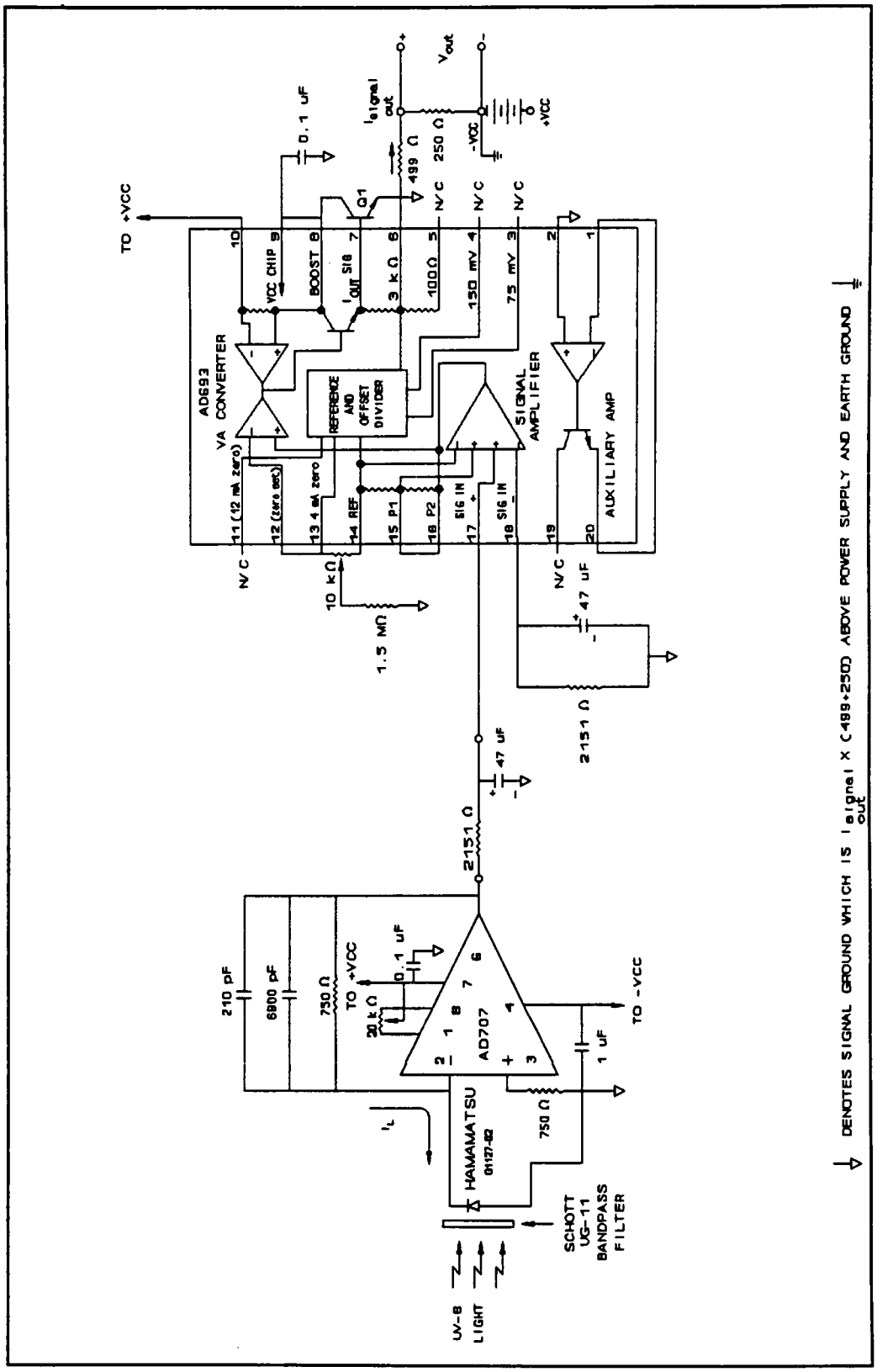

Figure 2.5. Schematic Diagram of Radiometer Circuit

3. FINAL DESIGN

The purpose of this section is to perform the necessary analyses to verify the individual components selected in Section 2.

3.1 Transimpedance Amplifier Frequency Stability Analysis

To obtain a more thorough analysis of the transimpedance amplifier, the op-amp's output series resistance and the transimpedance amplifier's low-pass filter load will be included in the loop transmission model as shown in Figure 3.1. The loop transmission is found by breaking the feedback loop at the output of the op-amp (a near-zero impedance point) and inserting a test voltage, v_t. The gain around the loop is calculated by finding the portion of the test voltage, v_t, that arrives at the output, v_{out}. Figure 3.1(b) shows the feedback loop broken and a test voltage source inserted. The loop transmission T(s), where $s = j\omega$, is found by dividing v_{out} by v_t. From Figure 3.1(b) it is evident that the portion of the v_t arriving at the inverting terminal of the op-amp, v_ϵ, is due to the voltage division between Z_{in} and Z_f and is given by

$$\frac{V_\epsilon}{V_t} = \frac{Z_{in}}{Z_{in} + Z_f} = \frac{\dfrac{R_{in}}{1 + sR_{in}C_{in}}}{\dfrac{R_{in}}{1 + sR_{in}C_{in}} + \dfrac{R_f}{1 + sR_fC_f}} \quad . \tag{3.1}$$

This expression can be further simplified to

$$\frac{V_\epsilon}{V_t} = \left(\frac{R_{in}}{R_{in} + R_f}\right)\left(\frac{1 + sR_fC_f}{1 + sR_{if}C_{if}}\right) \quad , \tag{3.2}$$

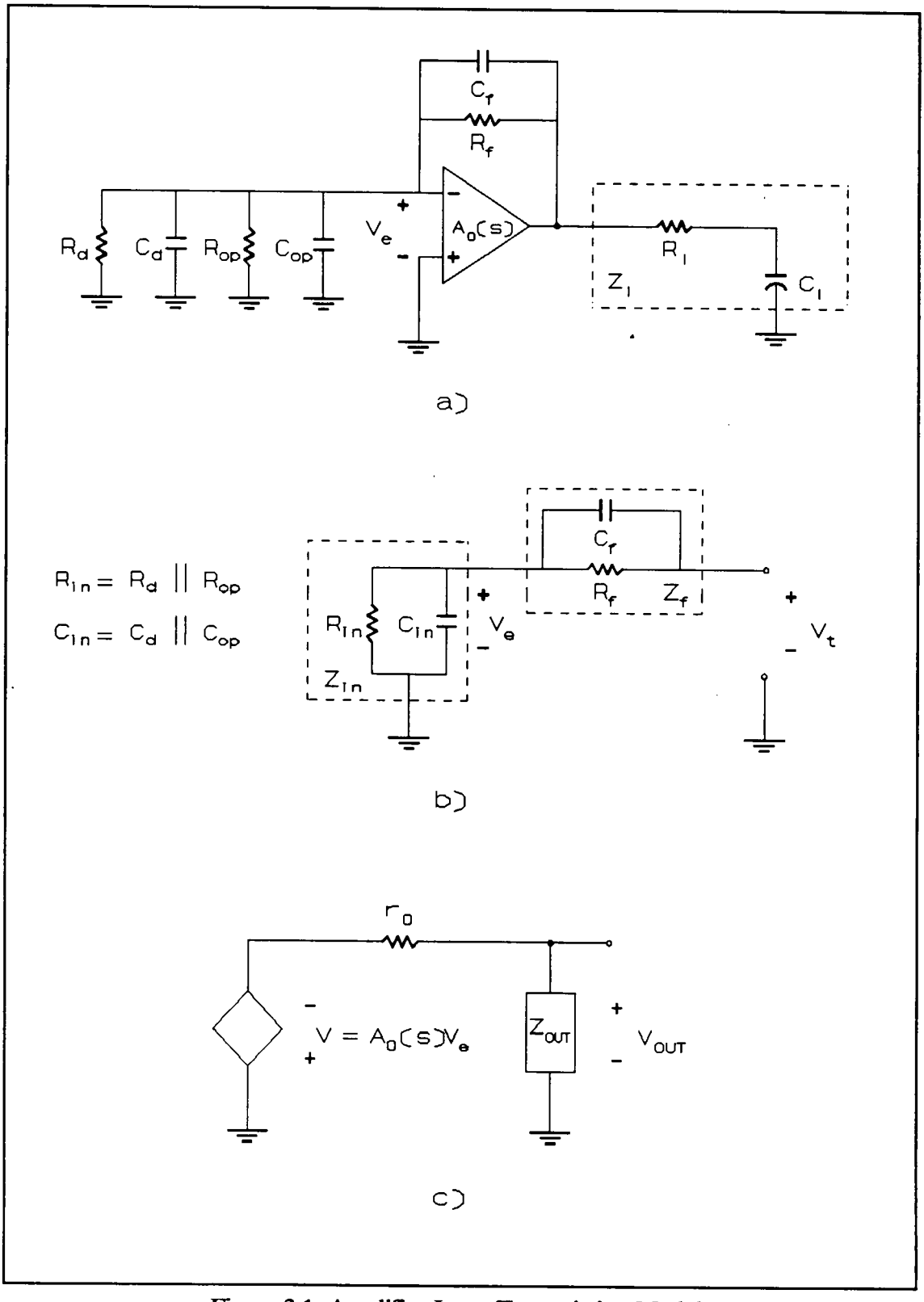

Figure 3.1. Amplifier Loop Transmission Model.

where

$$R_{if} = R_{in} \| R_f = \frac{R_{in} R_f}{R_{in} + R_f} \tag{3.3}$$

and

$$C_{if} = C_{in} + C_f \ . \tag{3.4}$$

The output voltage v_{out} can now be found from the transfer function

$$\frac{v_{out}}{v_\epsilon} = -A_o(s)\frac{Z_{out}}{r_o + Z_{out}} \ , \tag{3.5}$$

where

$$Z_{out} = Z_l \| (Z_{in} + Z_f) = \frac{Z_l(Z_{in} + Z_f)}{Z_l + (Z_{in} + Z_f)} \ , \tag{3.6}$$

$$(Z_{in} + Z_f) = \frac{(R_{in} + R_f)(1 + sR_{if}C_{if})}{(1 + sR_{in}C_{in})(1 + sR_fC_f)} \ , \tag{3.7}$$

$$Z_l = \frac{(1 + sR_lC_l)}{sC_l} \ , \tag{3.8}$$

and the AD707 open-loop transfer function, A_o, is given by the manufacturer (Analog Devices, 1988) to be

$$A_o = \frac{(13*10^6)}{\left(1 + \frac{jf}{0.1\,Hz}\right)\left(1 + \frac{jf}{8*10^6\,Hz}\right)} \quad . \tag{3.9}$$

Thus, the loop transmission T(s) is given by

$$T(s) = \frac{v_{out}}{v_i} = -A_o(s)\left(\frac{R_{in}}{R_{in} + R_f}\right)\left(\frac{1 + sR_fC_f}{1 + sR_{if}C_{if}}\right)\left(\frac{Z_{out}}{r_o + Z_{out}}\right) \quad . \tag{3.10}$$

Inserting the complex expressions for Z_{out} in Eq. (3.10) and factoring the last term of the loop transmission expression into easily identifiable poles and zeros becomes quite tedious. However, an approximation to Eq. (3.10) that will simplify the expression can be obtained if valid assumptions are made. Because $R_{in} >> R_f$ (R_f = 750 Ω and $R_{in} \sim$ 60 MΩ), then the magnitude of the second factored term in Eq. (3.10) approaches 1, and R_{if} in the denominator of the third factored term becomes R_f. Because $| r_o | << | Z_{out} |$, then the magnitude of the fourth factored term in Eq. (3.10) approaches 1. Thus, Eq. (3.10) can be approximated by

$$T(s) = -A_o(s)\left(\frac{1 + sR_fC_f}{1 + sR_f(C_f + C_{in})}\right) = -A_o(s)\left(\frac{1 + sR_fC_f}{1 + sR_fC_{if}}\right) \quad . \tag{3.11}$$

As can be seen from Eq. (3.11), the large diode capacitance produces a dominant pole in the loop transmission. The classic technique normally utilized to compensate for the input capacitance of an operational amplifier is to add a capacitor, C_f, in parallel with R_f, which allows this zero to cancel the input pole due to the input capacitance. Because

C_f is also in the pole term in Eq. (3.11), the pole and zero cannot be made to cancel directly. However, if C_f is made equal to C_{in}, then the 3-dB corner frequencies due to the pole and zero of Eq. (3.11) are located at the same order of magnitude (they differ by a factor of 2) in the frequency domain, and their effects on both the phase and magnitude of the loop transmission are effectively canceled.

The appendix contains a MathCad program named TACTUAL that calculates T(s) for Eq. (3.10) and a MathCad program named TAPPROX that calculates T(s) for Eq. (3.11). Figures 3.2 and 3.3 plot the magnitude of T(s) and the phase of T(s) for both equations respectively. As can be seen from these figures, the approximation yields close results for the magnitude of T(s); however, care must be taken in using the approximation for phase estimates to determine phase margin because the approximation is not as good at higher frequencies where the last factored term in Eq. (3.10) is contributing to the overall phase. Using a value for C_f of 7010 pF (6800 pf ‖ 210 pf), and Eq. (3.10), the gain margin was calculated to be 23 dB and the phase margin was calculated to be 52°. This will ensure that the transimpedance amplifier stage of the thesis radiometer circuit is stable.

3.2 Radiometer Noise Analysis

To determine the minimum amplifiable signal current that can be detected from the photodiode, a noise analysis of the radiometer must be performed. This analysis determines the level of photodiode current that must be present to exceed the input equivalent noise current (ENI) of the radiometer.

The model of the transimpedance amplifier shown in Figure 2.3 was extended to include sources that model the noise behavior of the various circuit components of the

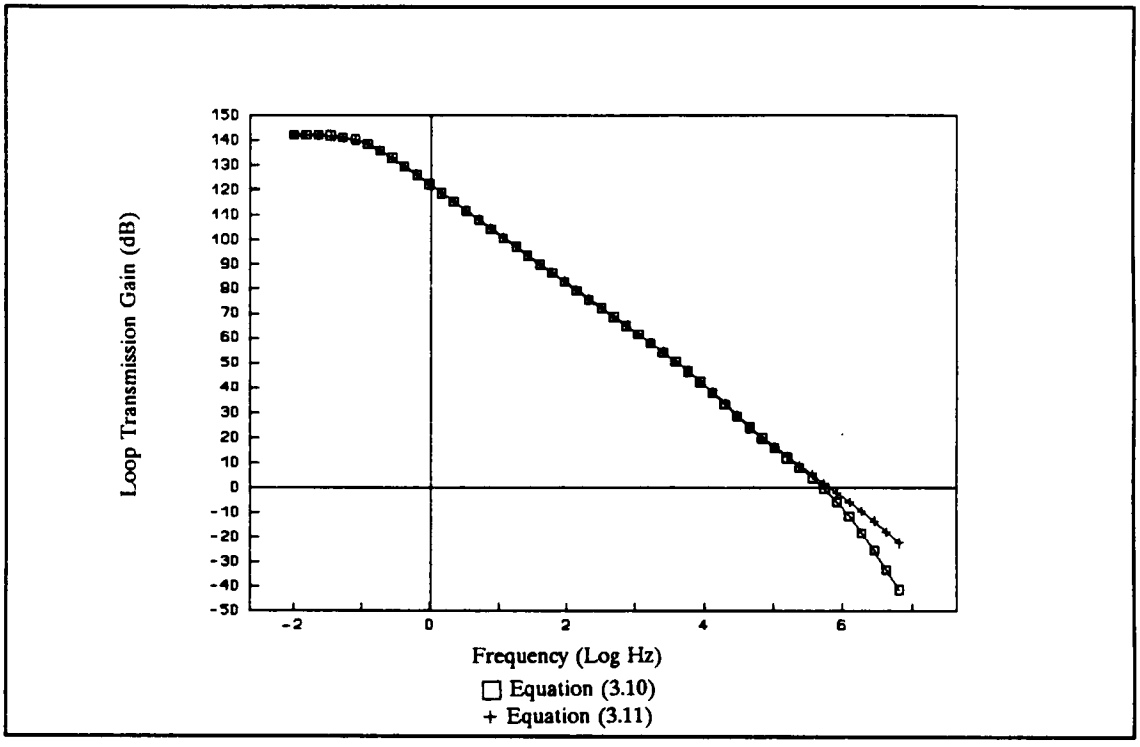

Figure 3.2. Amplifier Loop Transmission Gain.

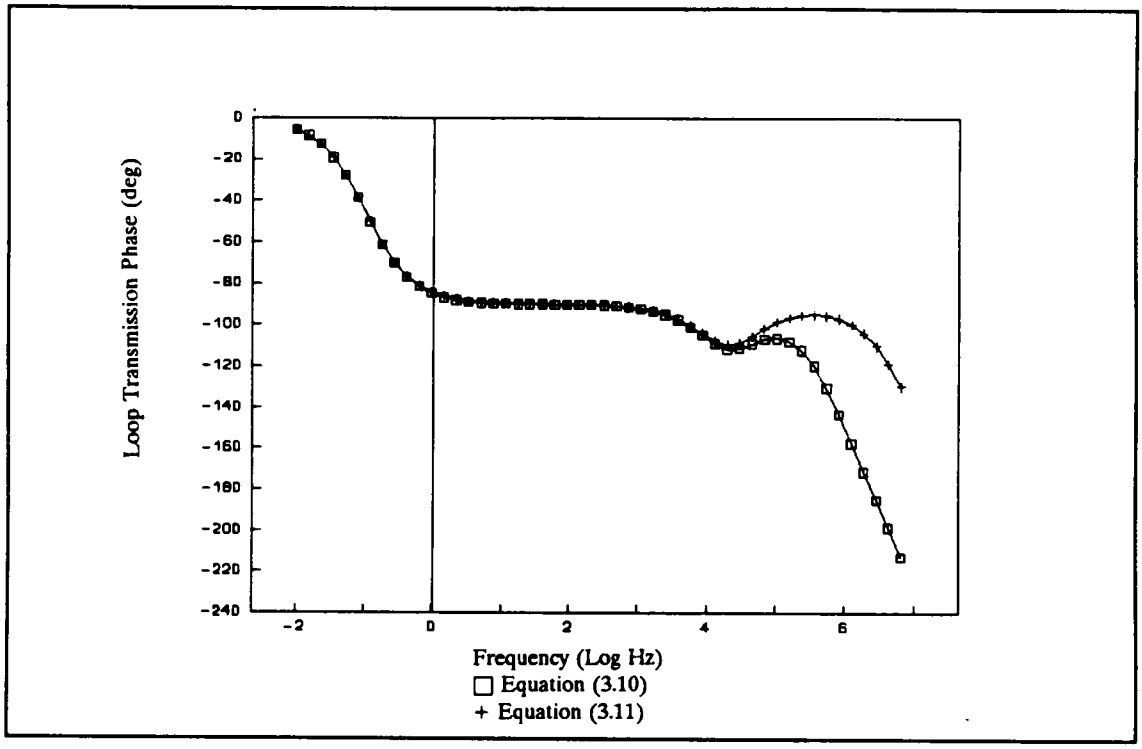

Figure 3.3. Amplifier Loop Transmission Phase.

radiometer including the photodiode, the op-amp, the AD693 and the resistors. This noise model is shown in Figure 3.4.

The voltage noise sources are denoted by "V" and the current noise sources are denoted by "I" in Figure 3.4; they are described by their noise power spectral densities (NPSDs), denoted by S(f). Subscripts on the noise sources defined in Figure 3.4 are used to indicate the origin of the noise source. The term power spectral density (PSD) is used here in the sense that the noise source described by the PSD would produce that power when loaded by a 1-Ω resistor (Wintenberg, 1989). For thermal noise or Johnson noise, the NPSD is constant as a function of frequency (white noise); however, many devices show an excess NPSD at low frequencies, which is often referred to as 1/f noise or pink noise (Kennedy, 1988). When appropriate and given by the manufacturer's specifications, low-frequency noise contributions from each noise source PSD will be included because the radiometer will have very little noise contributions from higher frequencies. This is due to the fact that the closed-loop transfer function of the radiometer has a dominant pole with a −3-dB corner frequency at ~1 Hz and a second pole whose −3-dB corner frequency is located at 500 Hz.

S_{Di} (f), given in Eq. (3.12), is the photodiode current NPSD where q is the electronic charge (1.6×10^{-19} coulomb). This NPSD is a function of the diode current composed of the photodiode dark current, i_d, and the photodiode light current, i_L. Because $i_L >> i_d$, the maximum light current of 80 μA will be used to calculate S_{Di}(f).

$$S_{Di}(f) = \left(2 * q * i_L = 2.56 \times 10^{-23}\right) \frac{A^2}{Hz} . \qquad (3.12)$$

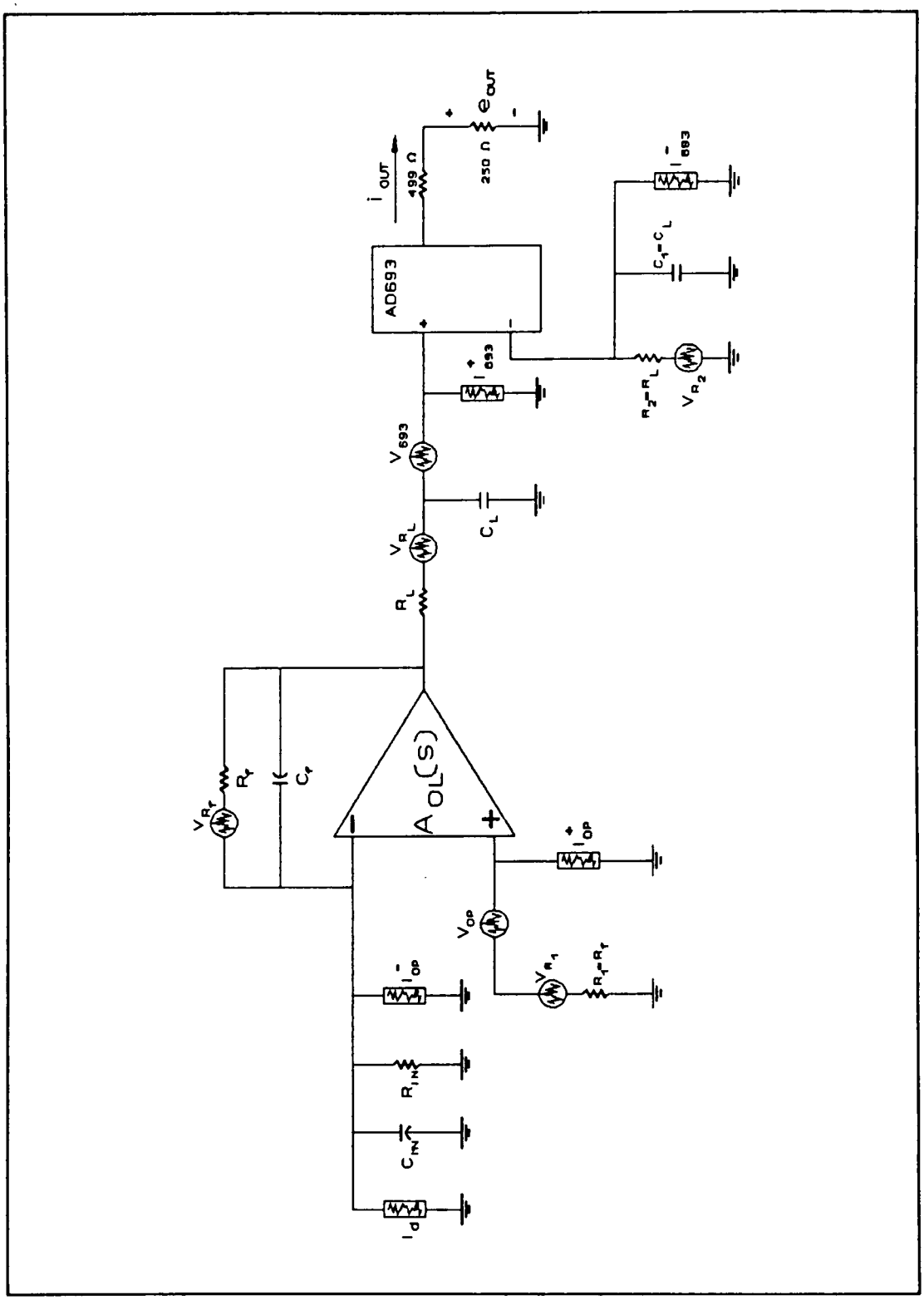

Figure 3.4. Radiometer Noise Model.

$S_{Opi}^{-}(f)$ and $S_{Opi}^{+}(f)$, given by $S_{Opi}(f)$ in Eq. (3.13), are the NPSDs of the input ENI sources for both the op-amp inverting and noninverting inputs, which have units of A^2/Hz (as listed in Table 2.2).

$$S_{Opi}(f) = 6.4 * 10^{-25} \quad (\text{for } f > 1 \text{ Hz})$$
$$S_{Opi}(f) = 6.4 * 10^{-25} \left(\frac{1\,\text{Hz}}{f}\right) \quad (\text{for } f < 1 \text{ Hz}) \ . \tag{3.13}$$

$S_{Ope}(f)$, shown in Eq. (3.14), is the NPSD of the equivalent input noise voltage (ENV) source for the op-amp having units of V^2/Hz (listed in Table 2.2).

$$S_{Ope}(f) = 1.69 * 10^{-16} \quad (\text{for } f > 1 \text{ Hz})$$
$$S_{Ope}(f) = 1.69 * 10^{-16} \left(\frac{1\ \text{Hz}}{f}\right) \quad (\text{for } f < 1 \text{ Hz}) \ . \tag{3.14}$$

The NPSDs for the noise voltage sources due to resistors R_f, R_L, R_1, and R_2 are shown in Eq. (3.15), where k is Boltzmann's constant, T is the absolute temperature in kelvins, R is given in ohms, and the units are V^2/Hz.

$$S_{Rf,\,Rl,\,R1,\,R2}(f) = 4kTR_{f,\,l,\,1,\,2} \ . \tag{3.15}$$

Carbon composition resistors can exhibit an NPSD value ten times that of the thermal noise equation given in Eq. (3.15) for frequencies < 100 Hz, whereas metal film and wire-wound resistors usually indicate nearly pure thermal noise as given by Eq. (3.15) to as low as 1 Hz (Kennedy, 1988). Because the resistors in the radiometer circuit are of metal film type, an assumption will be made that the noise is white and given purely by Eq. (3.15). It will be shown later in this section that the noise contribution from these resistors is

<0.5% combined. The noise contribution of the 499- and 250-Ω output resistors will be neglected because it can be shown that their contribution to calculating the radiometer input ENI would be insignificant since their magnitudes are small and their contribution to the input is divided by the gain blocks of the AD693 and the op-amp.

$S_{693e}(f)$, shown in Eq. (3.16), is the NPSD of the input ENV source of the AD693, having units of V^2/Hz (as listed in Table 2.3).

$$S_{693e}(f) = 2.5 * 10^{-15} \qquad (\text{for } f > 10 \text{ Hz})$$
$$S_{693e}(f) = 2.5 * 10^{-15} \left(\frac{10 \text{ Hz}}{f}\right) \qquad (\text{for } f < 10 \text{ Hz}) \ . \tag{3.16}$$

$S_{693i}^{-}(f)$ and $S_{693i}^{+}(f)$ given by $S_{693i}(f)$ in Eq. (3.17) are the NPSDs of the input ENI source of the AD693, having units of A^2/Hz (listed in Table 2.3).

$$S_{693i}(f) = 1.6 * 10^{-27} \qquad (\text{for } f > 80 \text{ Hz})$$
$$S_{693i}(f) = 1.6 * 10^{-27} \left(\frac{80 \text{ Hz}}{f}\right) \qquad (\text{for } f < 80 \text{ Hz}) \ . \tag{3.17}$$

The output NPSD, $S_{Xout}(j\omega)$, of an amplifier due to some input noise source, X, with power spectral density (PSD), $S_X(j\omega)$, is given by

$$S_{Xout}(j\omega) = S_X(j\omega) A_{cl}(j\omega) A_{cl}^{*}(j\omega)$$
$$S_{Xout}(j\omega) = S_X(j\omega) |A_{cl}(j\omega)|^2 \ , \tag{3.18}$$

where $A_{cl}(j\omega)$ is the actual closed-loop gain for the noise source, X, and $A_{cl}^{*}(j\omega)$ is its complex conjugate (Wintenberg, 1989). It is important to note that $A_{cl}(j\omega)$ may be different for each noise source (Wintenberg, 1989).

The total output NPSD of an amplifier is the sum of the output NPSDs due to all the noise sources if the sources are not correlated (Wintenberg, 1989); in other words, they are randomly related to each other in time and there is no systematic phase relationship. The author will assume for this analysis that the noise sources are not correlated.

To find the output noise power, e_{Xout}^2, for a particular noise source, X, in a bandwidth ranging from f_1 to f_2, the output PSD is integrated to give

$$e_{Xout}^2 = \int_{f1}^{f2} S_{Xout}(j2\pi f)\, df \quad , \tag{3.19}$$

where e_{Xout}^2 denotes the mean-squared output voltage; and therefore, the root-mean squared output noise voltage is given by the square root of e_{Xout}^2. The output noise power contributed by each source can now be identified.

The equivalent output noise power due to each source has been calculated in the MathCad program NOISE (see the appendix), where the transfer function for each noise source was derived using superposition techniques; these calculations are defined in Tables 3.1, 3.2, and 3.3. A practical limitation of low-frequency noise is reached when low-frequency noise is indiscernible from dc drift (Kennedy, 1988). A limit often imposed is 0.01 Hz, and this will be used for the lower limit of integration in the noise calculations. The upper limit of integration for the noise calculations was chosen to be 1000 Hz to stop the MathCad program's numerical integrations. Table 3.4 contains the output noise power expressions for each noise current source, and Table 3.5 contains the output noise power expressions for each noise voltage source. Table 3.6 contains the calculated output noise power of each source along with the percentage of its contribution to the total output

Table 3.1. Noise Calculation Ideal Closed-Loop Gain Terms

Gain	Definition
A_{f1}	$\frac{R_f}{\left(1 + jf2\pi R_f C_f\right)} = \frac{R_f}{\left(1 + \frac{jf}{30.3\ KHz}\right)}$
A_{f2}	$A_{f2} = \left[1 + \frac{\left(\frac{R_f}{1 + jf2\pi R_f C_f}\right)}{\left(\frac{R_{in}}{1 + jf2\pi R_{in} C_{in}}\right)}\right] = \left(1 + \frac{\frac{R_f}{1 + \frac{jf}{30.3\ Khz}}}{\frac{R_{in}}{1 + \frac{jf}{0.97\ Hz}}}\right)$
A_L	$\frac{1}{\left(1 + jf2\pi R_L C_L\right)} = \frac{1}{\left(1 + \frac{jf}{1.57\ Hz}\right)}$
A_{693}	$\left(0.2667\frac{A}{V}\right) * \frac{1}{\left(1 + \frac{jf}{500\ Hz}\right)} R_{out}$

Table 3.2. Resistor and Capacitor Values Used in Ideal Closed-Loop Gain Terms

Gain Term	Definition
R_f	750 Ω
R_{in}	2151 Ω
R_{in}	$R_d \parallel R_{op}$ = 1 GΩ ∣ 60 MΩ ≈ 60 MΩ
R_{out}	250 Ω
C_f	7010 pF
C_{in}	7000 pF
C_L	47 μF

Table 3.3. Noise Source Ideal Closed-Loop Transfer Functions

Noise Source Spectral Density	Noise Source Transfer Function
S_{Di}, S_{Opi}^-	$A_{f1} * A_L * A_{693}$
S_{Opi}^+, S_{R1}	$R_f * A_{f2} * A_L * A_{693}$
S_{Ope}	$A_{f2} * A_L * A_{693}$
S_{RL}, S_{R2}	$A_L * A_{693}$
S_{Rf}	$1/R_f * A_{f1} * A_L * A_{693}$
S_{693e}	A_{693}
S_{693i}^+, S_{693i}^-	$R_L * A_L * A_{693}$

Table 3.4. Output Noise Power of Current Noise Sources

Noise Source	Output Noise Power (V_{rms}^2)
I_D	$\int_{0.01\ Hz}^{1000\ Hz} S_{Di}(f)\,\lvert A_{f1}A_L A_{693}\rvert^2\,df$
I_{Opi}^-	$\int_{0.01\ Hz}^{1\ Hz} S_{Opi}(f)\,\lvert A_{f1}A_L A_{693}\rvert^2\,df + \int_{1\ Hz}^{1000\ Hz} S_{Opi}(f)\,\lvert A_{f1}A_L A_{693}\rvert^2\,df$
I_{Opi}^+	$\int_{0.01\ Hz}^{1\ Hz} S_{Opi(f)}\,\lvert R_f A_{f2}A_L A_{693}\rvert^2\,df + \int_{1\ Hz}^{1000\ Hz} S_{Opi}(f)\,\lvert R_f A_{f2}A_L A_{693}\rvert^2\,df$
I_{693i}^+ I_{693i}^-	$\int_{0.01\ Hz}^{80\ Hz} S_{693i}(f)\,\lvert R_f A_L A_{693}\rvert^2\,df + \int_{80\ Hz}^{1000\ Hz} S_{693i}(f)\,\lvert R_f A_L A_{693}\rvert^2\,df$

Table 3.5. Output Noise Power of Voltage Noise Sources

Source	Output Noise Power (V_{rms}^2)
V_{Ope}	$\int_{0.01\ Hz}^{1\ Hz} S_{Ope}(f)\,\lvert A_{f2}A_L A_{693}\rvert^2 df + \int_{1\ Hz}^{1000\ Hz} S_{Ope}(f)\,\lvert A_{f2}A_L A_{693}\rvert^2 df$
V_{R1} V_{R2}	$\int_{0.01\ Hz}^{1000\ Hz} S_{R2}(f),\ S_{R1}(f)\,\lvert A_L A_{693}\rvert^2 df$
V_{R1}	$\int_{0.01\ Hz}^{1000\ Hz} S_{R1}(f)\,\lvert R_f A_{f2}A_L A_{693}\rvert^2 df$
V_{Rf}	$\int_{0.01\ Hz}^{1000\ Hz} S_{Rf}(f)\,\lvert \frac{A_{f1}A_L A_{693}}{R_f}\rvert^2 df$
V_{693e}	$\int_{0.01\ Hz}^{10\ Hz} S_{693e}(f)\,\lvert A_{693}\rvert^2 df + \int_{10\ Hz}^{1000\ Hz} S_{693e}(f)\,\lvert A_{693}\rvert^2 df$

Table 3.6. Calculated Output Noise Power

Noise Source	Output Noise Power (V_{rms}^2)	Percentage of Total
I_D	6.1×10^{-13}	0.00
I_{Opi}^-	6.29×10^{-15}	0.00
I_{Opi}^+	5.90×10^{-15}	0.00
I_{693}^-	8.03×10^{-11}	1.03
I_{693}^+	8.03×10^{-11}	1.03
V_{Ope}	2.95×10^{-12}	0.04
V_{693}	7.59×10^{-9}	97.6
V_{Rf}	3.31×10^{-12}	0.04
V_{RI}	9.48×10^{-12}	0.12
V_{R1}	3.31×10^{-12}	0.04
V_{R2}	9.48×10^{-12}	0.12

Total output noise power: 7.78×10^{-9} V^2_{rms}
Total output noise voltage: 88 μV_{rms}

noise power. The total output noise power of the radiometer circuit is calculated to be 7.8×10^{-9} V^2.

It is now desirable to equate this output noise to an equivalent input noise source. This is equivalent to interpreting the noise of the amplifier as being due to a single noise source connected to the input. In this way, we can compare the noise source to a comparable signal at the input, which is the signal to be measured. This process is known as referring the noise to the input, and such a source is called an equivalent input noise source (Wintenberg, 1989). The equivalent output noise rms voltage, e_{nout}, is determined by taking the square root of the output noise power and is calculated to be 88 μV for the radiometer circuit. Thus, the equivalent input noise current is found by dividing the equivalent rms output noise voltage by the dc transimpedance gain of the op-amp and the AD693 and is given by

$$i_{neq} = \frac{e_{nout}}{250\ \Omega * 750\ \Omega * 0.267(A/V)} \quad . \tag{3.20}$$

The calculated rms input noise current is 1.8 nA. Table 3.6 shows that the major contributor to this noise is the AD693 input ENV source. This amount of noise is sufficiently lower than the smallest current change that could be detected by the data acquisition system (DAS) that monitors and records the thesis radiometer output. The DAS for the UV-B facility incorporates a 13-bit (other signals tied into the DAS require this resolution) analog-to-digital converter (ADC) for a 0- to 5-V input span. Because the output of the radiometer is 4 to 20 mA, the input to the ADC will be 1 to 5 V when the input is terminated with a 250-Ω resistor. This corresponds to a 4-V span at 6554 bits of resolution. Thus, the smallest current change that could be seen by the ADC would be

$$\frac{\left(\frac{4\,V}{6554\ bits}\right)}{\left(250\ \Omega\ *\ 750\ \Omega\ *\ 0.267\,\frac{A}{V}\right)} = \frac{12\,nA}{bit} \quad . \tag{3.21}$$

3.3 Radiometer Error Budget Analysis

To determine the overall accuracy of the radiometer, an error budget analysis must be performed to summarize the effects of dc offset conditions as well as the drift included due to temperature changes. The worst case (WC) values from the component specifications (Tables 2.1, 2.2, and 2.3) will be used in all calculations to ensure conservative results. The WC error will be calculated from the total algebraic error due to each parameter. A more realistic or probable error will be calculated as the square root of the sum of the squares of each error parameter.

Because the frequency response of the radiometer is very low and most of its noise contribution is from low-frequency noise, the total noise will be added to the final result because it may not be discernable from drift (Kennedy, 1988).

The error due to the finite loop transmission of the op-amp will be ignored because the minimum open-loop gain of the radiometer op-amp given in Table 2.2 is 8 V/μV (includes -40 to 85°C temperature range). Thus, the loop transmission is kept high, resulting in no significant contribution to the total error.

The photodiode has the lowest operating temperature range specifications (-10 to 60°C), and that range will be used to specify the temperature operating range of the radiometer. All temperature changes will be based on a maximum span of 35°C (-10 to 25°C or 25 to 60°C).

The photodiode light current, I_L, has a typical negative temperature coefficient of $-0.1\%/°C$. Thus, for a 35°C span, the maximum error would occur for $I_{L(max)}$, which would be the maximum photodiode current that would cause a full-scale output of 20 mA from the radiometer. For the radiometer design, $I_{L(max)}$ would be 80 μA, and the current output error due to the drift of I_L is given by

$$\Delta I_{out}(I_L) = \left(\frac{-0.001}{°C}\right)(35°C)\,(750\ \Omega)\left(0.267\frac{A}{V}\right)I_{L(max)}$$

$$\Delta I_{out}(I_L) = -560\ \mu A\ . \tag{3.22}$$

The AD707C has a maximum input offset voltage, V_{opos}, of ±15 μV maximum (Table 2.2), which includes the −40 to 85°C temperature range of the op-amp. Thus, the current output error due to V_{opos} is given by

$$\Delta I_{out}(V_{opos}) = (\pm 15\ \mu V)\left(1 + \frac{750\ \Omega}{1G\ \Omega}\right)\left(0.267\frac{A}{V}\right) = \pm 4.0\ \mu A\ . \tag{3.23}$$

The AD707C has a maximum differential input offset current, I_{opos}, of ±1.5 nA maximum (Table 2.2), which includes the −40 to 85°C temperature range of the op-amp. Thus, the current output error due to I_{opos} is given by

$$\Delta I_{out}(I_{opos}) = (\pm 1.5\ nA)(750\ \Omega)\left(0.267\frac{A}{V}\right)$$

$$\Delta I_{out}(I_{opos}) = \pm 0.3\ \mu A\ . \tag{3.24}$$

The feedback resistor, R_f, has an initial tolerance of ±1% with a temperature coefficient of ±50 ppm/°C. A WC error would occur when both drift and initial tolerance errors are in the same direction and the photodiode current, I_L, is a maximum of 80 μA. Thus, the current output WC error due to the feedback resistor tolerance errors is given by

$$\Delta I_{out}(R_f) = \pm \left| I_{L(\max)} R_f \left\{ \left(0.267\frac{A}{V}\right) 1 - (1.01) \left[1 + \left(\frac{50 * 10^{-6}}{^\circ C} \right) 35^\circ \right] \right\} \right| \text{(max)}$$

$$\Delta I_{out}(R_f) = \pm 216\,\mu A\ . \tag{3.25}$$

The AD693 has roughly a ±0.1% nonlinearity and transconductance error (Analog Devices, 1990). The WC error from this parameter would occur at a full-scale output of 20 mA (span of 16 mA); thus, the current output error due to the AD963 nonlinearity and transconductance error, 693_{nl}, is given by

$$\Delta I_{out}(693_{nl}) = (\pm 0.001)(16\ mA) = \pm 16\ \mu A\ . \tag{3.26}$$

The AD693 has an initial input offset current, I_{693os}, of ±3 nA maximum, which includes the −40 to 85°C operating temperature range. Thus, the current output error from I_{693os} is given by

$$\Delta I_{out}(I_{693os}) = (\pm 3\ nA)(2151\ \Omega)\left(0.267\frac{A}{V}\right)$$

$$\Delta I_{out}(I_{693os}) = \pm 1.72\ \mu A\ . \qquad (3.27)$$

The AD693 also has a differential input bias current offset because the input bias current of the inverting input increases with input signal voltage. The differential input current, I_{diff}, equals the inverting input current minus the noninverting input current. I_{diff} flowing into an input source impedance will cause an input voltage error that varies with signal. The change in differential input current with input signal is approximated as a linear function; therefore, the error caused by source impedance may be approximated as a span error that has a maximum value at full scale. I_{diff} will cause the voltage on the inverting terminal of the instrumentation amplifier front end of the AD693 to rise, causing a net decrease in output current. From the manufacturer's data sheets (Analog Devices, 1990), I_{diff} at full-scale input is equal to 1.8 times the typical input bias current of the AD693, which is 20 nA. Thus, the WC current output error due to I_{diff} is given by

$$\Delta I_{out}(I_{diff}) = (2151\ \Omega)(1.8)(-20\ \ nA)\left(0.267\frac{A}{V}\right) = -20.7\ \mu A\ . \qquad (3.28)$$

The total rms output noise voltage, e_{nout}, was calculated to be 88 μV (see Section 3.2). Using a 250-Ω resistor as a current-to-voltage converter for the front end of the DAS, the output current error due to e_{nout} is given by

$$\Delta I_{out}(e_{nout}) = \frac{\pm 88\ \mu V}{250\ \Omega} = \pm 0.35\ \mu A\ . \qquad (3.29)$$

Table 3.7 contains the tabulated output current error terms along with the percentage contribution of each parameter to the total error.

The total algebraic WC error is roughly −4.0% of full scale. The probable rms error is calculated to be −3.0% of full scale. The majority of the error is contributed by I_L and R_f. Almost all of the error from these terms can be eliminated if R_f can be chosen with a positive temperature coefficient of +0.1%/°C (+1000 ppm/°C), which will offset the negative temperature coefficient (−0.1%/°C) of the photodiode. A measurement of the initial value of this resistor can be made at room temperature to eliminate the initial tolerance of the resistor. Vishay Resistive Systems Group manufactures a wire-wound temperature-compensating resistor to compensate for circuit components that exhibit negative temperature coefficients. Specifically, they manufacture a 750-Ω, 1/8-W package, +1000 ppm/°C ±100 ppm, and an initial ±0.1% tolerance. The author was unable to purchase one of these in a timely manner to complete this thesis; however, they are commercially available.

The contribution of the output current error due to this combination of R_f and I_L yields

$$\Delta I_{out}(I_L, R_f) = \left[1 - \left(1 - \frac{0.001}{°C}\right)(35°C)\left(1 + \frac{0.001}{°C}\right)(35°)\right] * \left[I_{L_{max}} R_f \left(0.267 \quad \frac{A}{V}\right)\right]$$

$$\Delta I_{out}(I_L, R_f) = 0.16 \ \mu A \ . \tag{3.30}$$

Thus, the total algebraic WC error is drastically reduced because I_L and R_f errors almost cancel each other out, the total algebraic WC error now becomes −0.216%, and the WC probable rms error is −0.13%.

Table 3.7. Summary of Error Budget Analysis

Parameter	Output Current Error (νA)	Total (%)
I_L	−560	70.75
$V_{op\ os}$	±4.0	0.51
$I_{op\ os}$	±0.3	0.04
R_f	±188.5	23.81
693_{nl}	±16.0	2.02
$I_{693\ os}$	±1.7	0.21
I_{diff}	−20.7	2.62
e_{nout}	±0.35	0.04

Total algebraic worst-case error: −791.6 μA

Percentage of full-scale worst-case error: −4.0
(based on 20-mA full-scale output)

4. CALIBRATION

The purpose of this section is to derive and calculate the calibration factors needed to compare the output of the radiometer to a secondary calibration standard, which is a radiometer with its calibration traceable to NIST.

4.1 Correction Factor Derivation

To test the radiometer, the author acquired a radiometer that is sensitive to light in the UV-B region and has calibration traceable to NIST. This radiometer will be denoted as the UVX radiometer (Model UVX radiometer with Model UVX-31 midrange sensor, manufactured by UVP). The UVX radiometer is calibrated at the factory with a monochromatic source at 310 nm. The gain of the UVX meter is adjusted at the factory so that the unit reads correctly (in units of W/m^2) when exposed to a known irradiance at 310 nm. Thus, this radiometer has an absolute response value of 1 at 310 nm. At any other wavelength, the UVX radiometer will display either a higher or lower irradiance than is actually being measured based on the absolute meter response at that particular wavelength. Calibration at other wavelengths is not performed, but the manufacturer provides a relative response curve that can be normalized to the calibration wavelength at 310 nm. The calibration data or the absolute spectral response of the UVX radiometer normalized to 310 nm is shown in Figure 4.1.

For the thesis radiometer, the absolute spectral response can be obtained from the photodiode calibrated spectral response (mA/W) and the photosensitive area of the photodiode (21.16 mm^2) provided by the manufacturer. Likewise, the Schott UG-11 bandpass filter transmittance (ratio of the transmitted spectral radiant flux to the incident radiation flux) is provided by the manufacturer (Schott, 1984). Thus, the spectral response

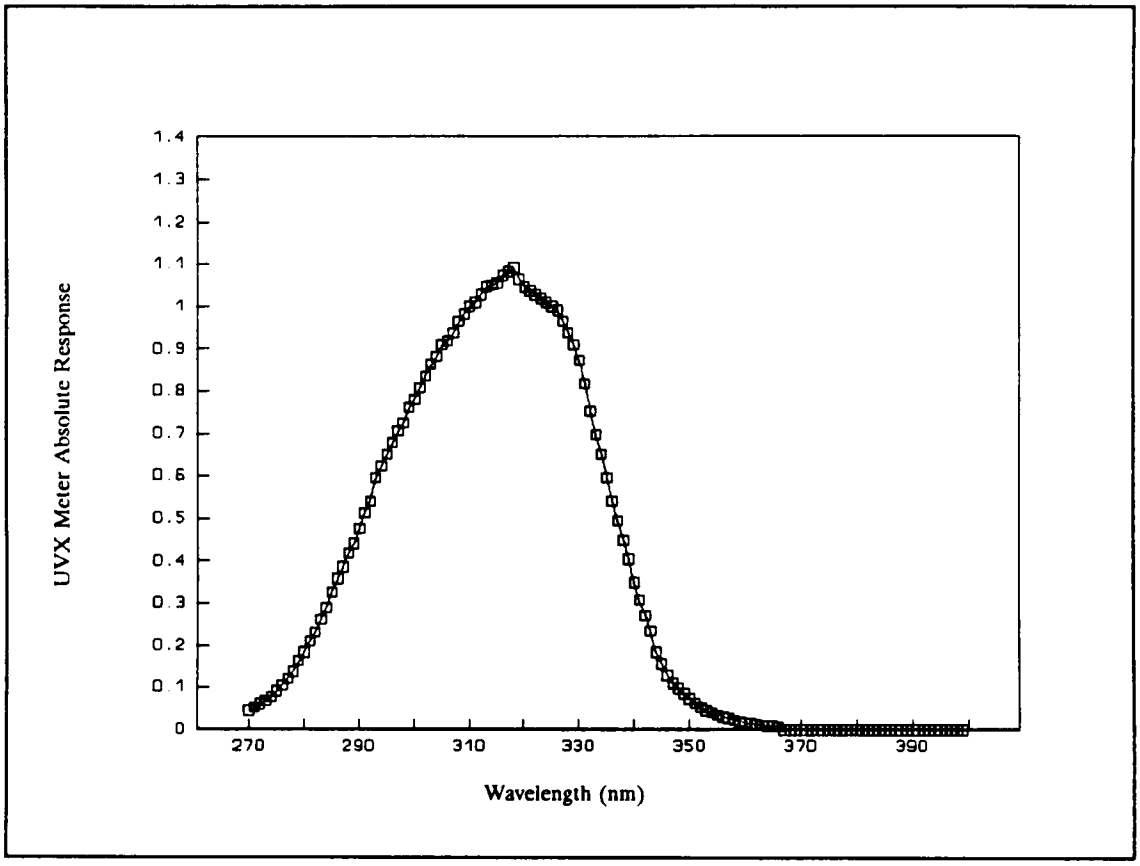

Figure 4.1. UVX Meter Absolute Response.

of the photodiode/filter assembly in units of $\mu A/W/m^2$ would be the product of the photodiode response and the filter transmittance at each wavelength.

At 310 nm, the thesis radiometer response is 0.8741 $\mu A/W/m^2$. The electronics of the radiometer are adjusted so that an 80-μA photodiode current will cause a full-scale output of 20 mA. This full-scale output would correspond to an irradiance of 91.52 W/m^2 for a 310-nm irradiance source. The spectral response of the thesis radiometer can now be normalized to 310 nm by dividing the individual spectral responses by the spectral response at 310 nm. This will permit easier comparisons between the two radiometers. The absolute spectral response of the thesis radiometer is shown in Figure 4.2. Thus, if the thesis radiometer were exposed to a monochromatic source at 310 nm, the absolute response would be 1 and the 4- to 20-mA output of this radiometer would be directly proportional to the full-scale range of 91.52 W/m^2.

The output of both radiometers is given by

$$UVX = \int_{-\infty}^{+\infty} B(\lambda)A(\lambda)d\lambda = k \int_{-\infty}^{+\infty} B(\lambda)D(\lambda)d\lambda \ , \tag{4.1}$$

where

$B(\lambda)$ = absolute spectral response of UVX or thesis radiometer (unitless);

$D(\lambda)$ = relative spectral power distribution of light source to be measured ($W/m^2/nm$);

k = amplitude multiplier for $D(\lambda)$—in other words, a function of source intensity or distance sensors are from the light source (unitless);

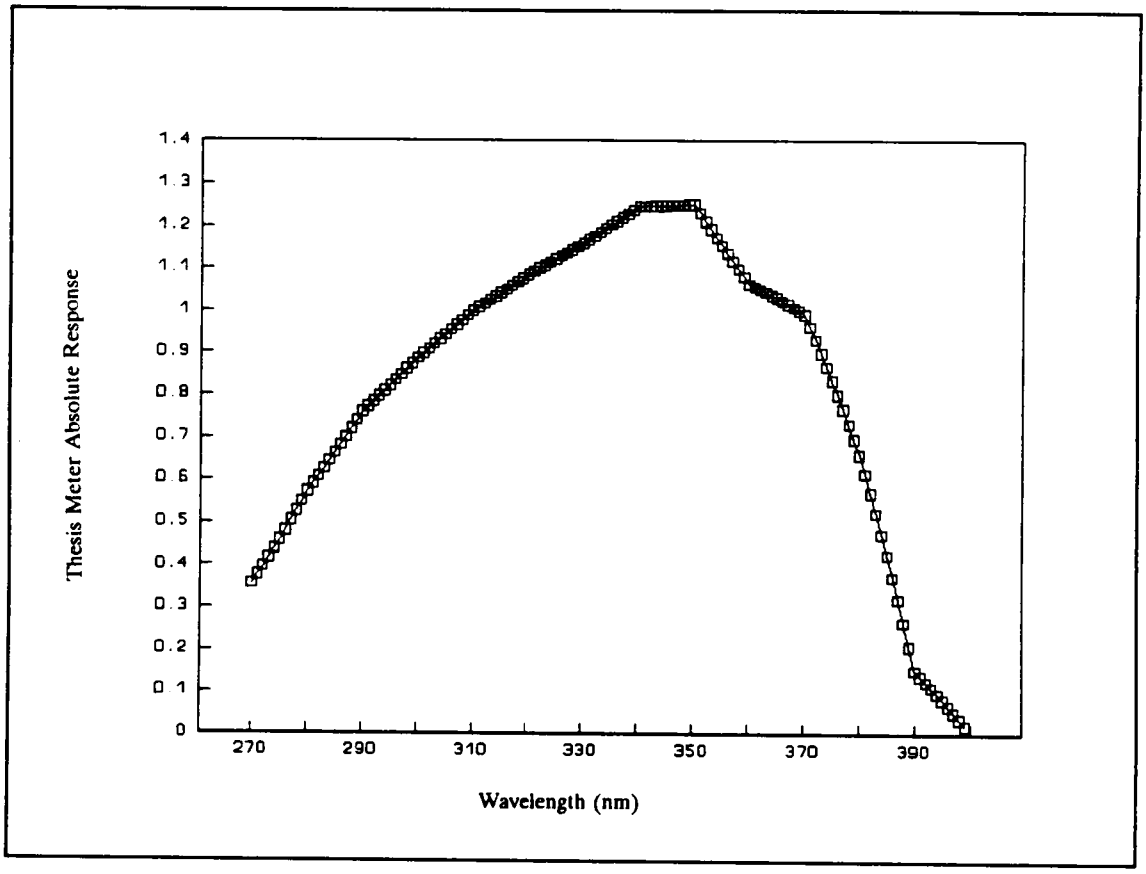

Figure 4.2. Thesis Meter Absolute Response.

$A(\lambda)$ = k * $D(\lambda)$, absolute spectral power distribution of light source to be measured ($W/m^2/nm$);

UVX = UVX or thesis radiometer output (W/m^2).

As shown in Figures 4.1 and 4.2 and from the spectral power data on the UVB-313 lamp sources and sunlight to be given later, the limits of integration in Eq. (4.1) can be limited to 270 to 400 nm because the product of $B(\lambda)*D(\lambda)$ is equal to zero outside this range for both radiometers. Thus, the total output of each radiometer is a function of the product of each radiometer's absolute spectral response with the spectral power distribution of the light source to be measured. Each radiometer has a different absolute spectral response; therefore, the corresponding output (in units of W/m^2) will be different for each one.

The desired measurement is not the total output of each radiometer. The desired measurement is the UV-B irradiance from 280 to 320 nm. A correction factor for both meters can be derived that will give the portion of the radiometer response due to only electromagnetic radiation in the UV-B region of interest. Solving for k in Eq. (4.1) gives

$$k = \frac{UVX}{\int_{270\ nm}^{400\ nm} B(\lambda)\,D(\lambda)\,d\lambda} \quad . \tag{4.2}$$

The desired measured UV-B irradiance is given by

$$\int_{280\ nm}^{320\ nm} A(\lambda)\,d\lambda = k \int_{280\ nm}^{320\ nm} D(\lambda)\,d\lambda \quad . \tag{4.3}$$

Substituting k from Eq. (4.2) into Eq. (4.3) gives

$$\int_{280\ nm}^{320\ nm} A(\lambda)\,d\lambda = \left(\frac{UVX}{\int_{270\ nm}^{400\ nm} B(\lambda)\,D(\lambda)\,d\lambda} \right) \int_{280\ nm}^{320\ nm} D(\lambda)\,d\lambda \quad . \tag{4.4}$$

Thus, a correction factor can be defined as

$$Correction\ Factor = \frac{\int_{280\ nm}^{320\ nm} D(\lambda)\,d\lambda}{\int_{270\ nm}^{400\ nm} B(\lambda)\,D(\lambda)\,d\lambda} \quad . \tag{4.5}$$

Thus, the desired output is given by

$$\int_{280\ nm}^{320\ nm} A(\lambda)\,d\lambda = (UVX) * (Correction\ Factor) \quad . \tag{4.6}$$

4.2 Ambient Sunlight Source

The spectral power distribution of ambient sunlight is shown in Figure 4.3. These data were obtained from the Q-Panel Company (Brennan, 1989) in Cleveland, Ohio, and will be used for $D(\lambda)$ in Eq. (4.5) to calculate the correction factor for the thesis and UVX radiometers when sensing sunlight. This is the same figure that was shown in Section 2.3 (Figure 2.4) using the 1-nm resolution provided by Q-Panel Company's data. These data were chosen over those of the SERI Model because the SERI data are given

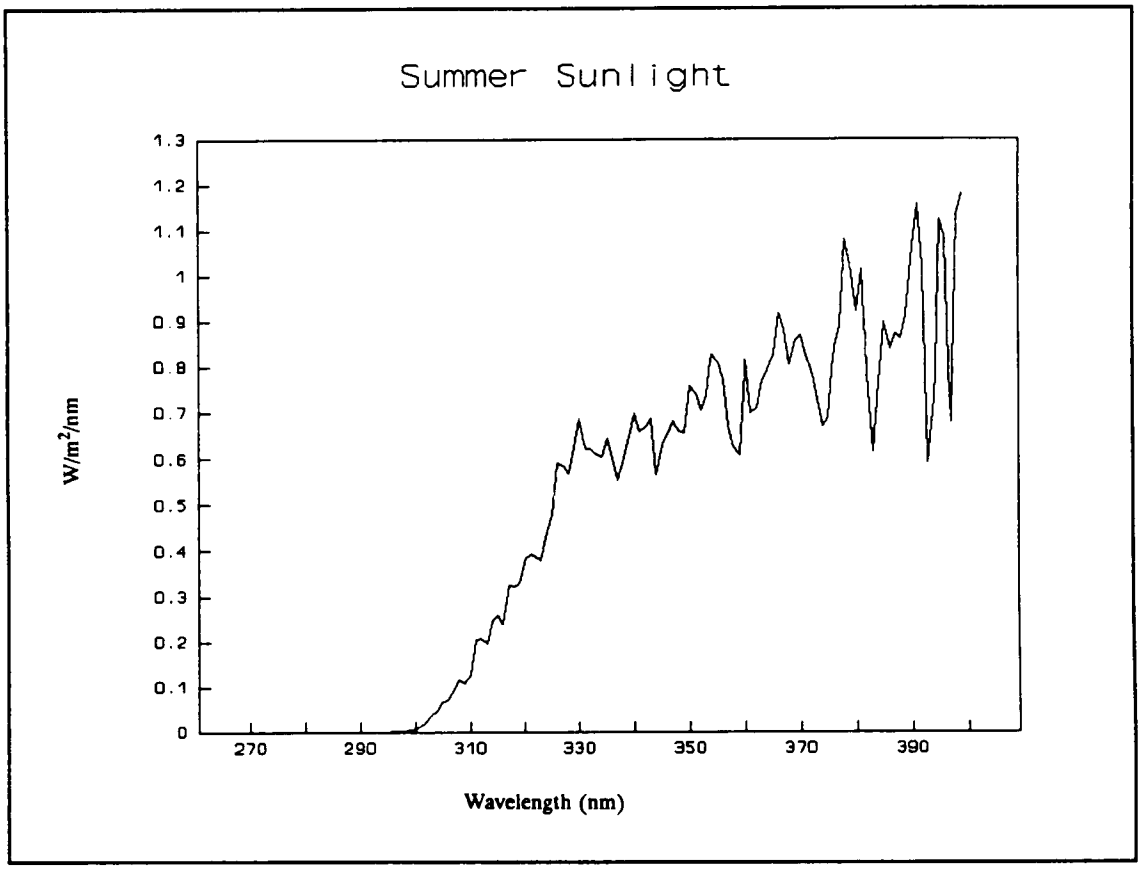

Figure 4.3. Summer Sunlight.

in bandwidths of 5 to 10 nm, whereas the Q-Panel data are given in 1-nm bandwidths. This makes it possible to use a smaller integration bandwidth for the calculations.

The correction factor for the thesis radiometer when it is exposed to sunlight is calculated in a MathCad program called UVB_CALS (see the appendix). This MathCad program performs the integrations and math required by Eq. (4.5). The thesis radiometer correction factor for ambient sunlight UV-B is calculated to be 0.0618.

The correction factor for the UVX radiometer when it is exposed to sunlight is calculated in a MathCad program called UVX_CALS (also contained in the appendix). This MathCad program performs the integrations and math required by Eq. (4.5). The UVX radiometer correction factor for ambient sunlight UV-B is calculated to be 0.2415.

4.3 UVB-313 Lamp Source

The spectral power distribution of the UVB-313 lamp source is shown in Figure 4.4. These data were obtained from the Q-Panel Company (Brennan, 1989), manufacturer of the UVB-313 lamp, and are used for $D(\lambda)$ in Eq. (4.5) to calculate the correction factor for the thesis and UVX radiometers when sensing the UVB-313 lamp.

The correction factor for the thesis radiometer when it is exposed to the UVB-313 lamp is calculated in a MathCad program called UVB_CALB (see the appendix), which performs the integrations and math required by Eq. (4.5). The thesis radiometer correction factor for the UVB-313 lamp UV-B is calculated to be 0.5521.

The correction factor for the UVX radiometer when it is exposed to the UVB-313 lamp is calculated in a MathCad program called UVX_CALB (see the appendix), which performs the integrations and math required by Eq. (4.5). The UVX radiometer correction factor for the UVB-313 lamp UV-B is calculated to be 0.7437.

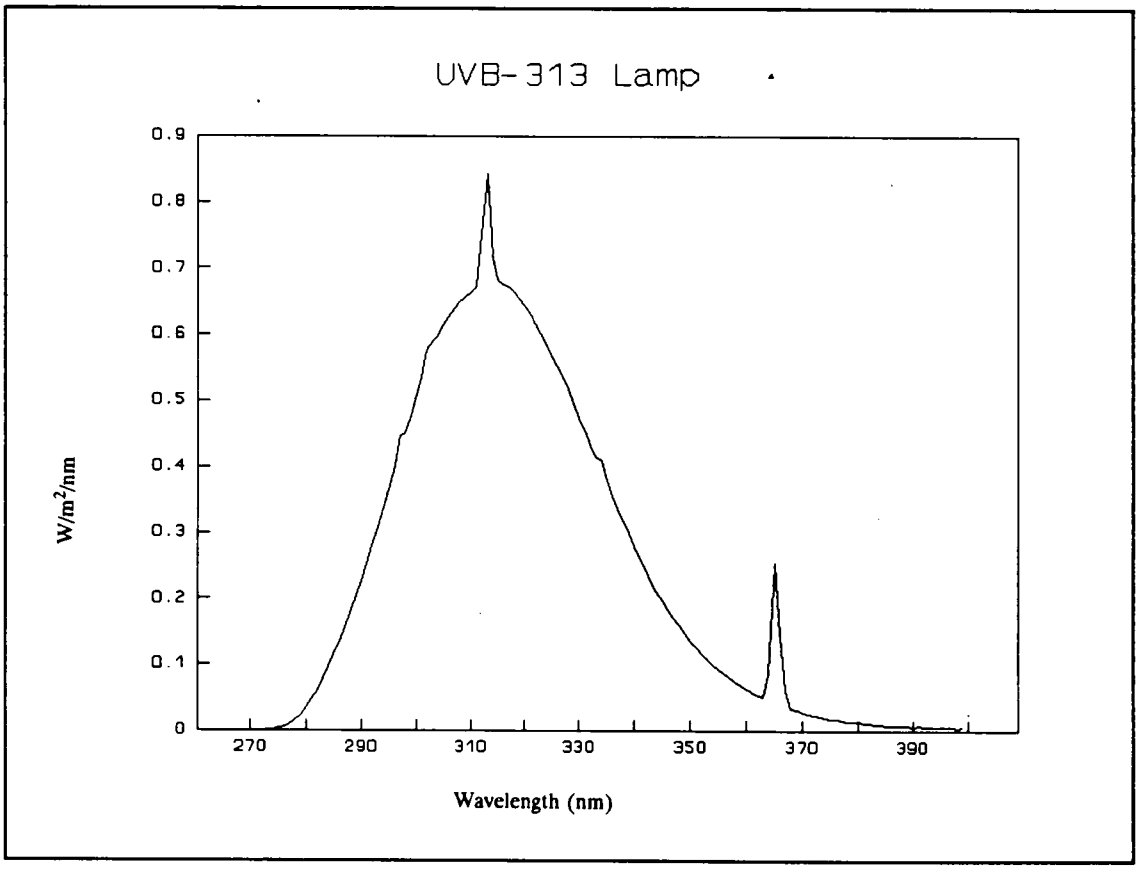

Figure 4.4. UVB-313 Spectral Power Distribution.

5. CIRCUIT CONSTRUCTION

This section describes the construction of the thesis UV-B sensor design and how it differs from the UVX sensor construction. The differences between the designs are important to the comparisons presented in Section 6.

5.1 Thesis UV-B Radiometer Construction

A diagram of the thesis UV-B sensor is shown in Figure 5.1. All electronics associated with the sensor are packaged in the enclosure with the photodiode and filter glass material. A printed circuit board was designed and fabricated to house all of the electrical components. For ease in replacing the photodiode, the photodiode leads are attached to the printed circuit board with single-socket pin holders designed to match the diameter of the lead wire on the photodiode. This results in good mechanical contact without having to solder the photodiode leads.

The top surface of the photodiode was positioned flush with the enclosure lid, directly under the Schott filter glass. This gives the sensor a fairly large field of view (discussed in Section 6.4). The photodiode and Schott filter glass were cleaned very carefully with alcohol to remove any foreign matter or fingerprints that would affect the calibration and measurement of the sensor. The Schott UG-11 filter glass is held in place by RTV adhesive and sealant. This sealant was also used around the lid mounting screws and the circuit board mounting screws to prevent any moisture from penetrating the enclosure. Likewise, sealant was applied along the outer lip of the lid and around the cable exit of the enclosure.

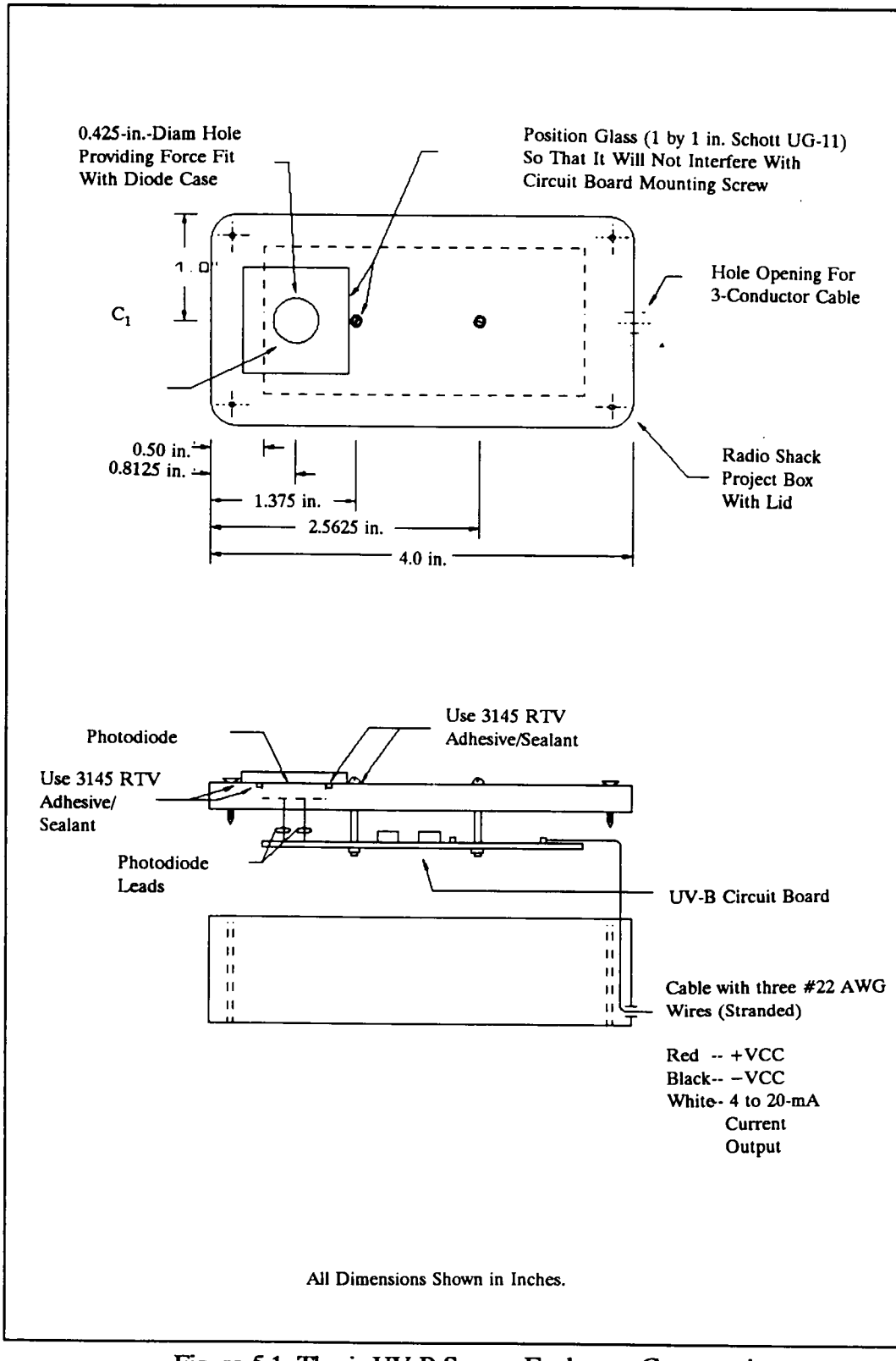

Figure 5.1. Thesis UV-B Sensor Enclosure Construction.

Four feet of 3-conductor, #22 AWG wire was soldered and strain relieved to the printed circuit board, and the other end was terminated with a three-prong male connector made for outdoor use. Connection to a dc power source and the DAS is then made by mating this connector with a field cable and its appropriate female mating connector.

5.2 UVX Sensor

The UVX radiometer is constructed such that the sensing element and a few electrical components are positioned in the sensor housing. The rest of the biasing and display electronics are housed in the hand-held display enclosure. A 3-ft cable assembly is used to mate the two components. Figure 5.2 is a sketch of the UVX sensor and how its photosensing surface is constructed. Note that the diffuser, filters, and photodiode are recessed below the surface of the sensor case. (The effects of this construction on the radiometer's performance will be discussed in Section 6.4). An external 0- to 2.0-V output is provided by a miniature female phone plug connection. The UVX sensor uses no sealer or gaskets around the sensor window and, thus, is not weatherproof. Likewise, the hand-held display and electronics were not designed for outdoor use.

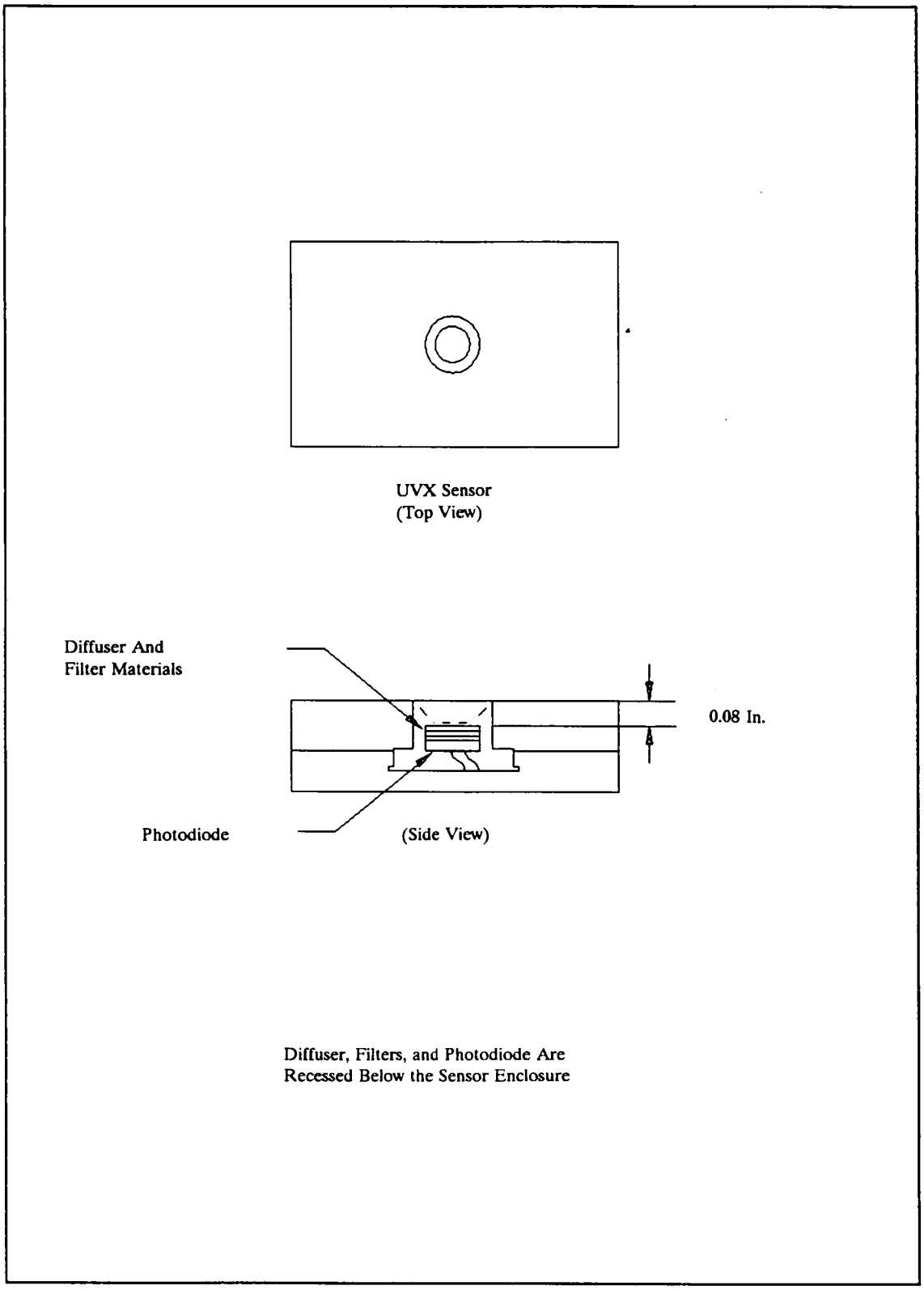

Figure 5.2. UVX Sensor Construction.

6. EXPERIMENTAL TECHNIQUES AND RESULTS

The purpose of this section is to describe the necessary experiments and measurements performed to verify the design in Section 3 and the calibration factors derived in Section 4.

6.1 Frequency Response and Gain Linearity

A variable-frequency current source to simulate the current output of the photodiode was needed to perform electrical measurements on the radiometer. Because variable-frequency function generators with voltage outputs are much more readily available than those with current outputs, the author designed a simple voltage-controlled current source using an operational amplifier, a reasonably fast transistor, and a resistor whose value was measured very accurately with a Keithly Model 191 digital multimeter that contains an automatic zeroing feature to subtract the lead resistance. When the current source was used in place of the photodiode, external capacitance was applied to the input of the op-amp to simulate the capacitance of the photodiode.

Figure 6.1 is a schematic diagram of the current source and the interconnections with the thesis UV-B radiometer and the biasing power supplies. The current source operates by applying a voltage, V_{Test}, to the noninverting terminal of the current source op-amp. This voltage due to feedback is seen at the inverting terminal of the op-amp, and a current flow through the transistor is developed by the voltage drop across the emitter resistor, R. This resistor was sized for a 1-V drop at 80 μA (full-scale radiometer photodiode current). Because the collector of the transistor is only a few volts above the radiometer's lower power supply bias voltage, two power supplies were used to bias the

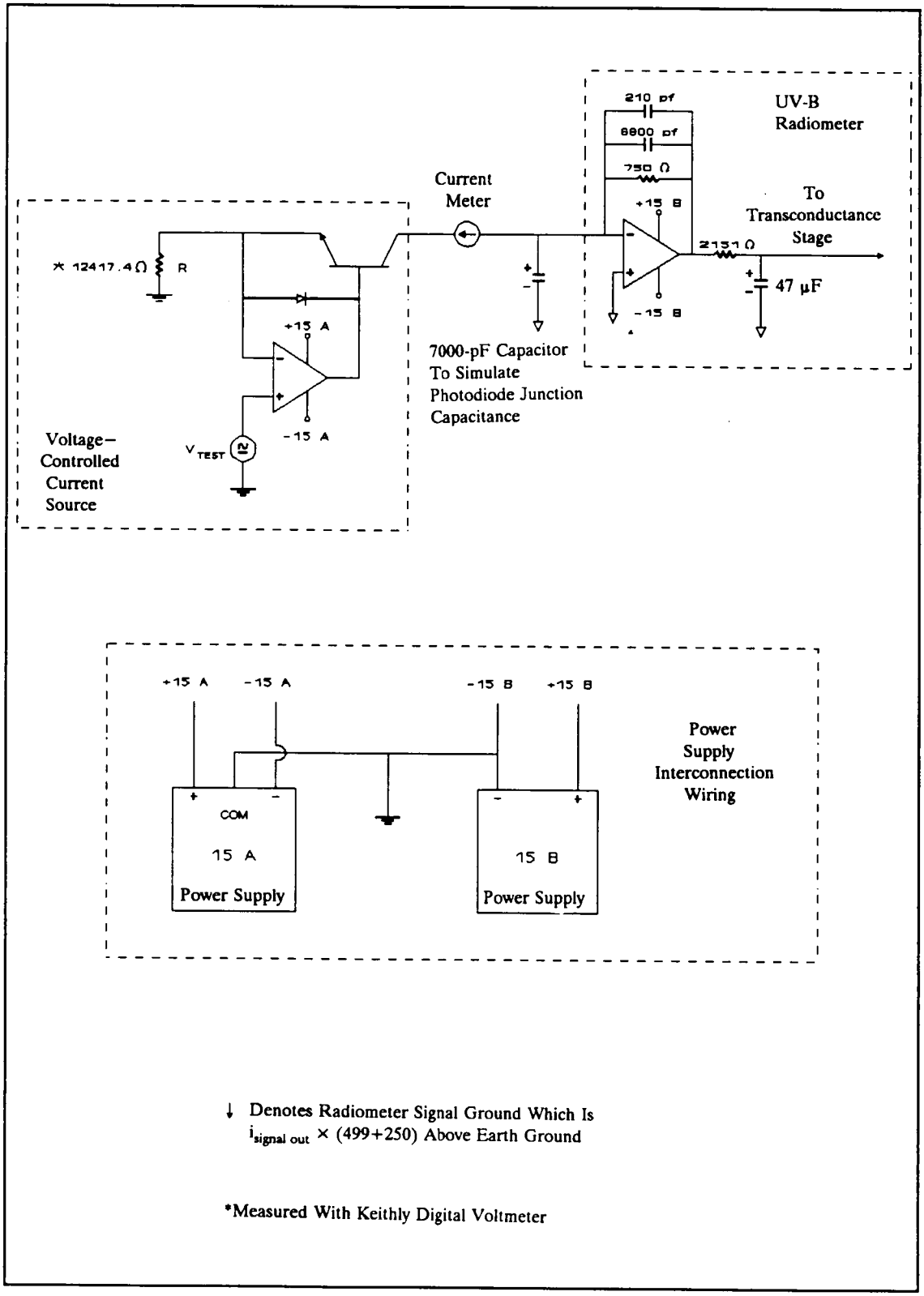

Figure 6.1. Radiometer Test Setup.

current source and the radiometer so that the output of the current source op-amp would have more than a few volts of "head room" above its lower power supply rail bias voltage. The power supplies and their interconnection to earth ground are also shown in Figure 6.1. Figure 6.1 also shows where a current meter (Triplett Model 3360 meter with current resolution of 0.1 μA) was positioned for some of the measurements.

Before any testing took place, the radiometer was zeroed by blocking all light to the photodiode. The output of the transimpedance amplifier was adjusted to zero voltage by using the 20-kΩ AD707 voltage offset potentiometer, and the output of the transconductance amplifier was adjusted to -4 mA by using the 10-kΩ AD693 zero offset potentiometer (see Figure 2.5).

An Analogic dc voltage standard, whose output display resolution is 0.1 mV, was used for the dc gain linearity checks. Using an accurately known resistor value, R, provides an emitter current resolution of ~0.01 μA (a MOSFET or JFET could be used in place of the transistor to eliminiate the base current error difference in the collector current). This is a factor of 10 better than using the Triplett multimeter, so this voltage display was used to determine the radiometer current for the gain linearity checks. Figure 6.2 is a graph of the measured vs expected output of the radiometer for the various test current source voltage inputs and shows the linearity to be very good (less than ± 0.25% of full scale). For the frequency response testing, a Philips Model PM5134 function generator was used for the current source test voltage, V_{Test}. Front panel adjustments on the function generator allowed selection of a 2.0 peak-to-peak voltage with a −6-dB attenuation to provide an output peak-to-peak voltage of ~1.00 V. The dc offset of the function generator was adjusted so that the 1.00-V peak-to-peak signal was from ground to 1.00 V. The test voltage frequency was varied from ~0.001 to 2000 Hz. The

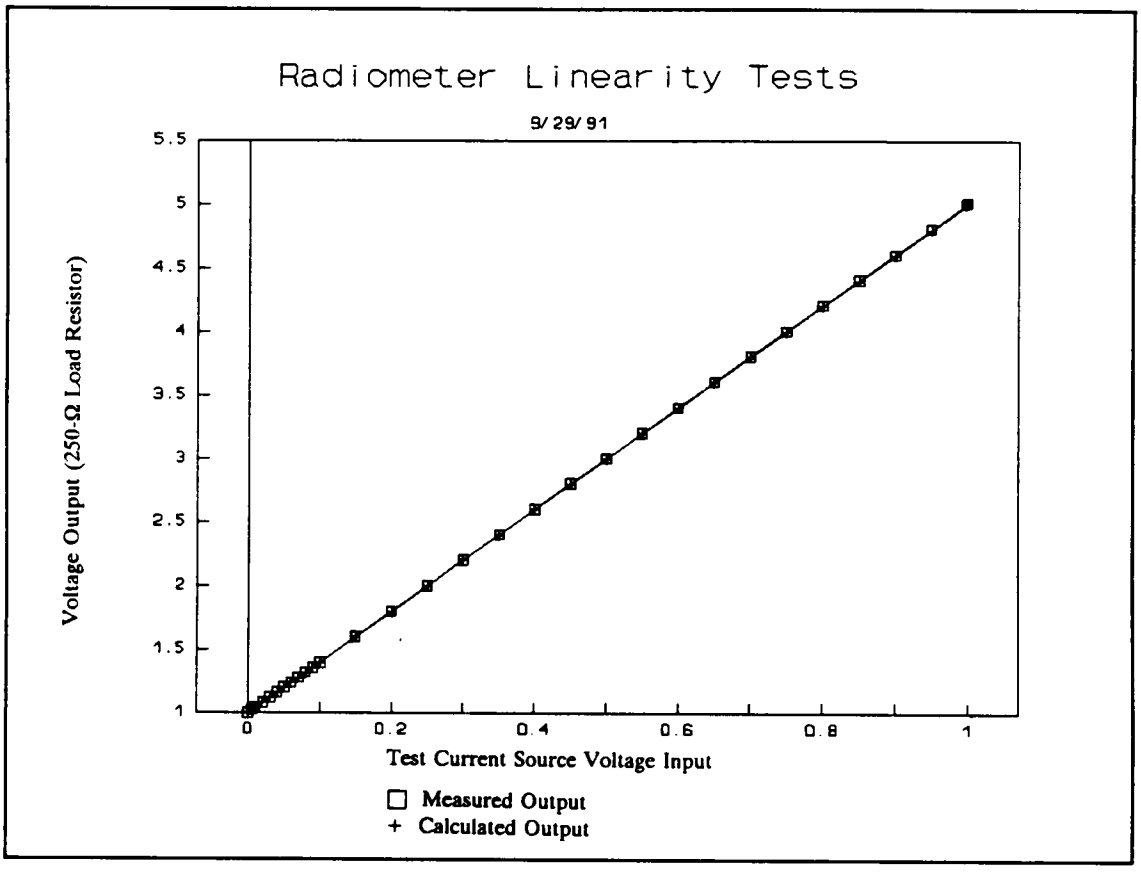

Figure 6.2. Radiometer Gain Linearity.

output of the radiometer was measured by using two instruments. For ~50% of the measurements, the peak voltage across a 250-Ω precision resistor (initial tolerance of ±0.1% with a temperature cofficient of ±50 ppm/°C) at the output of the radiometer's transconductance amplifier was measured by the Keithly Digital multimeter, whose voltage resolution is 10 μV on 2-V full scale. When the signal frequency started approaching the Keithly sample rate, the peak dc voltage from ground was measured by an oscilloscope. At the higher frequencies, the scope was ac voltage coupled to measure the peak-to-peak voltage so that low signal levels could be measured by blocking the 1-V dc offset output. Results of the frequency response testing are shown in Figure 6.3. These results show good agreement between the calculated and measured frequency responses of the radiometer.

6.2 Offset and Drift

The offset and temperature drift of the thesis radiometer were tested by placing the radiometer in an environmental chamber. Ideally, the drift of the instrument would be checked by using a stable UV-B source and measuring the drift with respect to changes in temperature, but this was not possible because the lamps were too large to be placed in the environmental chamber and because their output changes with temperature (Illuminating Engineering Society of America, 1981). A compromise approach was chosen in which the radiometer output would be monitored with the sensor seeing no UV-B and thus looking at the effects of changes in the photodiode dark current and the drift of the electronics for a zero condition. While the radiometer was inside in the dark environmental chamber, the 4- to 20-mA output signal was monitored with a precision 250-Ω resistor (initial tolerance of ±0.1% with a temperature coefficient of ±50 ppm/°C)

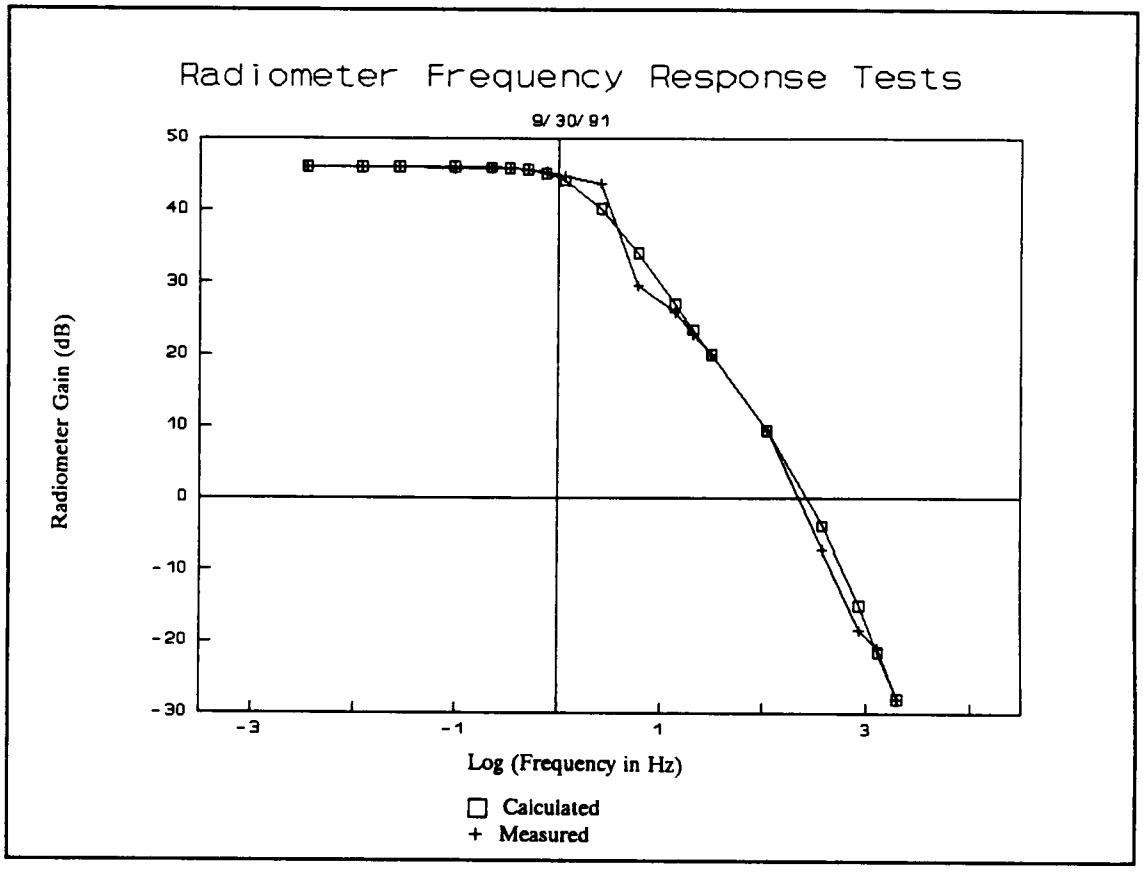

Figure 6.3. Radiometer Frequency Response.

and the Keithly Digital voltmeter located outside the chamber. The chamber temperature was varied from 0 to 50°C in 10°C steps. At each temperature test point setting, 30 min was allowed for the radiometer to reach thermal equilibrium with its surroundings.

The results of this test are shown in Figure 6.4. Figure 6.5 is a plot of the radiometer output zero current error based on the 20°C room temperature test point and shows the maximum zero shift to be <0.2% for the temperature range of 0 to 50°C. For the specified operating temperature range of −10 to 60°C (a span of 35°C from a midpoint room temperature of 25°C), the error is estimated to be 0.3%, which was calculated from the steepest slope (10 to 40°C) for a 35°C span (Figure 6.4.)

6.3 Output Noise Voltage

The peak-to-peak output noise voltage was measured with the thesis UV-B radiometer sensor exposed to total darkness. This measurement was made using a Tektronix oscilloscope with a resolution of 1 mV per division. The peak-to-peak noise voltage measured across a 250-Ω output resistor was 0.6 mV. The peak-to-peak noise voltage is ~6 to 7 times the output rms noise voltage (Wait, Huelsman, and Korn, 1975). Using a value of 6.5, the measured peak-to-peak voltage of 0.6 mV corresponds to an rms voltage of 92 μV. The calculated rms noise voltage (Section 3.2) was 88 μV, which shows good agreement between the calculated and measured output peak-to-peak noise voltage of the radiometer.

6.4 Radiometer Performance Comparisons

Many parameters that are a function of a sensor's design can affect radiant incidence measurements. One of these, spectral response, has been discussed and taken

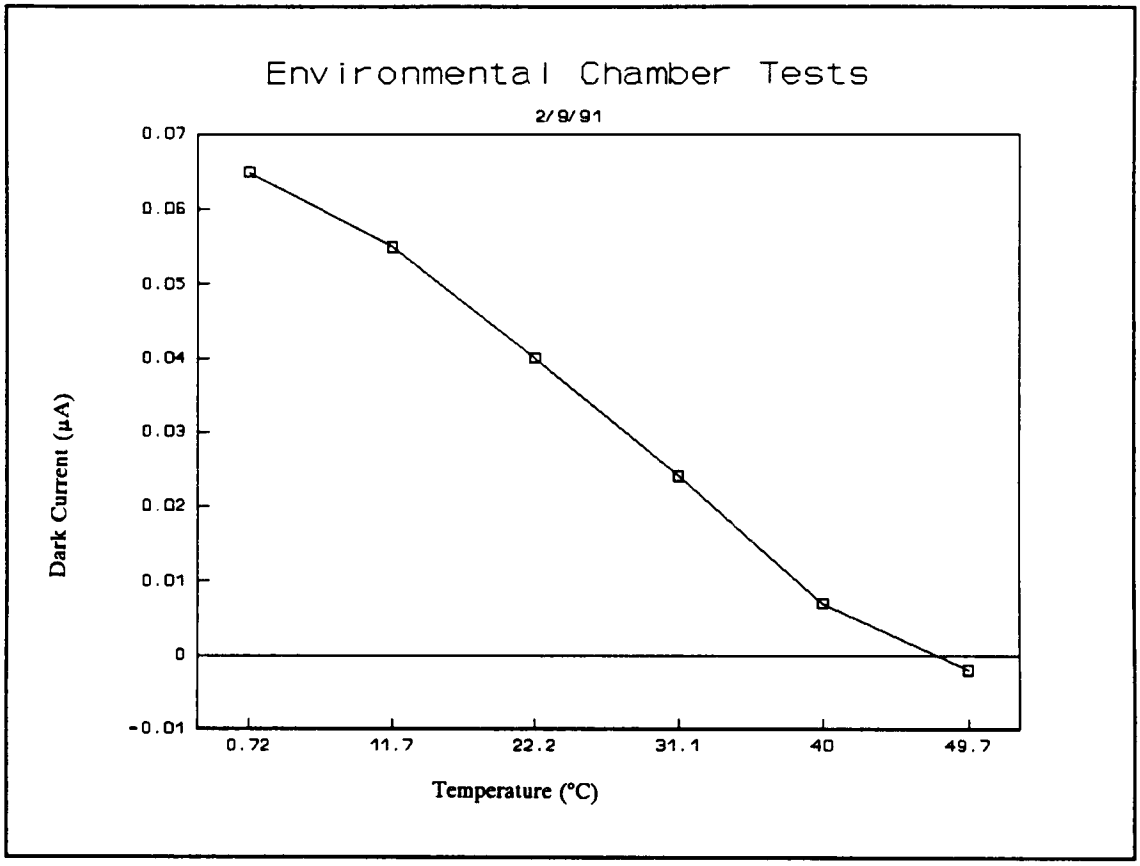

Figure 6.4. Temperature Drift Results of Thesis Radiometer.

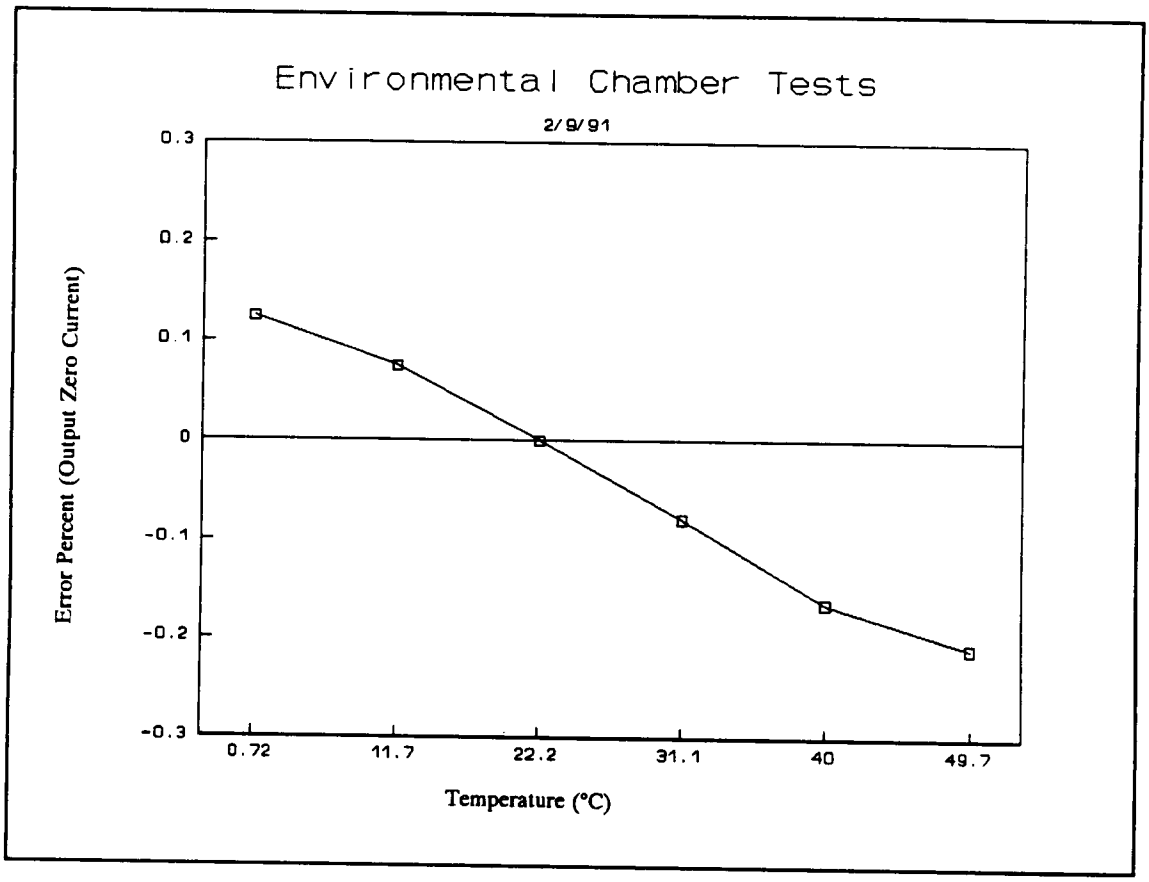

Figure 6.5. Percentage of Drift Error for 4-mA Zero Current.

into consideration in the derivation of correction factors for the various sensors. In addition, field of view and cosine response are also important specifications of a radiometer.

Figure 6.6 (Ultraviolet Products, Inc., 1990b) shows two different sensors measuring the output from an extended lamp source. Sensor S_1 has a larger field of view or acceptance angle than that of sensor S_2. Because it is radiant incidence that is being measured, sensor S_1 will yield a larger output than sensor S_2 because the emission from the total lamp length is being sensed (Ultraviolet Products, Inc., 1990b). Light emission comes from the ends of the lamp as well as from the middle and from the entire lamp length. It is obvious (see Section 5) that the thesis radiometer will have a larger field of view than that of the UVX sensor because its photosensing surface is not being shaded by the radiometer housing, whereas the UVX photosensing surface is recessed in its case, causing it to be more shaded.

Another important sensor specification is cosine response. For a sensor to measure irradiance accurately, it is necessary that it preserve a cosine relationship that depends on the angle of incident radiation, θ (Ultraviolet Products, Inc., 1990b). As can be seen from Figure 6.7, this relationship is a function of the projected area of the sensor as seen in a plane normal to the incident light. Because the projected area is proportional to the power intercepted by the sensor, the irradiance measured for radiation incident at an angle θ will be given by

$$I = I_o Cos(\theta) \quad , \tag{6.1}$$

where I_o is the irradiance that would be measured if the sensor were pointed directly toward the incident region (Ultraviolet Products, Inc., 1990b). Sensors that scale their

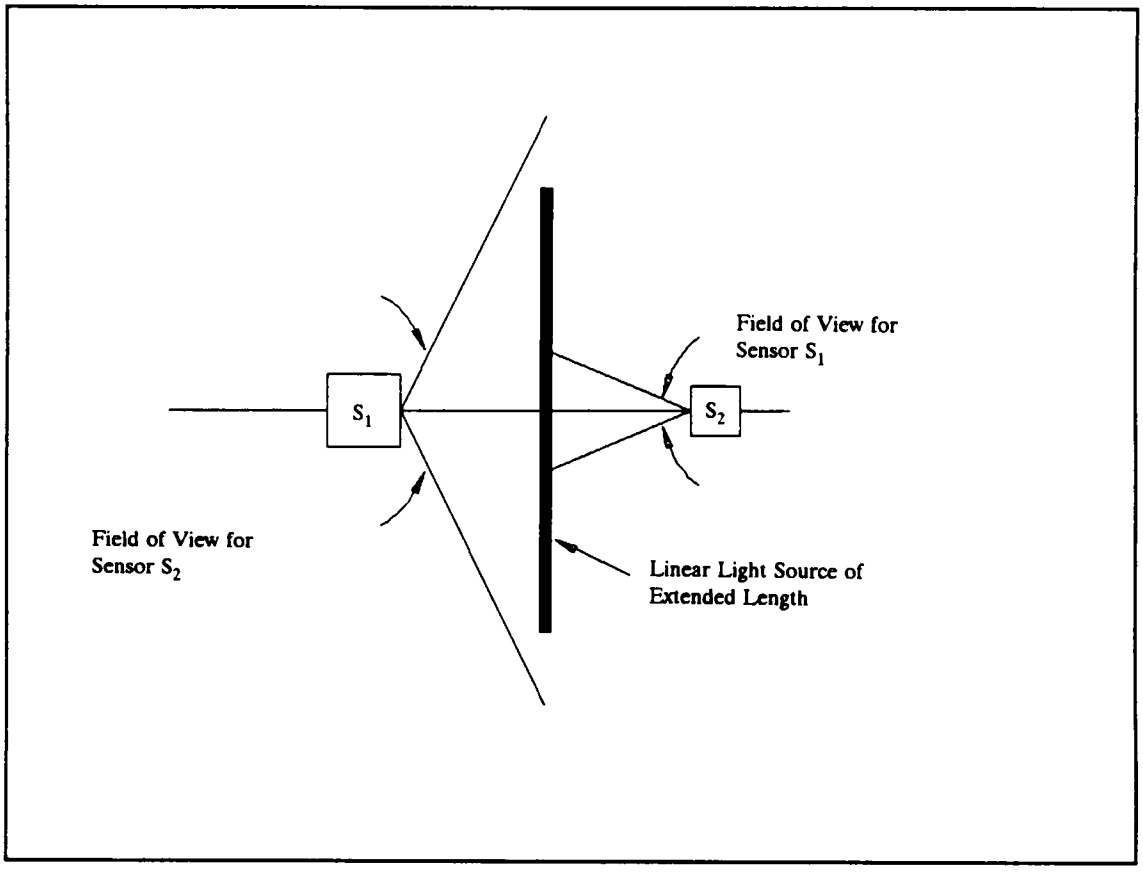

Figure 6.6. Sensor Field of View Illustration.

Source: Redrawn with permission from Ultraviolet Products, Inc., *UVX Radiometer Manual*, San Gabriel, California, 1990.

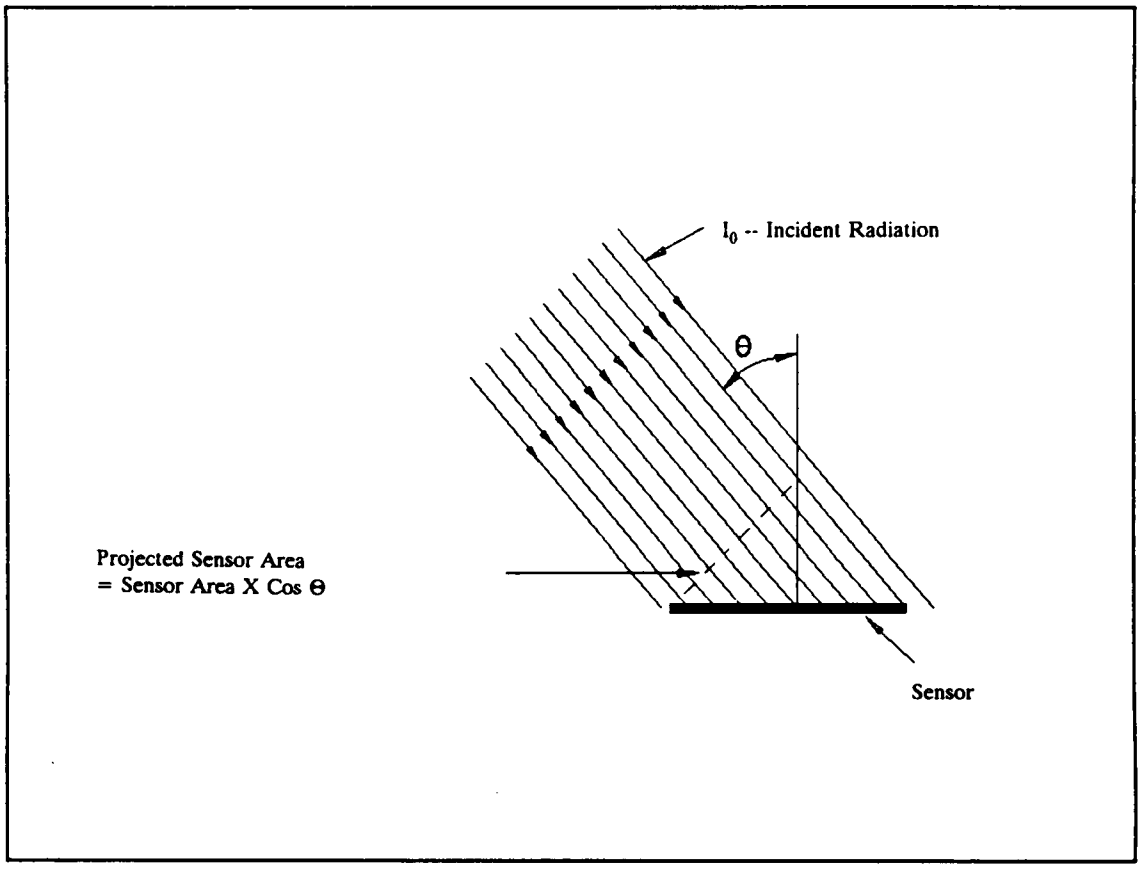

Figure 6.7. Sensor Cosine Response Illustration.

Source: Redrawn with permission from Ultraviolet Products, Inc., *UVX Radiometer Manual*, San Gabriel, California, 1990.

response in this manner are said to be cosine corrected. Plots of the measurements of the thesis and UVX radiometers' cosine responses and the ideal cosine response are shown in Figure 6.8. These measurements were made by positioning the sensor at some distance away from a vertical UV-B line source. Each sensor was fixed on an assembly containing a precision rotator that would allow it to rotate along its centerline while measuring the angular position. The sensor was roughly positioned normal to the line source and adjusted until a peak in the output was noted. The position where the peak occurred was noted, and this was taken as the normal incident position with the output value recorded as I_o. The sensor was then rotated in both directions to obtain the cosine response data shown in Figure 6.8.

Initial comparison testing of the thesis and UVX radiometers with UV-B lamps was performed in the laboratory to minimize unwanted variables. Two UVB-313 lamps were mounted in a standard 4-ft fluorescent shop fixture assembly. The lamps were positioned ~7 ft above the floor. A test fixture assembly was used to position the sensors with respect to the lamps so that each sensor could be positioned in exactly the same location. Irradiance readings were made at various distances from the lamps. Two measurements for both sensors were made at each elevation. A zero measurement was made by exposing both sensors to no light, and these values were used to subtract any offsets. The results of this initial indoor testing with the UVB-313 lamps are shown in Figure 6.9.

As can be seen from Figure 6.9, there is a ratio difference between the two measurements with the average ratio being 1.64. Various hypotheses were formed, but the most likely theory is that there was a difference in the field of view of each sensor, with the thesis radiometer having a larger field of view. To verify this hypothesis, a point UV-B light source was created by shielding the entire length of one UVB-313 lamp and

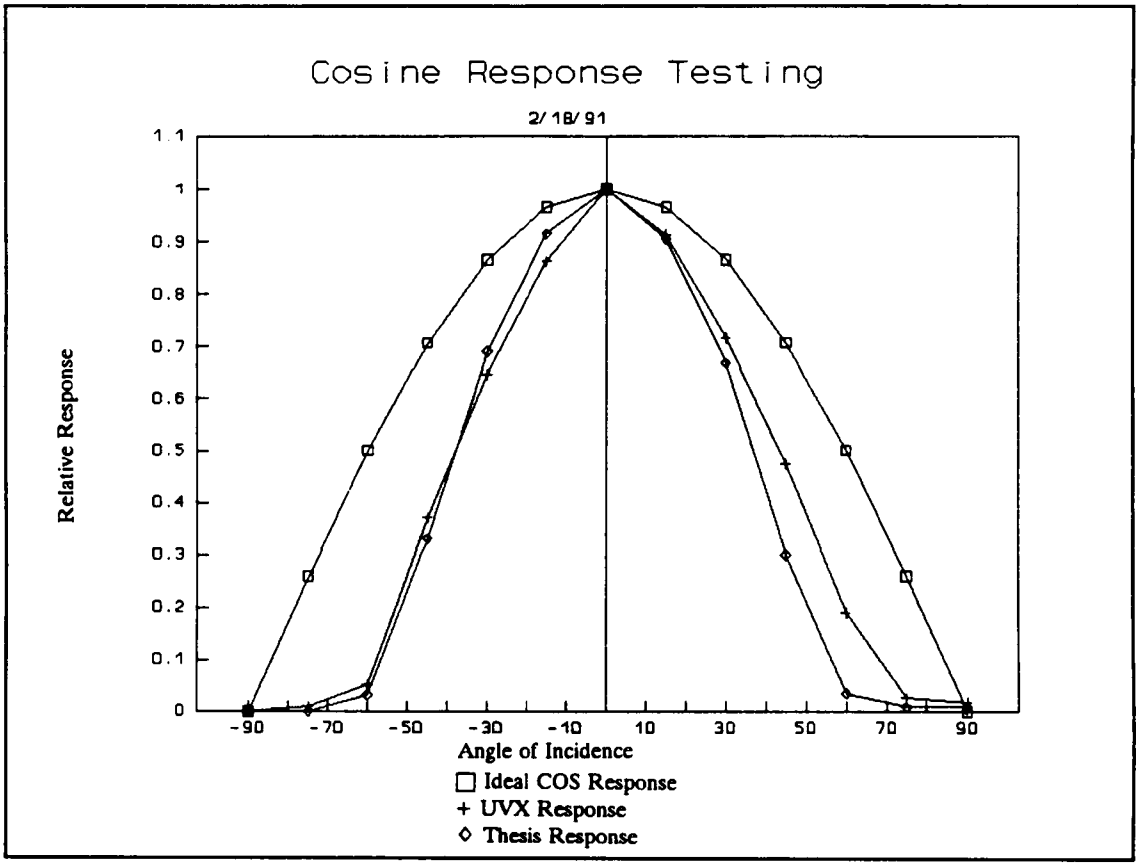

Figure 6.8. Cosine Response of Sensors.

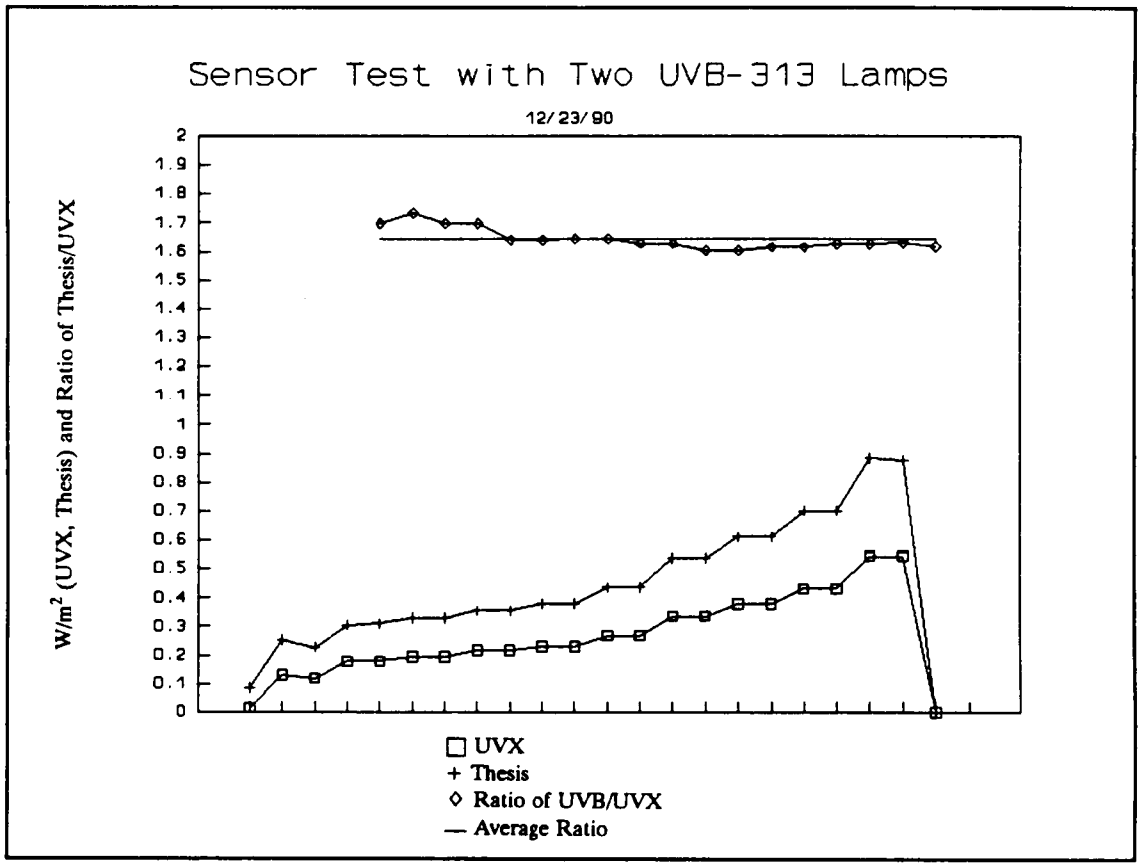

Figure 6.9. Initial Comparison Testing with UVB-313 Lamps.

creating two pinholes of different diameters through the shield material. This ensured that the total amount of light area irradiating from the pinholes would be smaller than each of the sensing areas when each sensor was positioned near each pinhole. Figure 6.10 is a diagram of the setup for the pinhole testing, showing the position and distance of each sensor from the pinhole source. The distance from the sensor lamp platform and the lamp were fixed. Throughout all testing, the UVX sensor had a spacer glued to its bottom side so that the top surface was even with the thesis UV-B sensor when positioned on a flat surface. Because the UVX sensor is recessed in it case ~0.08 in., this distance must be taken into consideration when comparing the two readings because both sensors must be positioned close to the pinhole source to ensure that all light is seen by each photosensing element. For field measurements when the lamps are positioned many feet above the sensors, this distance is insignificant and can be ignored. The magnitude of irradiance from a point source follows the inverse square law as given by

$$E = \frac{I}{d^2} . \tag{6.2}$$

Tests were made with both sensors on the two pinhole sources. The differences in distance from the sensors to the point source were factored into the UV-B irradiance measurements and are shown in Table 6.1.

The percentage difference between the two radiometer measurements is now much better and probably would be lower if a laboratory test were performed with the proper optical equipment. According to the ORNL Environmental Sciences Division, where measurements of the lamps with the UVX radiometer were compared to measurements of an ORIEL spectral radiometer in September 1990, the spectral radiometer UV-B

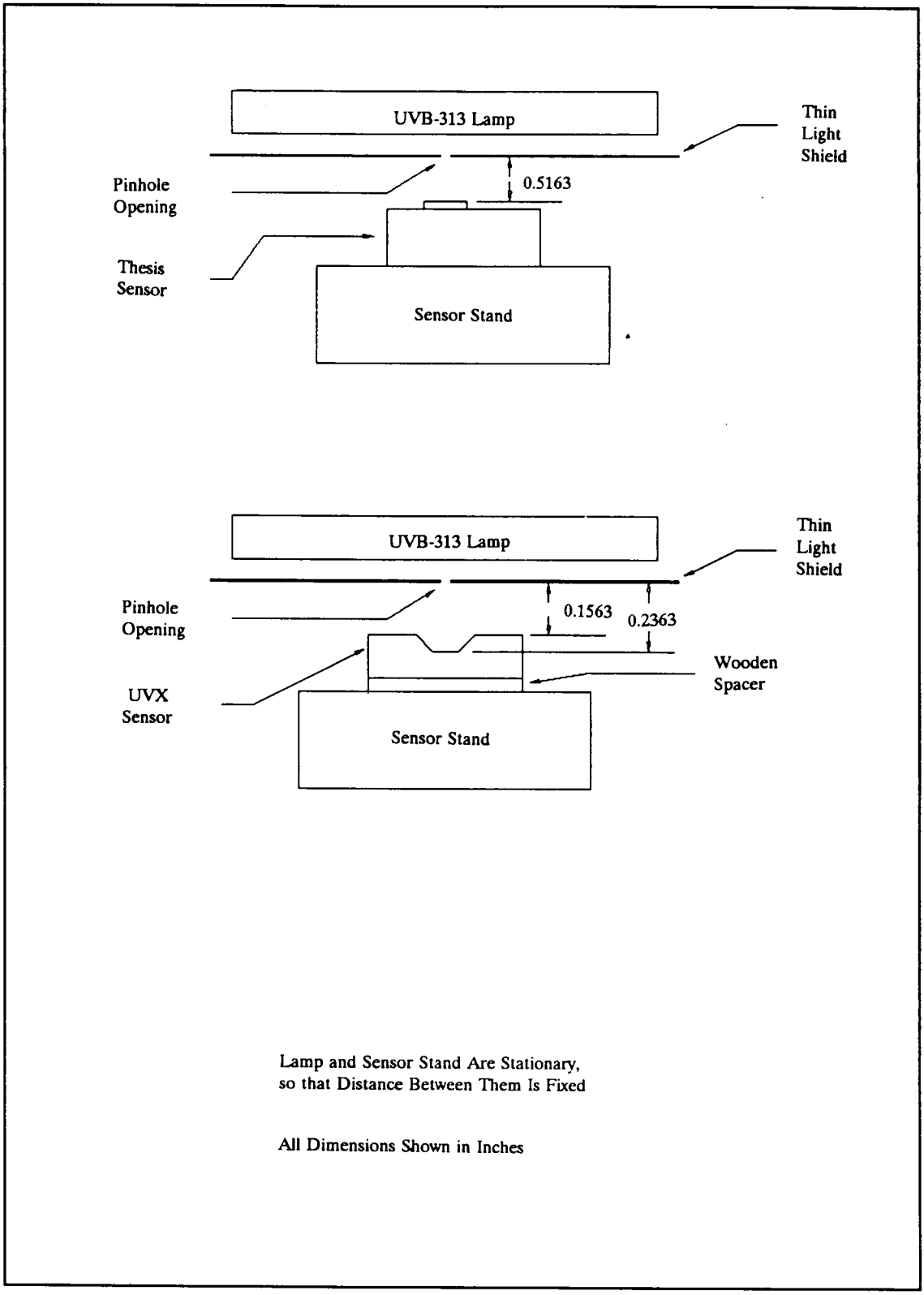

Figure 6.10. Pinhole Testing Configuration.

Table 6.1. Pinhole Test Data on UV-B Sensors

Pinhole Test No.	UVX UV-B (W/m^2)	Thesis UV-B (W/m^2)	Difference (%)
1 (small hole)	0.208	0.239	13.0
2 (smaller hole)	0.163	0.193	15.5

measurements were more than 100% greater than the integrated amount seen by the UVX sensor. Thus, the author believes it is a valid assumption that both sensors are measuring the irradiance correctly; however, the thesis radiometer has a wider field of view. The ultimate use of this radiometer would be for measuring the total UV-B exposure from sunlight, skylight, and extended UV-B lamps; therefore, a wide field of view is more desirable.

Field measurements comparing the two sensors under the lamp bank assemblies at the outdoor UV-B facility at ORNL were made at night. This lamp bank assembly is composed of a 4-ft^2 frame containing eight 4-ft UVB-313 lamps positioned ~6 in. on centers, producing a planar lamp source. The measurements were made with the sensors lying side by side under the UV-B planar lamp source. Two tests were made at two different lamp distances from the sensors. For the first test, the lamp plane was positioned ~68 in. from the sensors. The lamp intensity controller was adjusted from 100 to 40% output in 30% increments. At each of the three controller settings, the output was held constant for 15 min. During each of these 15-min periods, the DAS at the UV-B facility was used to store the sensors' output data at 1-min intervals. Figure 6.11 shows the data taken during the first test, in which the three changes in controller outputs are evident. The ratio of the output of the thesis UV-B sensor to the output of the UVX sensor and the average value of 1.65 is also shown, emphasizing the larger field of view of the thesis sensor.

Figure 6.12 contains data taken from the second test, in which the lamp plane assembly was lowered so that the distance between the sensors and the lamp plane assembly was 41 in. The higher irradiance due to the reduced distance between the sensors and the lights is evident, as are the three controller settings. Fluctuations in the

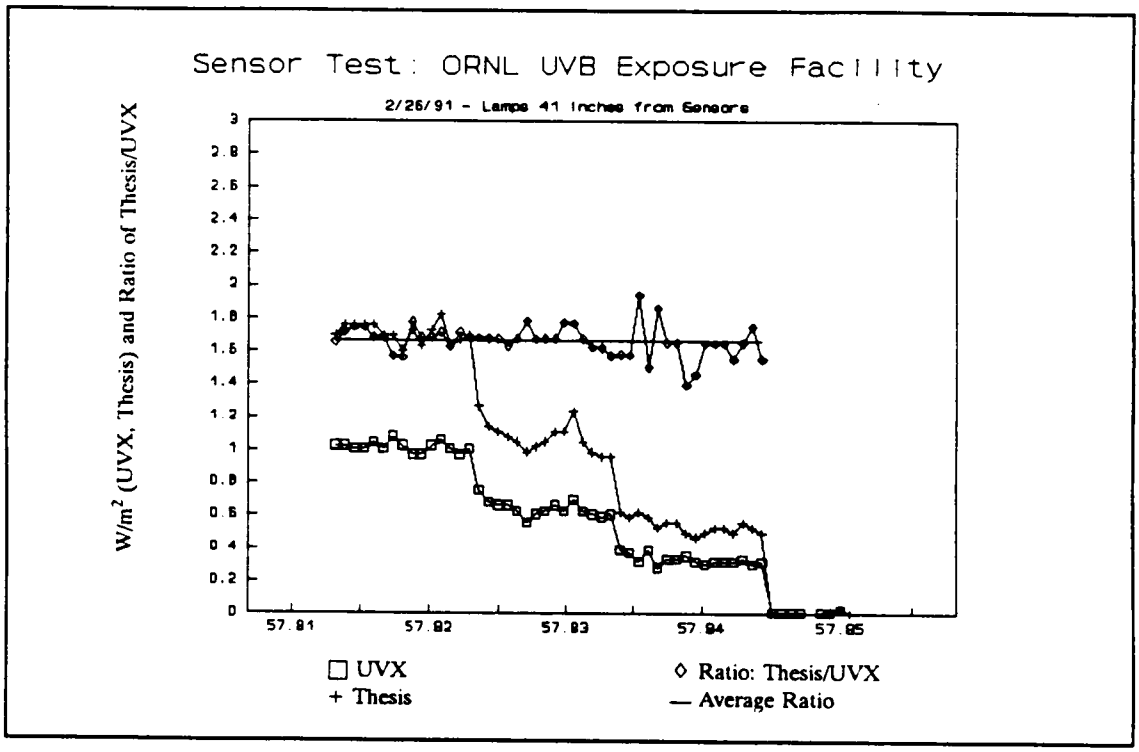

Figure 6.11. Sensor Testing at Lamp Distance of 41 Inches.

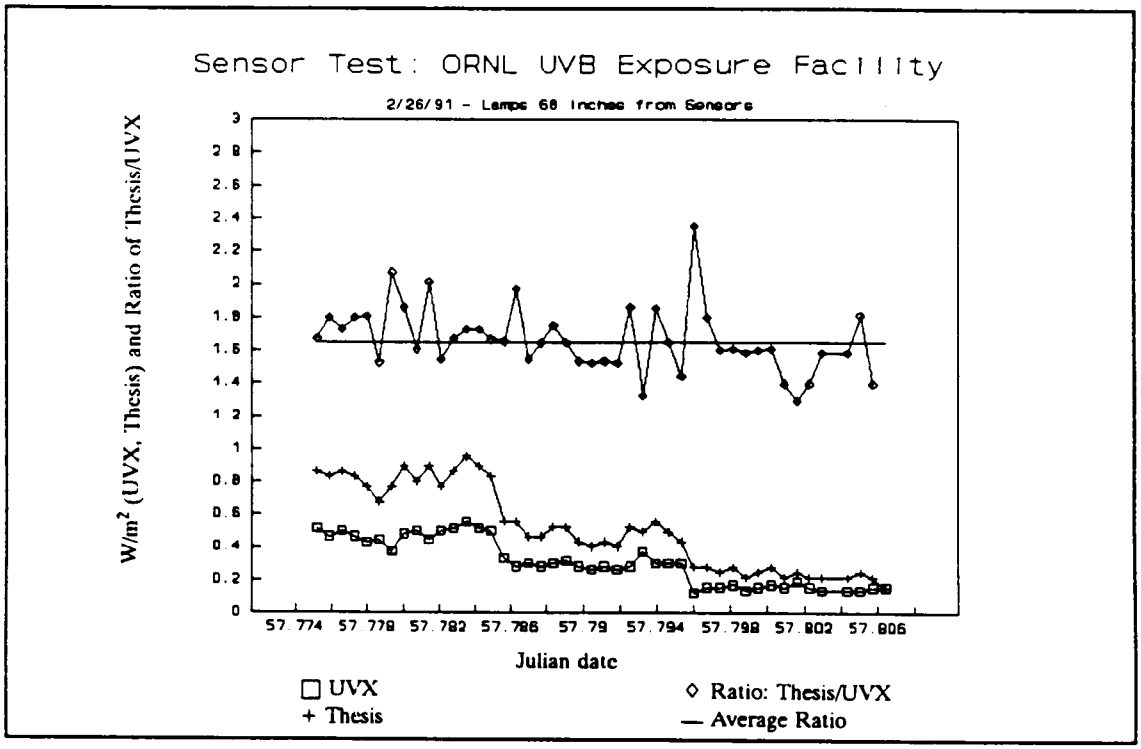

Figure 6.12. Sensor Testing at Lamp Distance of 68 Inches.

irradiance are due primarily to fluctuations in bulb temperatures caused by changes in wind currents. Sensor output ratios and their average of 1.66 are also shown in Figure 6.12.

Field measurements comparing the two sensors when exposed to ambient sun and skylight are shown in Figure 6.13. These data were taken from sunrise to sunset on February 27, 1991, which was a fairly clear day with few clouds. The sensors were positioned side by side on a flat horizontal surface. The ratio of thesis to UVX sensor output for this test and the average ratio of 1.62 are shown in Figure 6.14. Field measurements comparing the two sensors' outputs when exposed to ambient sun and skylight on a partly cloudy day are shown in Figure 6.15. These data were taken from sunrise to sunset on February 28, 1991. For this measurement, the sensors were positioned on a solar tracking platform so that their surfaces were constantly normal to the direct sunlight. Cloud passage over the sensors is evident by sharp reductions in UV-B irradiance. Figure 6.16 is a plot of ratio of thesis to UVX sensor output for this test and the average ratio of 1.67.

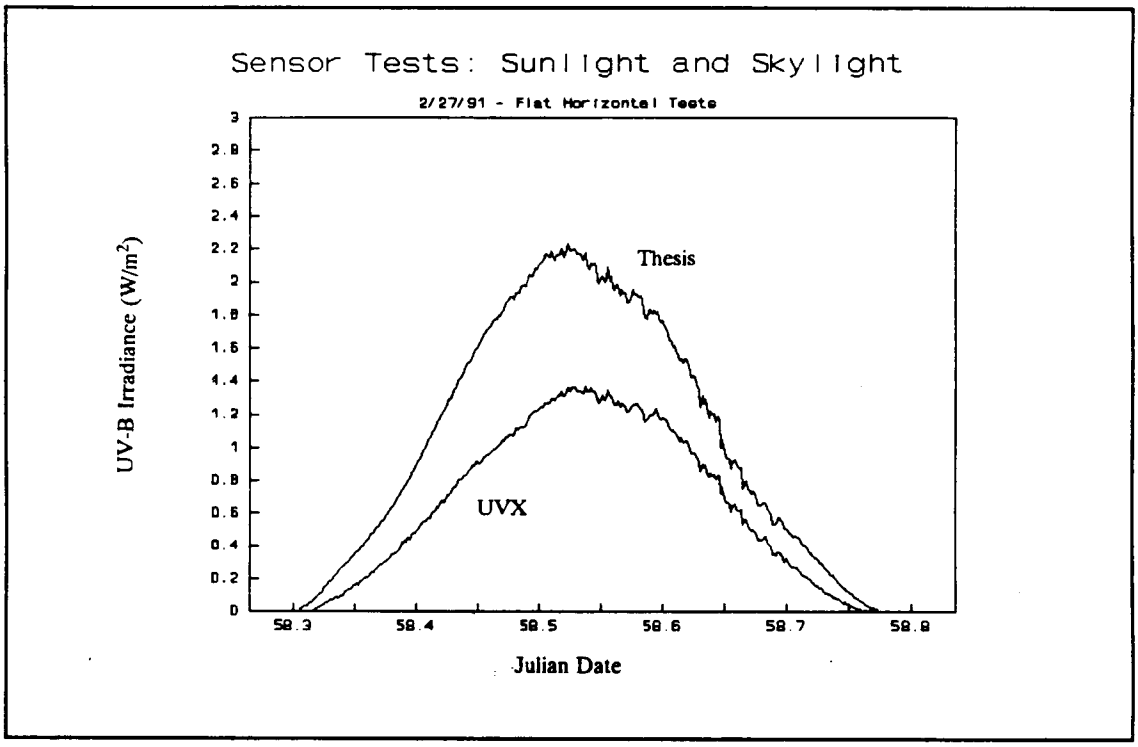

Figure 6.13. Sunlight Testing on Horizontal Surface.

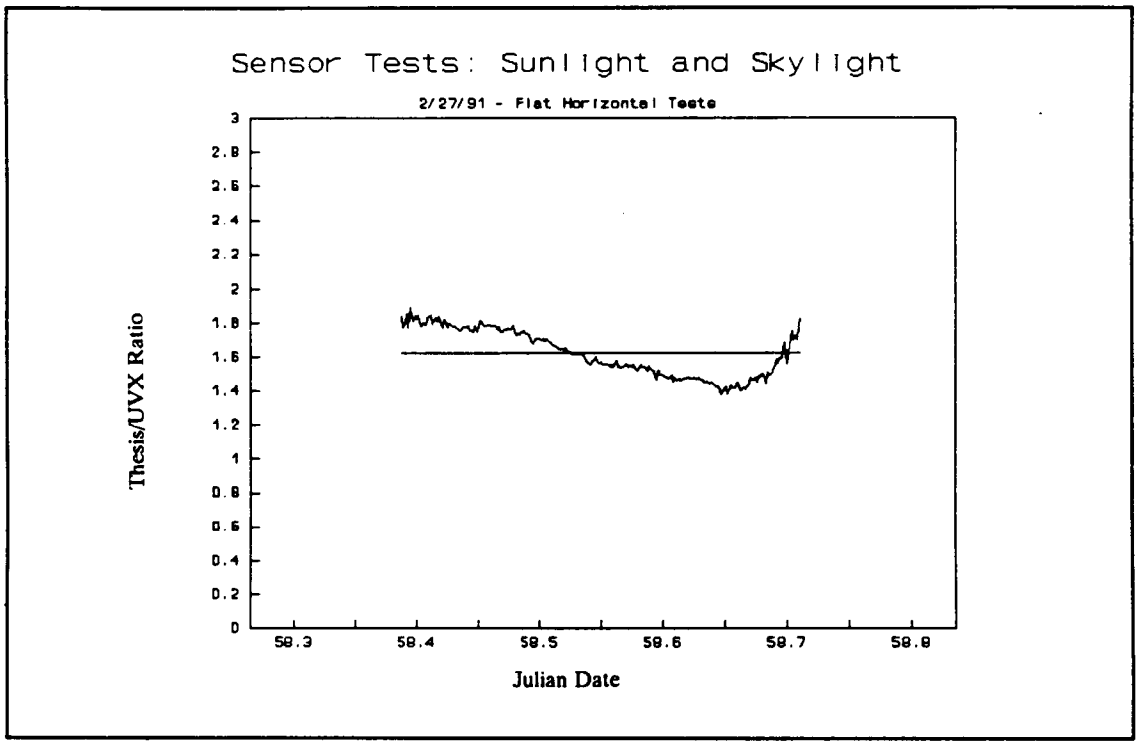

Figure 6.14. Ratio of Sensors in Sunlight - Horizontal.

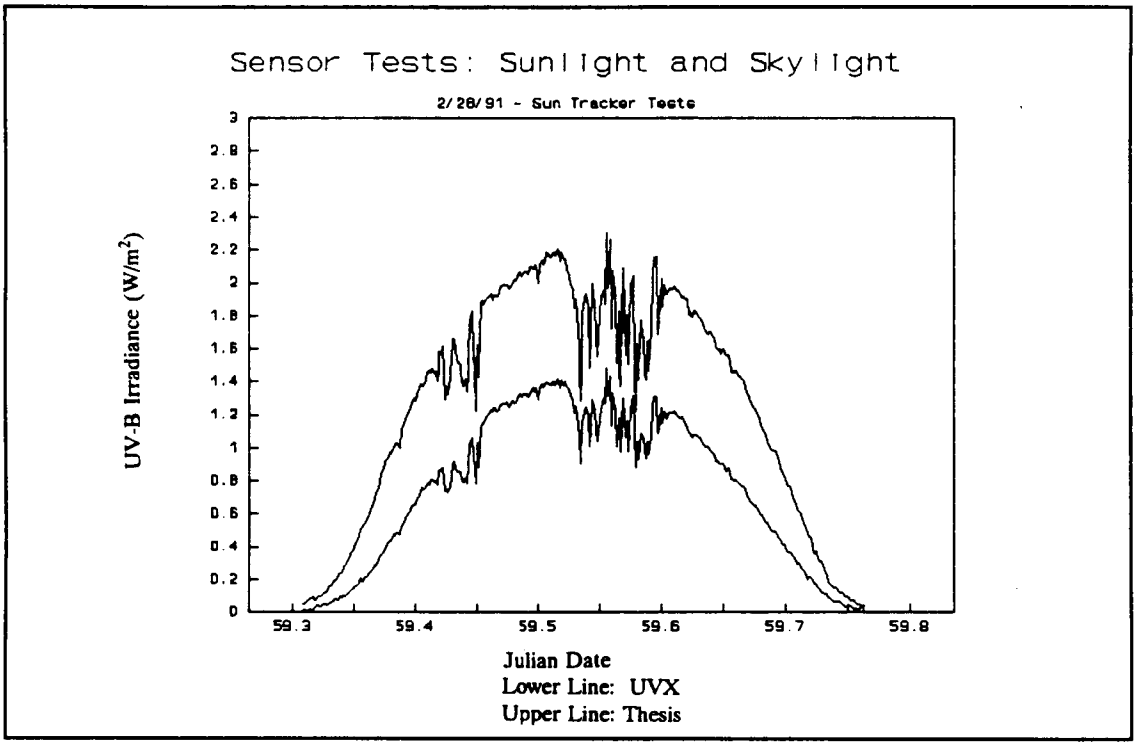

Figure 6.15. Sunlight Testing - Sun Tracker.

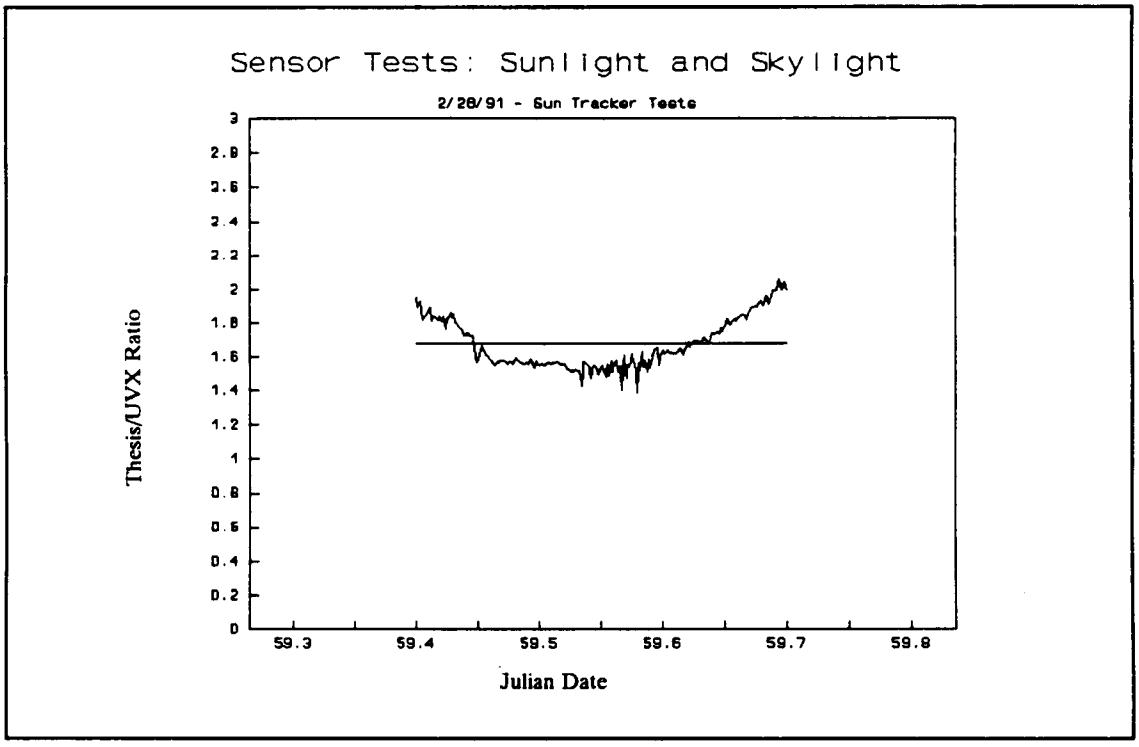

Figure 6.16. Ratio of Sensors - Sun Tracker.

7. SUMMARY AND CONCLUSIONS

The goal of this thesis was to design, build, and test a field-usable UV-B radiometer to measure UV-B irradiances of 280 to 320 nm in solar sunlight and under an artificial UV-B lamp source. The results of the tests demonstrate that this goal was achieved.

Further improvements to the design of the radiometer could be made by implementing the special temperature-compensating resistor to minimize circuit drift. Environmental testing of the circuit could then be performed by using a stable source of UV-B light that possibly could be brought into a chamber via a fiber optic cable, thereby permitting drift measurements at higher light current levels.

A spherical diffuser over the filter and the photodiode could improve the sensor by improving the acceptance angle of the radiometer to give it an even larger field of view. The diffuser would result in some loss of signal, but it would greatly reduce the sensitivity of alignment of the source with the sensor (ORIEL, 1989) by reducing the effect of angle change on beam strength. The decrease in signal strength would require the circuit gain to be increased.

The filter optics could be improved by using a narrower band filter to allow a greater percentage of the radiometer's sensitivity to be in only the UV-B region.

It should be noted that the UV-B sensors will be used for measuring ambient UV-B light and for controlling the UV-B light from the UVB-313 lamps. Periodic quantitative absolute measurements of the spectral irradiance of the lamps and ambient sunlight will be made by using an ORIEL spectral radiometer at the UV-B Exposure Facility.

LIST OF REFERENCES

AND

BIBLIOGRAPHY

LIST OF REFERENCES

Analog Devices, Inc., 1988, *AD707 Ultralow-Drift Op-Amp Data Sheet*, Norwood, Massachusetts.

Analog Devices, Inc., 1990, *Linear Products Databook*, Norwood, Massachusetts.

Brennan, P., 1989, *Facsimile Message Containing Spectral Power Distribution Data for Q-Panel Company UVB-313 Lamp and for Summer Sunlight*, Q-Panel Company, Cleveland, Ohio.

Hamamatsu Corporation, 1988, *Catalog: Photodiodes*, Bridgewater, New Jersey.

Illuminating Engineering Society of America, 1981, *IES Light. Handb.*, Waverly Press, Baltimore.

Kennedy, E. J., 1988, *Operational Amplifier Circuits: Theory and Applications*, Holt, Rinehart, and Winston, New York.

ORIEL Corporation, 1989, *Light Sources, Monochromators, and Detection Systems*, Vol. II, Stratford, Connecticut.

Schott, 1984, *Catalog: Optical Glass Filters*, Schott Glass Technologies, Inc., Duryea, Pennsylvania.

Solar Energy Research Institute, 1990, *FORTRAN Program: Spectral 2 Model*, Denver, Colorado.

Ultraviolet Products, Inc., 1990a, "Guide to Optical Radiation Measurements," Application Note AN-1167, San Gabriel, California.

Ultraviolet Products, Inc., 1990b, *UVX Radiometer Manual*, San Gabriel, California.

Wait, J. V., L. P. Huelsman and G. A. Korn, 1975, *Introduction to Operational Amplifier Theory and Applications*, McGraw-Hill, New York.

Wilson, A. D., and H. Lyall, 1986a, "Design of an Ultraviolet Radiometer. 1: Detector Electrical Characteristics," *Appl. Opt.* 25(24), 4530–39.

Wilson, A. D., and H. Lyall, 1986b, "Design of an Ultraviolet Radiometer. 2: Detector Optical Characteristics," *Appl. Opt.* 25(24), 4540–46.

Wintenberg, A. L., 1989, *Development of a Measurement System Optimized for Detecting Prebreakdown Currents in Liquid Dielectrics*, PhD dissertation, The University of Tennessee, Knoxville.

BIBLIOGRAPHY

CRC Press, Inc., 1989, *70th Edition of CRC Handbook of Chemistry and Physics*, CRC Press, Boca Raton, Florida.

Green, A. E. S., 1989, *Stratospheric Ozone Depletion Seminar*, Oak Ridge National Laboratory, Oak Ridge, Tennessee (March).

Hewlett Packard, 1977, *Optoelectronics Applications Manual*, McGraw-Hill, New York.

Mims III, F. M., 1990, "The Amateur Scientist: How to Monitor Ultraviolet Radiation from the Sun," *Sci. Am.*, pp. 106–9 (August).

National Academy of Sciences, 1982, *Causes and Effects of Stratospheric Ozone Reduction: An Update*, National Academy Press, Washington, D.C.

Smith, W. J., 1990, *Modern Optical Engineering, The Design of Optical Systems*, 2d Ed., McGraw-Hill, New York.

Vishay Intertechnology, Inc., 1990, *Catalog VW1000A: Elliott Jordan–Precision Wirewound Resistors*, Malvern, Pennsylvania.

APPENDIX

MATHCAD PROGRAMS

MathCad Program ZFBGAIN0

This MathCad program uses solar spectral irradiance data obtained from the SERI solar irradiance FORTRAN Model SPECTRL2 to calculate the maximum value of the feedback resistor "R" for the UV-B optical detector transimpedance amplifier, assuming the maximum input to the transconductance amplifier to be 60 mV. R is then recalculated for an additional photocurrent increase of 50% above ambient. This increase would represent the maximum percentage above ambient controller setpoint at which the UV-B facility would ever likely operate. See the MathCad program ENGRUNIT for definitions of engineering units used in this program.

Variable Definitions:

λ = Light wavelength in nanometers.

Diode = Radiant sensitivity calibration data of the G1127-02 diode in units of amperes/watts/square meter.

UG = Transmittance of the Schott UG 11 optical bandpass filter (unit less ratio of the transmitted spectral radiant flux to the incident radiation flux).

S = Solar spectral irradiance data obtain from the SERI solar irradiance FORTRAN Model SPECTRL2.

Out = vector containing products of the diode radiant sensitivity, bandpass filter transmittance, and solar spectral power in units of amperes/nanometer.

PhotoI = the integral of "Out," calculated by using the trapezoidal rule, which contains the total photocurrent produced by the diode in units of amperes.

R = Maximum value for the feedback resistor in the UV-B optical detector transimpedance amplifier.

$\lambda := 200 \cdot nm, 210 \cdot nm \ldots 400 \cdot nm$ Range of λ that assures no more contribution to the photocurrent.

λ / nm	Diode
200	.588
210	.525
220	.483
230	.441
240	.441
250	.546
260	.636
270	.672
280	.777
290	.903
300	.987
310	1.071
320	1.134
330	1.197
340	1.302
350	1.323
360	1.197
370	1.302
380	1.428
390	1.638
400	1.827

Diode := $\begin{bmatrix} .588 \\ .525 \\ .483 \\ .441 \\ .441 \\ .546 \\ .636 \\ .672 \\ .777 \\ .903 \\ .987 \\ 1.071 \\ 1.134 \\ 1.197 \\ 1.302 \\ 1.323 \\ 1.197 \\ 1.302 \\ 1.428 \\ 1.638 \\ 1.827 \end{bmatrix} \cdot 10^{-6} \cdot \begin{bmatrix} \frac{amp}{watt} \\ \frac{}{2} \\ m \end{bmatrix}$

λ / nm	S	UG
200	0	0
210	0	0
220	0	0
230	0	0
240	0	.00009
250	0	.03
260	0	.23
270	0	.46
280	0	.64
290	0	.73
300	.0120223	.78
310	.1533886	.81
320	.3426000	.83
330	.5949277	.84
340	.6056044	.83
350	.6901587	.82
360	.7171115	.77
370	.8493336	.66
380	.8608554	.40
390	.8264664	.08
400	1.2086804	.002

S := $\begin{bmatrix} 0 \\ 0 \\ 0 \\ 0 \\ 0 \\ 0 \\ 0 \\ 0 \\ 0 \\ 0 \\ .0120223 \\ .1533886 \\ .3426000 \\ .5949277 \\ .6056044 \\ .6901587 \\ .7171115 \\ .8493336 \\ .8608554 \\ .8264664 \\ 1.2086804 \end{bmatrix} \cdot \frac{watt}{2 \cdot nm}$ UG := $\begin{bmatrix} 0 \\ 0 \\ 0 \\ 0 \\ .00009 \\ .03 \\ .23 \\ .46 \\ .64 \\ .73 \\ .78 \\ .81 \\ .83 \\ .84 \\ .83 \\ .82 \\ .77 \\ .66 \\ .40 \\ .08 \\ .002 \end{bmatrix}$

$$Out_{\frac{\lambda-200\cdot nm}{10\cdot nm}} := Diode_{\frac{\lambda-200\cdot nm}{10\cdot nm}} \cdot UG_{\frac{\lambda-200\cdot nm}{10\cdot nm}} \cdot S_{\frac{\lambda-200\cdot nm}{10\cdot nm}}$$

$\lambda := 200\cdot nm, 210\cdot nm \,..\, 390\cdot nm$

Reset range for λ so subscript in equation below is not out of range.

$$PhotoI := \left[\sum_{\lambda} \frac{Out_{\frac{\lambda-200\cdot nm}{10\cdot nm}} + Out_{\frac{\lambda-200\cdot nm}{10\cdot nm}+1}}{2} \right] \cdot 10\cdot nm$$

$PhotoI = 4.459\cdot 10^{-5}\cdot amp$

$$R := 60\cdot \frac{mvolt}{PhotoI}$$

$R = 1.346\cdot 10^{3}\cdot ohm$

$PhotoI := 1.50\cdot PhotoI$

Allow for additional photocurrent from facility operating at 50% above ambient UV-B.

$$R := 60\cdot \frac{mvolt}{PhotoI}$$

Calculate the maximum value for the feedback resistor R.

$R = 897\cdot ohm$

MathCad Program ZFBGAIN1

This MathCad program uses solar spectral irradiance data from the Q-Panel Company to calculate the maximum value of the feedback resistor "R" for the UV-B optical detector transimpedance amplifier, assuming the maximum input to the transconductance amplifier to be 60 mV. R is then recalculated for an additional photocurrent increase of 50% above ambient. This increase would represent the maximum percentage above ambient controller setpoint at which the UV-B facility would ever likely operate. See the MathCad program ENGRUNIT for definitions of engineering units used in this program.

Variable Definitions:

λ = Light wavelength in nanometers.

Diode = Radiant sensitivity calibration data of the G1127-02 Diode in units of (amp/watt/square-meter).

UG = Transmittance of the Schott UG 11 optical bandpass filter (unit less ratio of the transmitted spectral radiant flux to the incident radiation flux).

S = Solar spectral power distribution data obtained from actual summer sunlight data taken in Cleveland, Ohio, by the Q-Panel Company in units of watts/square meters/nanometers.

Out = Vector containing products of the diode radiant sensitivity, bandpass filter transmittance, and the solar spectral power in units of amperes/nanometer.

PhotoI = The integral of "Out," calculated by using the trapezoidal rule, which contains the total photocurrent produced by the diode in units of amperes.

R" = Maximum value for the feedback resistor in the UV-B optical detector transimpedance amplifier.

$\lambda := 200 \cdot nm, 210 \cdot nm \ldots 400 \cdot nm$ Range of λ that assures no more contribution to the photocurrent.

λ / nm
200
210
220
230
240
250
260
270
280
290
300
310
320
330
340
350
360
370
380
390
400

$$Diode := \begin{bmatrix} .588 \\ .525 \\ .483 \\ .441 \\ .441 \\ .546 \\ .636 \\ .672 \\ .777 \\ .903 \\ .987 \\ 1.071 \\ 1.134 \\ 1.197 \\ 1.302 \\ 1.323 \\ 1.197 \\ 1.302 \\ 1.428 \\ 1.638 \\ 1.827 \end{bmatrix} \cdot 10^{-6} \cdot \left[\frac{amp}{\frac{watt}{m^2}} \right]$$

λ / nm
200
210
220
230
240
250
260
270
280
290
300
310
320
330
340
350
360
370
380
390
400

$$UG := \begin{bmatrix} 0 \\ 0 \\ 0 \\ 0 \\ .00009 \\ .03 \\ .23 \\ .46 \\ .64 \\ .73 \\ .78 \\ .81 \\ .83 \\ .84 \\ .83 \\ .82 \\ .77 \\ .66 \\ .40 \\ .08 \\ .002 \end{bmatrix} \qquad S := \begin{bmatrix} 0.0 \\ 0.0 \\ 0.0 \\ 0.0 \\ 0.0 \\ 0.0 \\ 0.0 \\ 0.0 \\ 0.0 \\ 0.0 \\ .0076 \\ .1276 \\ .3827 \\ .6871 \\ .6973 \\ .7592 \\ .8152 \\ .8682 \\ .9195 \\ 3 \\ 1.200 \end{bmatrix} \cdot \left[\frac{watt}{m^2 \cdot nm} \right]$$

$$Out_{\frac{\lambda-200\cdot nm}{10\cdot nm}} := Diode_{\frac{\lambda-200\cdot nm}{10\cdot nm}} \cdot UG_{\frac{\lambda-200\cdot nm}{10\cdot nm}} \cdot S_{\frac{\lambda-200\cdot nm}{10\cdot nm}}$$

$\lambda := 200\cdot nm, 210\cdot nm \,..\, 390\cdot nm$ Reset range for λ so subscript in equation below is not out of range.

$$PhotoI := \left[\sum_{\lambda} \frac{Out_{\frac{\lambda-200\cdot nm}{10\cdot nm}} + Out_{\frac{\lambda-200\cdot nm}{10\cdot nm}+1}}{2} \right] \cdot 10\cdot nm$$

$$PhotoI = 5.163\cdot 10^{-5}\cdot amp$$

$$R := 60\cdot \frac{mvolt}{PhotoI}$$

$$R = 1.162\cdot 10^{3}\cdot ohm$$

$PhotoI := 1.50\cdot PhotoI$ Allow for additional photocurrent from facility operating at 50% above ambient UV-B.

$$R := 60\cdot \frac{mvolt}{PhotoI}$$ Calculate the maximum value for the feedback resistor R.

$$R = 774.8\cdot ohm$$

MathCad Program TAPPROX

This MathCad program calculates the approximate loop transmission of the transimpedance amplifier as defined in Eq. (3.11). The variables used in this program correspond to the labeling associated with Figure 3.1. The output of this program is the tabulated values of loop gain (dB) and phase margin (degrees), which were used to create Figures 3.2 and 3.3 respectively. See MathCad program ENGRUNIT for definitions of engineering units used in this program.

Variables defined in Figure 3.1:

$R_f := 750 \cdot ohm$

$C_d := 7000 \cdot pF$ $C_f := 7010 \cdot pF$

Variables used to generate frequency range:

$min := 1 \cdot 10^{-2}$ Minimum frequency in Hz.

$max := 1 \cdot 10^{7}$ Maximum frequency in Hz.

$r := \ln\left[\frac{max}{min}\right]$ Log ratio of maximum and minimum frequencies. This will be used to generate equally spaced values on the logarithmic plot.

$n := 40$ Number of calculation points.

$i := 0 \,..\, n$ Range variable.

$s_i := min \cdot e^{i \cdot \frac{r}{n}} \cdot j \cdot hz$ S plane variable equally spaced over frequency range of calculations.

Transimpedance amplifier variables:

$\omega_0 := .1 \cdot hz$ — Dominant pole location of AD707 open-loop response.

$\omega_1 := 8 \cdot 10^6 \cdot hz$ — Second pole location of AD707 open-loop response.

$A_o := 13 \cdot 10^6$ — AD707 open-loop dc gain

Transimpedance amplifier model variables:

$$A(s) := \frac{A_o}{\left[1 + \frac{s}{\omega_0}\right] \cdot \left[1 + \frac{s}{\omega_1}\right]}$$

AD707 open-loop transfer function.

$C_{in} := C_d$ — Total input capacitance is equal to (C.d + C.op), but C.d >> C.op, therefore C.in is approximately equal to C.d.

$C_{if} := C_d + C_f$ — Parallel combination of C_d with C_f. From Eq. (3.4).

Transimpedance amplifier loop expression from Eq. (3.11).

$$T(s) := -A(s) \cdot \left[\frac{1 + s \cdot R_f \cdot C_f}{1 + s \cdot R_f \cdot C_{if}}\right]$$

$T_{db}(s) := 20 \cdot \log(|T(s)|)$ — Transimpedance amplifier loop gain in dB.

$T_{Phase}(s) := \arg(-T(s))$ — Transimpedance amplifier phase in degrees.

Tabular data of loop transmission calculations using Eq. (3.13).

Frequency (Hz) $\frac{s}{i}$ $j \cdot hz$	Magnitude (dB) $T_{db}\left[\begin{smallmatrix}s\\i\end{smallmatrix}\right]$	Phase (degrees) $T_{Phase}\left[\begin{smallmatrix}s\\i\end{smallmatrix}\right]$ deg
0.01	142.236	-5.711
0.0168	142.158	-9.53
0.0282	141.947	-15.74
0.0473	141.402	-25.321
0.0794	140.154	-38.461
0.1334	137.841	-53.134
0.2239	134.489	-65.931
0.3758	130.482	-75.101
0.631	126.171	-80.995
1.0593	121.74	-84.609
1.7783	117.265	-86.785
2.9854	112.774	-88.087
5.0119	108.277	-88.866
8.414	103.778	-89.335
14.1254	99.279	-89.621
23.7137	94.779	-89.803
39.8107	90.279	-89.932
66.8344	85.779	-90.041
112.2018	81.279	-90.162
188.3649	76.778	-90.327
316.2278	72.277	-90.582
530.8844	67.775	-90.996
891.2509	63.268	-91.681
1496.2357	58.747	-92.819
2511.8864	54.191	-94.688
4216.965	49.538	-97.656
7079.4578	44.652	-101.938
11885.0223	39.318	-106.769
19952.6231	33.476	-109.55
33496.5439	27.549	-108.013
56234.1325	22.065	-103.622
94406.0876	17.079	-99.34
158489.3192	12.379	-96.489
266072.506	7.801	-95.138
446683.5922	3.266	-95.131
749894.2093	-1.268	-96.51
1258925.4118	-5.84	-99.631
2113489.0398	-10.528	-105.209
3548133.8923	-15.515	-114.162
5956621.4353	-21.151	-126.816
10000000	-27.822	-141.427

MathCad Program TACTUAL

This MathCad program calculates the actual loop transmission of the transimpedance amplifier as defined in Eq. (3.10). The variables used in this program correspond to the labeling associated with Figure 3.1. The output of this program is the tabulated values of loop gain (dB) and Phase Margin (degrees), which were used to create Figures 3.2 and 3.3. See the MathCad program ENGRUNIT for definitons of engineering units used in this program.

Variables defined in Figure 3.1:

$R_d := 1 \cdot 10^{9} \cdot ohm$ $r_o := 60 \cdot ohm$ $R_l := 2.151 \cdot 10^{3} \cdot ohm$

$R_f := 750 \cdot ohm$ $R_{op} := 60 \cdot 10^{6} \cdot ohm$

$C_d := 7000 \cdot pF$ $C_l := 47 \cdot \mu F$ $C_f := 7010 \cdot pF$

Variables used to generate frequency range:

$min := 1 \cdot 10^{-2}$ Minimum frequency in Hz.

$max := 1 \cdot 10^{7}$ Maximum frequency in Hz.

$r := \ln\left[\frac{max}{min}\right]$ Log ratio of maximum and minimum frequencies. This will be used to generate equally spaced values on the logarithmic plot.

$n := 40$ Number of calculation points.

$i := 0 \,..\, n$ Range variable.

$s_i := min \cdot e^{i \cdot \frac{r}{n}} \cdot j \cdot hz$ S plane variable equally spaced over frequency range of calculations.

Transimpedance amplifier variables:

$\omega_0 := .1 \cdot hz$ Dominant pole location of AD707 open-loop response.

$\omega_1 := 8 \cdot 10^6 \cdot hz$ Second pole location of AD707 open-loop response.

$A_o := 13 \cdot 10^6$ AD707 open-loop dc gain

Transimpedance amplifier model variables:

$$A(s) := \frac{A_o}{\left[1 + \frac{s}{\omega_0}\right] \cdot \left[1 + \frac{s}{\omega_1}\right]}$$

AD707 open-loop transfer function.

$$Z_f(s) := \frac{R_f}{1 + s \cdot R_f \cdot C_f}$$

Feedback impedance or parallel combination of R.f with (1/sC.f).

$$Z_{in}(s) := \frac{\frac{R_{op} \cdot R_d}{R_{op} + R_d}}{1 + s \cdot \frac{R_{op} \cdot R_d}{R_{op} + R_d} \cdot C_d}$$

Input impedance or parallel combination of R.op, R.d, and (1/sC.d).

$$Z_l(s) := R_l + \frac{1}{s \cdot C_l}$$

Output load impedance or R.1 in series with (1/sC.1).

$$Z(s) := \frac{Z_{in}(s)}{Z_{in}(s) + Z_f(s)}$$

Portion of test voltage arriving at the inverting terminal of the op-amp due to the voltage division between Z.in and Z.f.

$$Z_{out}(s) := \frac{Z_l(s) \cdot \left[Z_f(s) + Z_{in}(s)\right]}{Z_l(s) + \left[Z_f(s) + Z_{in}(s)\right]}$$

Parallel combination of Z.1 with (Z.f + Z.in).

Transimpedance Amplifier loop expression:

$$T(s) := -\left[A(s) \cdot Z(s) \cdot \left[\frac{Z_{out}(s)}{r_o + Z_{out}(s)}\right]\right]$$

$T_{db}(s) := 20 \cdot \log(|T(s)|)$

Transimpedance amplifier loop gain in dB.

$T_{Phase}(s) := \arg(-T(s))$

Transimpedance amplifier phase in degrees.

Tabular data of loop transmission calculations using Eq. (3.10).

Frequency (Hz) $\frac{s}{i}$ $j \cdot hz$	Magnitude (dB) $T_{db}\left[\frac{s}{i}\right]$	Phase (degrees) $T_{Phase}\left[\frac{s}{i}\right]$ deg
0.01	142.236	-5.721
0.0168	142.158	-9.547
0.0282	141.947	-15.769
0.0473	141.401	-25.369
0.0794	140.154	-38.542
0.1334	137.839	-53.269
0.2239	134.484	-66.154
0.3758	130.468	-75.462
0.631	126.137	-81.545
1.0593	121.664	-85.343
1.7783	117.129	-87.566
2.9854	112.586	-88.733
5.0119	108.059	-89.313
8.414	103.547	-89.618
14.1254	99.042	-89.794
23.7137	94.541	-89.91
39.8107	90.04	-89.999
66.8344	85.54	-90.087
112.2018	81.04	-90.2
188.3649	76.539	-90.368
316.2278	72.038	-90.636
530.8844	67.536	-91.078
891.2509	63.028	-91.815
1496.2357	58.507	-93.039
2511.8864	53.947	-95.054
4216.965	49.286	-98.253
7079.4578	44.382	-102.883
11885.0223	39.012	-108.173
19952.6231	33.125	-111.529
33496.5439	27.161	-110.848
56234.1325	21.645	-107.954
94406.0876	16.612	-106.295
158489.3192	11.801	-107.885
266072.506	6.93	-113.729
446683.5922	1.662	-124.533
749894.2093	-4.447	-139.9
1258925.4118	-11.708	-157.409
2113489.0398	-20.015	-174.629
3548133.8923	-29.142	168.445
5956621.4353	-39.142	150.773
10000000	-50.264	133.111

MathCad Program NOISE

This MathCad program calculates the contribution from each noise source to the total output noise power of the radiometer. See MathCad program ENGRUNIT for definitions of engineering units used in this program.

Variables defined in Figure 3.1

$R_d := 1 \cdot 10^{9} \cdot ohm$ $R_1 := 2151 \cdot ohm$ $R_f := 750 \cdot ohm$

$R_1 := 750 \cdot ohm$ $R_{op} := 60 \cdot 10^{6} \cdot ohm$ $R_{out} := 250 \cdot ohm$

$C_f := 7010 \cdot pF$ $C_{in} := 7000 \cdot pF$ $C_1 := 47 \cdot \mu F$

$R_2 := 2151 \cdot ohm$ $R_{in} := \frac{R_d \cdot R_{op}}{R_d + R_{op}}$ $r_o := 60 \cdot ohm$

$k := 1.38 \cdot 10^{-23} \cdot \frac{joule}{K}$ Boltzmann's Constant

$T := 300 \cdot K$ Absolute temperature in degrees Kelvin

Frequency terms used in the MathCad program NOISE

$f_{lo} := .01 \cdot hz$ Lower noise bandwidth limit

$f_{hi} := 1000 \cdot hz$ Upper noise bandwidth limit

$f_6 := 500 \cdot hz$ AD693 3dB closed-loop corner frequency

$$f_1 := \frac{1}{2 \cdot \pi \cdot C_1 \cdot R_1}$$ 3dB Corner frequency of low-pass filter

$$f_f := \frac{1}{2 \cdot \pi \cdot C_f \cdot R_f}$$ 3dB Corner frequency of op-amp feedback impedance

$$f_{in} := \frac{1}{2 \cdot \pi \cdot C_{in} \cdot R_{in}}$$ 3dB Corner frequency of op-amp input impedance

Noise source closed-loop transfer functions as defined in Table 3.1.

$$A_6(f) := .267 \cdot \frac{amp}{volt} \cdot R_{out} \cdot \frac{1}{1 + \left[j \cdot \frac{f}{f_6} \right]}$$

$$A_{f1}(f) := \frac{R_f}{1 + \left[j \cdot \frac{f}{f_f} \right]}$$

$$A_1(f) := \frac{1}{1 + \left[j \cdot \frac{f}{f_1} \right]}$$

$$A_{f2}(f) := 1 + \left[\frac{\frac{R_f}{1 + \left[\frac{j \cdot f}{f_f} \right]}}{\frac{R_{in}}{1 + \left[\frac{j \cdot f}{f_{in}} \right]}} \right]$$

$$A_{Opip}(f) := R_f \cdot A_{f2}(f) \cdot A_1(f) \cdot A_6(f)$$

Noise source spectral densities as defined in Eqs. (3.14) through (3.21).

$$S_{Di} := 2.56 \cdot 10^{-23} \cdot \frac{amp^2}{hz}$$

$$S_{Opi} := 6.4 \cdot 10^{-25} \cdot \frac{amp^2}{hz}$$

$$S_{Ope} := 1.69 \cdot 10^{-16} \cdot \frac{volt^2}{hz}$$

$$S_{6i} := 1.6 \cdot 10^{-27} \cdot \frac{amp^2}{hz}$$

$$S_{6e} := 2.5 \cdot 10^{-15} \cdot \frac{volt^2}{hz}$$

$$S_{Rf} := 4 \cdot k \cdot T \cdot R_f$$

$$S_{Rl} := 4 \cdot k \cdot T \cdot R_1$$

$$S_{R1} := 4 \cdot k \cdot T \cdot R_1$$

$$S_{R2} := 4 \cdot k \cdot T \cdot R_2$$

Output noise power calculations as defined in Tables 3.4 and 3.5.

$$e_D := \sqrt{\int_{f_{lo}}^{f_{hi}} S_{Di} \cdot \left[\left|A_{f1}(f) \cdot A_1(f) \cdot A_6(f)\right|\right]^2 df}$$

$$e_{Opin.lo} := \sqrt{\int_{f_{lo}}^{1 \cdot hz} S_{Opi} \cdot \left[\left|A_{f1}(f) \cdot A_1(f) \cdot A_6(f)\right|\right]^2 \cdot \left[1 \cdot \frac{hz}{f}\right] df}$$

$$e_{Opin.hi} := \sqrt{\int_{1 \cdot hz}^{f_{hi}} S_{Opi} \cdot \left[\left|A_{f1}(f) \cdot A_1(f) \cdot A_6(f)\right|\right]^2 df}$$

$$e_{Opin} := \sqrt{e_{Opin.lo}^2 + e_{Opin.hi}^2}$$

$$e_{Opip.lo} := \sqrt{\int_{f_{lo}}^{1 \cdot hz} S_{Opi} \cdot \left[\left|A_{Opip}(f)\right|\right]^2 \cdot \left[1 \cdot \frac{hz}{f}\right] df}$$

Continuation of output noise power calculations as defined in Tables 3.4 and 3.5.

$$e_{Opip.hi} := \sqrt{\int_{f_{lo}}^{1\cdot hz} S_{Opi} \cdot \left[\left|A_{Opip}(f)\right|\right]^2 df}$$

$$e_{Opip} := \sqrt{e_{Opip.lo}^2 + e_{Opip.hi}^2}$$

$$e_{6ip.lo} := \sqrt{\int_{f_{lo}}^{80\cdot hz} S_{Opi} \cdot \left[\left|R_1 \cdot A_1(f) \cdot A_6(f)\right|\right]^2 \cdot \left[80 \cdot \frac{hz}{f}\right] df}$$

$$e_{6ip.hi} := \sqrt{2 \cdot \left[\int_{80\cdot hz}^{f_{hi}} S_{Opi} \cdot \left[\left|R_1 \cdot A_1(f) \cdot A_6(f)\right|\right]^2 df\right]}$$

$$e_{6ip} := \sqrt{e_{6ip.lo}^2 + e_{6ip.hi}^2}$$

Continuation of output noise power calculations as defined in Tables 3.3 and 3.4.

$$e_{6in.hi} := e_{6ip.hi}$$

$$e_{6in.lo} := e_{6ip.lo}$$

$$e_{6in} := \sqrt{e_{6in.lo}^{2} + e_{6in.hi}^{2}}$$

$$e_{Ope.lo} := \sqrt{\int_{f_{lo}}^{1\cdot hz} S_{Ope} \cdot \left[\left|A_{1}(f)\cdot A_{6}(f)\right|\right]^{2} \cdot \left[1\cdot \frac{hz}{f}\right] df}$$

$$e_{Ope.hi} := \sqrt{\int_{1\cdot hz}^{f_{hi}} S_{Ope} \cdot \left[\left|A_{1}(f)\cdot A_{6}(f)\right|\right]^{2} df}$$

$$e_{Ope} := \sqrt{e_{Ope.lo}^{2} + e_{Ope.hi}^{2}}$$

Continuation of output noise power calculations as defined in Tables 3.4 and 3.5.

$$e_{6e.lo} := \sqrt{\int_{f_{lo}}^{10\cdot hz} S_{6e} \cdot \left[\left|A_6(f)\right|\right]^2 \cdot \left[10\cdot\frac{hz}{f}\right] df}$$

$$e_{6e.hi} := \sqrt{\int_{10\cdot hz}^{f_{hi}} S_{6e} \cdot \left[\left|A_6(f)\right|\right]^2 df}$$

$$e_{6e} := \sqrt{e_{6e.lo}^2 + e_{6e.hi}^2}$$

$$e_{Rf} := \sqrt{\int_{f_{lo}}^{f_{hi}} S_{Rf} \cdot \left[\left|\frac{A_{f1}(f)\cdot A_1(f)\cdot A_6(f)}{R_f}\right|\right]^2 df}$$

$$e_{Rl} := \sqrt{\int_{f_{lo}}^{f_{hi}} S_{Rl} \cdot \left[\left|A_1(f)\cdot A_6(f)\right|\right]^2 df}$$

Continuation of Output noise power calculations as defined in Tables 3.3 and 3.4.

$$e_{R1} := \sqrt{\int_{f_{lo}}^{f_{hi}} S_{R1} \cdot \left[\left|A_{f2}(f) \cdot A_{1}(f) \cdot A_{6}(f)\right|\right]^2 df}$$

$$e_{R2} := \sqrt{\int_{f_{lo}}^{f_{hi}} S_{R2} \cdot \left[\left|A_{1}(f) \cdot A_{6}(f)\right|\right]^2 df}$$

Calcualted rms output noise voltages:

$e_D = 7.811 \cdot 10^{-7} \cdot volt$

$e_{Opin} = 7.93 \cdot 10^{-8} \cdot volt$

$e_{Ope} = 1.718 \cdot 10^{-6} \cdot volt$

$e_{6ip} = 8.96 \cdot 10^{-6} \cdot volt$

$e_{6in} = 8.96 \cdot 10^{-6} \cdot volt$

$e_{6e} = 8.712 \cdot 10^{-5} \cdot volt$

$e_{Rf} = 1.818 \cdot 10^{-6} \cdot volt$

$e_{R1} = 3.079 \cdot 10^{-6} \cdot volt$

$e_{R1} = 1.818 \cdot 10^{-6} \cdot volt$

$e_{R2} = 3.079 \cdot 10^{-6} \cdot volt$

$e_{Opip} = 7.679 \cdot 10^{-8} \cdot volt$

Calculations to determine total output rms noise voltage:

$$e_{out.i.2} := e_D^2 + e_{Opin}^2 + e_{Opip}^2 + e_{6ip}^2 + e_{6in}^2$$

$$e_{out.v.2} := e_{Ope}^2 + e_{6e}^2 + e_{Rf}^2 + e_{Rl}^2 + e_{R1}^2 + e_{R2}^2$$

$$e_{out.2} := e_{out.i.2} + e_{out.v.2}$$

$$e_{out} := \sqrt{e_{out.2}}$$

$$e_{out} = 8.82 \cdot 10^{-5} \cdot volt$$

Calculate total equivalent input noise current:

$$Equ_{I.Noise} := \frac{e_{out}}{(250 \cdot ohm) \cdot \left[.26667 \cdot \frac{amp}{volt}\right] \cdot R_f}$$

$$Equ_{I.Noise} = 1.764 \cdot 10^{-9} \cdot amp$$

MathCad Program UVB_CALS

This MathCad program performs the necessary integrations to calculate the correction factor of Eq. (4.6) in Sect. 4.1. This will define the portion of the thesis Radiometer output that corresponds to the measured UV-B irradiance from 280 to 320 nm for the solar irradiance source. See MathCad program ENGRUNIT for definitions of engineering units used in this program.

$\lambda 1_{min} := 270 \cdot nm$ minimum wavelength of first region

$\lambda 1_{max} := 314 \cdot nm$ maximum wavelength of first region

$\lambda 2_{min} := 314 \cdot nm$ minimum wavelength of second region

$\lambda 2_{max} := 358 \cdot nm$ maximum wavelength of second region

$\lambda 3_{min} := 358 \cdot nm$ minimum wavelength of third region

$\lambda 3_{max} := 399 \cdot nm$ maximum wavelength of third region

$\lambda_{bw} := 1 \cdot nm$ nominal integration bandwidth

$\lambda 1 := \lambda 1_{min}, \lambda 1_{min} + \lambda_{bw} .. \lambda 1_{max}$ region 1 variable range

$\lambda 2 := \lambda 2_{min}, \lambda 2_{min} + \lambda_{bw} .. \lambda 2_{max}$ region 2 variable range

$\lambda 3 := \lambda 3_{min}, \lambda 3_{min} + \lambda_{bw} .. \lambda 3_{max}$ region 3 variable range

First array set containing solar spectral irradiance distribution and absolute response of the thesis radiometer.

$\lambda 1$ (nm)	L1	UVB1
270	0	.3563
271	0	.3761
272	0	.3962
273	0	.4168
274	0	.4379
275	0	.4593
276	0	.4812
277	0	.505
278	0	.5264
279	0	.5496
280	0	.5732
281	0	.5907
282	0	.6085
283	0	.6265
284	0	.6447
285	0	.6633
286	0	.6821
287	0	.7011
288	0	.7204
289	0	.74
290	0	.7599
291	0	.7722
292	0	.7846
293	0	.7971
294	0	.8097
295	0	.8224
296	.0012	.8352
297	.0020	.8481
298	.0031	.8611
299	.0054	.8742
300	.0076	.8874
301	.0139	.8984
302	.0213	.9095
303	.0404	.9206
304	.0478	.9318
305	.0667	.943
306	.0719	.9543
307	.0944	.9656
308	.1169	.977
309	.1071	.9885
310	.1276	1.0
311	.2042	1.0084
312	.2071	1.0168
313	.1954	1.0252
314	.2464	1.0336

$L1 := \cdot \frac{watt}{m^2 \cdot nm}$ $\quad UVB1 :=$

Second array set containing solar spectral irradiance distribution and absolute response of the thesis radiometer.

$\frac{\lambda 2}{nm}$	L2 :=	$\cdot \frac{watt}{m^2 \cdot nm}$	UVB2 :=
314	.2464		1.0336
315	.2578		1.0421
316	.2375		1.0506
317	.3244		1.0592
318	.3211		1.0677
319	.3314		1.0763
320	.3827		1.085
321	.3921		1.0923
322	.3876		1.0997
323	.3770		1.107
324	.4429		1.1144
325	.4770		1.1218
326	.5884		1.1292
327	.5844		1.1367
328	.5676		1.1441
329	.6247		1.1516
330	.6871		1.159
331	.6197		1.1678
332	.6223		1.1766
333	.6090		1.1853
334	.6046		1.194
335	.6431		1.2027
336	.6002		1.2113
337	.5520		1.22
338	.5997		1.2286
339	.6476		1.2371
340	.6973		1.2457
341	.6592		1.2462
342	.6691		1.2467
343	.6864		1.2472
344	.5631		1.2477
345	.6290		1.2482
346	.6508		1.2487
347	.6796		1.2491
348	.6587		1.2496
349	.6555		1.2501
350	.7592		1.2505
351	.7416		1.2311
352	.7019		1.2118
353	.7371		1.1926
354	.8268		1.1736
355	.8094		1.1547
356	.7730		1.1359
357	.6681		1.1174
358	.6251		1.0989

Third array set containing solar spectral irradiance distribution and absolute response of the thesis radiometer.

$\frac{\lambda 3}{nm}$	L3 :=	$\cdot \frac{watt}{m^2 \cdot nm}$	UVB3 :=
358	.6251		1.0989
359	.6069		1.0806
360	.8152		1.0625
361	.6964		1.0565
362	.7102		1.0502
363	.7678		1.0437
364	.7921		1.0369
365	.8264		1.0298
366	.9167		1.0225
367	.8799		1.0149
368	.8039		1.0071
369	.8557		.9989
370	.8682		.9906
371	.8228		.9607
372	.7842		.9302
373	.7260		.8989
374	.6703		.8668
375	.6855		.8339
376	.84		.8003
377	.8886		.766
378	1.0805		.7309
379	1.0216		.695
380	.9195		.6584
381	1.0147		.6147
382	.7846		.5694
383	.6130		.5225
384	.7671		.4741
385	.8965		.4241
386	.8385		.3726
387	.8720		.3195
388	.8603		.2649
389	.9118		.2088
390	1.0630		.1511
391	1.1577		.1379
392	1.0164		.1244
393	.5890		.1106
394	.7280		.0964
395	1.1219		.0819
396	1.0843		.067
397	.6763		.0518
398	1.1316		.0363
399	1.1800		.0204

Array containing product of solar spectral irradiance and thesis radiometer absolute response for first array set.

$$Z1_{\frac{\lambda 1-\lambda 1_{min}}{\lambda_{bw}}} := L1_{\frac{\lambda 1-\lambda 1_{min}}{\lambda_{bw}}} \cdot UVB1_{\frac{\lambda 1-\lambda 1_{min}}{\lambda_{bw}}}$$

Array containing product of solar spectral irradiance and thesis radiometer absolute response for second array set.

$$Z2_{\frac{\lambda 2-\lambda 2_{min}}{\lambda_{bw}}} := L2_{\frac{\lambda 2-\lambda 2_{min}}{\lambda_{bw}}} \cdot UVB2_{\frac{\lambda 2-\lambda 2_{min}}{\lambda_{bw}}}$$

Array containing product of solar spectral irradiance and thesis radiometer absolute response for third array set.

$$Z3_{\frac{\lambda 3-\lambda 3_{min}}{\lambda_{bw}}} := L3_{\frac{\lambda 3-\lambda 3_{min}}{\lambda_{bw}}} \cdot UVB3_{\frac{\lambda 3-\lambda 3_{min}}{\lambda_{bw}}}$$

Set integration range variables for calculating the integration of the product of the solar spectral irradiance and the thesis radiometer absolute response.

$$\lambda 1 := \lambda 1_{min}, \lambda 1_{min} + \lambda_{bw} .. \left[\lambda 1_{max} - \lambda_{bw}\right]$$

$$\lambda 2 := \lambda 2_{min}, \lambda 2_{min} + \lambda_{bw} .. \left[\lambda 2_{max} - \lambda_{bw}\right]$$

$$\lambda 3 := \lambda 3_{min}, \lambda 3_{min} + \lambda_{bw} .. \left[\lambda 3_{max} - \lambda_{bw}\right]$$

Calculate individual areas for 1-nm bandwidths for the product of the solar spectral irradiance and the thesis radiometer absolute response for all three regions.

$$T_{DL1}(\lambda 1) := \left[Z1_{\frac{\lambda 1-\lambda 1_{min}}{\lambda_{bw}}} + Z1_{\frac{\lambda 1-\lambda 1_{min}}{\lambda_{bw}}+1} \right] \cdot \frac{\lambda_{bw}}{2}$$

$$T_{DL2}(\lambda 2) := \left[Z2_{\frac{\lambda 2-\lambda 2_{min}}{\lambda_{bw}}} + Z2_{\frac{\lambda 2-\lambda 2_{min}}{\lambda_{bw}}+1} \right] \cdot \frac{\lambda_{bw}}{2}$$

$$T_{DL3}(\lambda 3) := \left[Z3_{\frac{\lambda 3-\lambda 3_{min}}{\lambda_{bw}}} + Z3_{\frac{\lambda 3-\lambda 3_{min}}{\lambda_{bw}}+1} \right] \cdot \frac{\lambda_{bw}}{2}$$

Calculate total area under product of solar spectral irradiance and thesis radiometer absolute response:

$$T_{DL} := \left[\sum_{\lambda 1} T_{DL1}(\lambda 1) \right] + \left[\sum_{\lambda 2} T_{DL2}(\lambda 2) \right] + \left[\sum_{\lambda 3} T_{DL3}(\lambda 3) \right]$$

$$T_{DL} = 52.529 \cdot \frac{watt}{m^2}$$

Set integration ranges for calculating area under solar spectral irradiance distribution for UV-B region.

$$\lambda 1 := 280 \cdot nm, 280 \cdot nm + \lambda_{bw} .. \left[\lambda 1_{max} - \lambda_{bw}\right]$$

$$\lambda 2 := \lambda 2_{min}, \lambda 2_{min} + \lambda_{bw} .. \left[320 \cdot nm - \lambda_{bw}\right]$$

Calculate individual areas for 1-nm bandwidth for the solar spectral irradiance distribution for all UV-B region.

$$T_{L1}(\lambda 1) := \left[L1_{\frac{\lambda 1 - \lambda 1_{min}}{\lambda_{bw}}} + L1_{\frac{\lambda 1 - \lambda 1_{min}}{\lambda_{bw}} + 1} \right] \cdot \frac{\lambda_{bw}}{2}$$

$$T_{L2}(\lambda 2) := \left[L2_{\frac{\lambda 2 - \lambda 2_{min}}{\lambda_{bw}}} + L2_{\frac{\lambda 2 - \lambda 2_{min}}{\lambda_{bw}} + 1} \right] \cdot \frac{\lambda_{bw}}{2}$$

Calculate the total area under the solar spectral irradiance distribution for the UV-B region.

$$T_L := \left[\sum_{\lambda 1} T_{L1}(\lambda 1)\right] + \left[\sum_{\lambda 2} T_{L2}(\lambda 2)\right]$$

$$T_L = 3.244 \cdot \frac{watt}{m^2}$$

Calculate the correction factor for the thesis radiometer when sensing solar sunlight.

$$UVB\_CAL\_S_{Correction.Factor} := \frac{T_L}{T_{DL}}$$

$$UVB\_CAL\_S_{Correction.Factor} = 0.0618$$

MathCad Program UVX_CALS

This Mathcad program performs the necessary integrations to calculate the correction factor of Eq. (4.6) in Sect. 4.1. This will define the portion of the UVX radiometer output that corresponds to the measured UV-B irradiance from 280 to 320 nm from the solar irradiance source. See the MathCad program ENGRUNIT for definitions of engineering units used in this program.

$\lambda 1_{min} := 270 \cdot nm$ minimum wavelength of first region

$\lambda 1_{max} := 314 \cdot nm$ maximum wavelength of first region

$\lambda 2_{min} := 314 \cdot nm$ minimum wavelength of second region

$\lambda 2_{max} := 358 \cdot nm$ maximum wavelength of second region

$\lambda 3_{min} := 358 \cdot nm$ minimum wavelength of third region

$\lambda 3_{max} := 399 \cdot nm$ maximum wavelength of third region

$\lambda_{bw} := 1 \cdot nm$ nominal bandwidth

$\lambda 1 := \lambda 1_{min}, \lambda 1_{min} + \lambda_{bw} .. \lambda 1_{max}$

$\lambda 2 := \lambda 2_{min}, \lambda 2_{min} + \lambda_{bw} .. \lambda 2_{max}$

$\lambda 3 := \lambda 3_{min}, \lambda 3_{min} + \lambda_{bw} .. \lambda 3_{max}$

UVXCAL := 1.09 UVX radiometer absolute response at 310 nm.

First array set containing solar spectral irradiance distribution and absolute response of the UVX radiometer.

$\lambda 1$ (nm)	L1	UVX1
270	0.0	.05
271	0.0	.057
272	0.0	.066
273	0.0	.075
274	0.0	.084
275	0.0	.10
276	0.0	.115
277	0.0	.132
278	0.0	.150
279	0.0	.178
280	0.0	.20
281	0.0	.228
282	0.0	.252
283	0.0	.285
284	0.0	.315
285	0.0	.355
286	0.0	.390
287	0.0	.420
288	0.0	.455
289	0.0	.480
290	0.0	.52
291	0.0	.560
292	0.0	.590
293	0.0	.650
294	0.0	.680
295	0.0	.71
296	.0012	.740
297	.0020	.770
298	.0031	.790
299	.0054	.830
300	.0076	.85
301	.0139	.880
302	.0213	.910
303	.0404	.940
304	.0478	.960
305	.0667	.990
306	.0719	1.0
307	.0944	1.02
308	.1169	1.05
309	.1071	1.07
310	.1276	1.09
311	.2042	1.10
312	.2071	1.12
313	.1954	1.14
314	.2464	1.145

$L1 := \cdot \frac{watt}{m^2 \cdot nm}$ $\quad UVX1 := \cdot \frac{1}{UVXCAL}$

Second array set containing solar spectral irradiance distribution and absolute response of the UVX radiometer.

$\lambda 2$ (nm)	L2	UVX2
314	.2464	1.145
315	.2578	1.15
316	.2375	1.17
317	.3244	1.18
318	.3211	1.19
319	.3314	1.16
320	.3827	1.14
321	.3921	1.13
322	.3876	1.12
323	.3770	1.11
324	.4429	1.10
325	.4770	1.09
326	.5884	1.08
327	.5844	1.05
328	.5676	1.02
329	.6247	.99
330	.6871	.950
331	.6197	.890
332	.6223	.820
333	.6090	.760
334	.6046	.710
335	.6431	.650
336	.6002	.590
337	.5520	.540
338	.5997	.490
339	.6476	.440
340	.6973	.38
341	.6592	.335
342	.6691	.295
343	.6864	.255
344	.5631	.20
345	.6290	.170
346	.6508	.140
347	.6796	.120
348	.6587	.106
349	.6555	.092
350	.7592	.079
351	.7416	.067
352	.7019	.057
353	.7371	.050
354	.8268	.0445
355	.8094	.038
356	.7730	.0325
357	.6681	.0290
358	.6251	.0250

$L2 := \begin{bmatrix} .2464 \\ .2578 \\ .2375 \\ .3244 \\ .3211 \\ .3314 \\ .3827 \\ .3921 \\ .3876 \\ .3770 \\ .4429 \\ .4770 \\ .5884 \\ .5844 \\ .5676 \\ .6247 \\ .6871 \\ .6197 \\ .6223 \\ .6090 \\ .6046 \\ .6431 \\ .6002 \\ .5520 \\ .5997 \\ .6476 \\ .6973 \\ .6592 \\ .6691 \\ .6864 \\ .5631 \\ .6290 \\ .6508 \\ .6796 \\ .6587 \\ .6555 \\ .7592 \\ .7416 \\ .7019 \\ .7371 \\ .8268 \\ .8094 \\ .7730 \\ .6681 \\ .6251 \end{bmatrix} \cdot \frac{\text{watt}}{\text{m}^2 \cdot \text{nm}}$

$UVX2 := \begin{bmatrix} 1.145 \\ 1.15 \\ 1.17 \\ 1.18 \\ 1.19 \\ 1.16 \\ 1.14 \\ 1.13 \\ 1.12 \\ 1.11 \\ 1.10 \\ 1.09 \\ 1.08 \\ 1.05 \\ 1.02 \\ .99 \\ .950 \\ .890 \\ .820 \\ .760 \\ .710 \\ .650 \\ .590 \\ .540 \\ .490 \\ .440 \\ .38 \\ .335 \\ .295 \\ .255 \\ .20 \\ .170 \\ .140 \\ .120 \\ .106 \\ .092 \\ .079 \\ .067 \\ .057 \\ .050 \\ .0445 \\ .038 \\ .0325 \\ .0290 \\ .0250 \end{bmatrix} \cdot \frac{1}{\text{UVXCAL}}$

Third array set containing solar spectral irradiance distribution and absolute response of the UVX radiometer.

$\lambda 3$ (nm)	L3	UVX3
358	.6251	.0250
359	.6069	.0215
360	.8152	.0175
361	.6964	.016
362	.7102	.0135
363	.7678	.0118
364	.7921	.01
365	.8264	.009
366	.9167	.008
367	.8799	0.0
368	.8039	0.0
369	.8557	0.0
370	.8682	0.0
371	.8228	0.0
372	.7842	0.0
373	.7260	0.0
374	.6703	0.0
375	.6855	0.0
376	.84	0.0
377	.8886	0.0
378	1.0805	0.0
379	1.0216	0.0
380	.9195	0.0
381	1.0147	0.0
382	.7846	0.0
383	.6130	0.0
384	.7671	0.0
385	.8965	0.0
386	.8385	0.0
387	.8720	0.0
388	.8603	0.0
389	.9118	0.0
390	1.0630	0.0
391	1.1577	0.0
392	1.0164	0.0
393	.5890	0.0
394	.7280	0.0
395	1.1219	0.0
396	1.0843	0.0
397	.6763	0.0
398	1.1316	0.0
399	1.1800	0.0

$L3 := \cdot \frac{watt}{m^2 \cdot nm}$ $\quad UVX3 := \cdot \frac{1}{UVXCAL}$

Array containing product of solar spectral irradiance and UVX radiometer absolute response for first array.

$$Z1_{\lambda 1-\lambda 1_{min}} := \frac{L1_{\lambda 1-\lambda 1_{min}}}{\lambda_{bw}} \cdot \frac{UVX1_{\lambda 1-\lambda 1_{min}}}{\lambda_{bw}}$$

Array containing product of solar spectral irradiance and UVX radiometer absolute response for second array.

$$Z2_{\lambda 2-\lambda 2_{min}} := \frac{L2_{\lambda 2-\lambda 2_{min}}}{\lambda_{bw}} \cdot \frac{UVX2_{\lambda 2-\lambda 2_{min}}}{\lambda_{bw}}$$

Array containing product of solar spectral irradiance and UVX radiometer absolute response for third array.

$$Z3_{\lambda 3-\lambda 3_{min}} := \frac{L3_{\lambda 3-\lambda 3_{min}}}{\lambda_{bw}} \cdot \frac{UVX3_{\lambda 3-\lambda 3_{min}}}{\lambda_{bw}}$$

Set integration range variables for calculating the integration of the product of the solar spectral irradiance and the UVX radiometer absolute response.

$$\lambda 1 := \lambda 1_{min}, \lambda 1_{min} + \lambda_{bw} .. \lceil \lambda 1_{max} - \lambda_{bw} \rceil$$

$$\lambda 2 := \lambda 2_{min}, \lambda 2_{min} + \lambda_{bw} .. \lceil \lambda 2_{max} - \lambda_{bw} \rceil$$

$$\lambda 3 := \lambda 3_{min}, \lambda 3_{min} + \lambda_{bw} .. \lceil \lambda 3_{max} - \lambda_{bw} \rceil$$

Calculate individual areas for 1-nm bandwidths for the product of the solar spectral irradiance and the UVX radiometer absolute response for all three regions.

$$T_{DL1}(\lambda 1) := \left[Z1_{\frac{\lambda 1 - \lambda 1_{min}}{\lambda_{bw}}} + Z1_{\frac{\lambda 1 - \lambda 1_{min}}{\lambda_{bw}} + 1} \right] \cdot \frac{\lambda_{bw}}{2}$$

$$T_{DL2}(\lambda 2) := \left[Z2_{\frac{\lambda 2 - \lambda 2_{min}}{\lambda_{bw}}} + Z2_{\frac{\lambda 2 - \lambda 2_{min}}{\lambda_{bw}} + 1} \right] \cdot \frac{\lambda_{bw}}{2}$$

$$T_{DL3}(\lambda 3) := \left[Z3_{\frac{\lambda 3 - \lambda 3_{min}}{\lambda_{bw}}} + Z3_{\frac{\lambda 3 - \lambda 3_{min}}{\lambda_{bw}} + 1} \right] \cdot \frac{\lambda_{bw}}{2}$$

Calculate total area under product of solar spectral irradiance and UVX radiometer absolute response.

$$T_{DL} := \sum_{\lambda 1} T_{DL1}(\lambda 1) + \sum_{\lambda 2} T_{DL2}(\lambda 2) + \sum_{\lambda 3} T_{DL3}(\lambda 3)$$

$$T_{DL} = 13.434 \cdot \frac{watt}{m^2}$$

Set integration ranges for calculating area under solar spectral irradiance distribution for UV-B region.

$$\lambda 1 := 280\cdot nm, 280\cdot nm + \lambda_{bw} .. \left[\lambda 1_{max} - \lambda_{bw}\right]$$

$$\lambda 2 := \lambda 2_{min}, \lambda 2_{min} + \lambda_{bw} .. \left[320\cdot nm - \lambda_{bw}\right]$$

Calculate individual areas for 1-nm bandwidth for the solar spectral irradiance distribution for the UV-B region.

$$T_{L1}(\lambda 1) := \left[L1_{\frac{\lambda 1 - \lambda 1_{min}}{\lambda_{bw}}} + L1_{\frac{\lambda 1 - \lambda 1_{min}}{\lambda_{bw}} + 1} \right] \cdot \frac{\lambda_{bw}}{2}$$

$$T_{L2}(\lambda 2) := \left[L2_{\frac{\lambda 2 - \lambda 2_{min}}{\lambda_{bw}}} + L2_{\frac{\lambda 2 - \lambda 2_{min}}{\lambda_{bw}} + 1} \right] \cdot \frac{\lambda_{bw}}{2}$$

Calculate the total area under the solar spectral irradiance distribution for the UV-B region.

$$T_L := \left[\sum_{\lambda 1} T_{L1}(\lambda 1)\right] + \left[\sum_{\lambda 2} T_{L2}(\lambda 2)\right]$$

$$T_L = 3.244\cdot \frac{watt}{m^2}$$

Calculate the correction factor for the UVX radiometer when sensing a solar spectrum.

$$\text{UVX\_CAL\_S Correction.Factor} := \frac{T_L}{T_{DL}}$$

$$\text{UVX\_CAL\_S Correction.Factor} = 0.24148$$

MathCad Program UVB_CALB

This MathCad program performs the necessary integrations to calculate the correction factor of Eq. (4.6) in Sect. 4.1. This will define the portion of the thesis radiometer output that corresponds to the measured UV-B irradiance from 280 to 320 nm from the UVB-313 irradiance lamp source. See the MathCad program ENGRRUNIT for definitions of engineering units used in this program.

$\lambda 1_{min} := 270 \cdot nm$ minimum wavelength of first region

$\lambda 1_{max} := 314 \cdot nm$ maximum wavelength of first region

$\lambda 2_{min} := 314 \cdot nm$ minimum wavelength of second region

$\lambda 2_{max} := 358 \cdot nm$ maximum wavelength of second region

$\lambda 3_{min} := 358 \cdot nm$ minimum wavelength of third region

$\lambda 3_{max} := 399 \cdot nm$ maximum wavelength of third region

$\lambda_{bw} := 1 \cdot nm$ nominal integration bandwidth

$\lambda 1 := \lambda 1_{min}, \lambda 1_{min} + \lambda_{bw} .. \lambda 1_{max}$

$\lambda 2 := \lambda 2_{min}, \lambda 2_{min} + \lambda_{bw} .. \lambda 2_{max}$

$\lambda 3 := \lambda 3_{min}, \lambda 3_{min} + \lambda_{bw} .. \lambda 3_{max}$

First array set containing UVB-313 lamp spectral irradiance distribution and absolute response of the thesis radiometer.

$\lambda 1$ (nm)	L1 (watt / m² · nm)	UVB1
270	0.0	.3563
271	0.0	.3761
272	0.0	.3962
273	.0012	.4168
274	.0021	.4379
275	.0037	.4593
276	.0062	.4812
277	.0103	.505
278	.0156	.5264
279	.0235	.5496
280	.0359	.5732
281	.0465	.5907
282	.0614	.6085
283	.0787	.6265
284	.0963	.6447
285	.1149	.6633
286	.1344	.6821
287	.1550	.7011
288	.1767	.7204
289	.2043	.74
290	.2259	.7599
291	.2515	.7722
292	.2788	.7846
293	.3087	.7971
294	.3364	.8097
295	.3648	.8224
296	.4007	.8352
297	.4467	.8481
298	.4507	.8611
299	.4782	.8742
300	.5076	.8874
301	.5355	.8984
302	.5771	.9095
303	.5895	.9206
304	.5979	.9318
305	.6147	.943
306	.6271	.9543
307	.6391	.9656
308	.6489	.977
309	.6566	.9885
310	.6627	1.0
311	.6719	1.0084
312	.7497	1.0168
313	.8422	1.0252
314	.7174	1.0336

Second array set containing UVB-313 lamp spectral irradiance distribution and absolute response of the thesis radiometer.

$\lambda 2$ (nm)	L2 :=	UVB2 :=
314	.7174	1.0336
315	.6803	1.0421
316	.6757	1.0506
317	.6705	1.0592
318	.6626	1.0677
319	.6531	1.0763
320	.6417	1.085
321	.6307	1.0923
322	.6172	1.0997
323	.6015	1.107
324	.5852	1.1144
325	.5691	1.1218
326	.5531	1.1292
327	.5356	1.1367
328	.5170	1.1441
329	.4959	1.1516
330	.4751	1.159
331	.4551	1.1678
332	.4338	1.1766
333	.4159	1.1853
334	.4093	1.194
335	.3798	1.2027
336	.3565	1.2113
337	.3371	1.22
338	.3175	1.2286
339	.2989	1.2371
340	.2792	1.2457
341	.2607	1.2462
342	.2431	1.2467
343	.2250	1.2472
344	.2104	1.2477
345	.1966	1.2482
346	.1830	1.2487
347	.1706	1.2491
348	.1582	1.2496
349	.1469	1.2501
350	.1360	1.2505
351	.1253	1.2311
352	.1164	1.2118
353	.1079	1.1926
354	.1006	1.1736
355	.0933	1.1547
356	.0864	1.1359
357	.0806	1.1174
358	.0746	1.0989

$\cdot \frac{watt}{2}$

$m \cdot nm$

Third array set containing UVB-313 lamp spectral irradiance distribution and absolute response of the thesis radiometer.

$\lambda 3$ (nm)	L3 (watt / $m^2 \cdot nm$)	UVB3
358	.0746	1.0989
359	.0689	1.0806
360	.0634	1.0625
361	.0585	1.0565
362	.0535	1.0502
363	.0502	1.0437
364	.0859	1.0369
365	.2539	1.0298
366	.1450	1.0225
367	.0614	1.0149
368	.0336	1.0071
369	.0307	.9989
370	.0276	.9906
371	.0255	.9607
372	.0236	.9302
373	.0217	.8989
374	.0197	.8668
375	.0181	.8339
376	.0170	.8003
377	.0159	.766
378	.0144	.7309
379	.0136	.695
380	.0125	.6584
381	.0116	.6147
382	.0107	.5694
383	.0098	.5225
384	.0089	.4741
385	.0084	.4241
386	.0081	.3726
387	.0075	.3195
388	.0072	.2649
389	.0068	.2088
390	.0066	.1511
391	.0071	.1379
392	.0055	.1244
393	.0053	.1106
394	.0054	.0964
395	.0051	.0819
396	.0048	.067
397	.0049	.0518
398	.0046	.0363
399	.0047	.0204

Array containing product of UVB-313 lamp source spectral irradiance and thesis radiometer absolute response for first array set.

$$Z1_{\lambda 1-\lambda 1_{min}} := \frac{L1_{\lambda 1-\lambda 1_{min}}}{\lambda_{bw}} \cdot \frac{UVB1_{\lambda 1-\lambda 1_{min}}}{\lambda_{bw}}$$

Array containing product of UVB-313 lamp source spectral irradiance and thesis radiometer absolute response for second array set.

$$Z2_{\lambda 2-\lambda 2_{min}} := \frac{L2_{\lambda 2-\lambda 2_{min}}}{\lambda_{bw}} \cdot \frac{UVB2_{\lambda 2-\lambda 2_{min}}}{\lambda_{bw}}$$

Array containing product of UVB-313 lamp source spectral irradiance and thesis radiometer absolute response for third array set.

$$Z3_{\lambda 3-\lambda 3_{min}} := \frac{L3_{\lambda 3-\lambda 3_{min}}}{\lambda_{bw}} \cdot \frac{UVB3_{\lambda 3-\lambda 3_{min}}}{\lambda_{bw}}$$

Set integration range variables for calculating the integration of the product of the UVB-313 lamp irradiance and the thesis radiometer absolute response.

$$\lambda 1 := \lambda 1_{min}, \lambda 1_{min} + \lambda_{bw} .. \lceil \lambda 1_{max} - \lambda_{bw} \rceil$$

$$\lambda 2 := \lambda 2_{min}, \lambda 2_{min} + \lambda_{bw} .. \lceil \lambda 2_{max} - \lambda_{bw} \rceil$$

$$\lambda 3 := \lambda 3_{min}, \lambda 3_{min} + \lambda_{bw} .. \lceil \lambda 3_{max} - \lambda_{bw} \rceil$$

Calculate individual areas for 1-nm bandwidths for the product of the UVB-313 lamp source spectral irradiance and the thesis radiometer absolute response for all three regions:

$$T_{DL1}(\lambda 1) := \left[Z1_{\left(\frac{\lambda 1 - \lambda 1_{min}}{\lambda_{bw}}\right)} + Z1_{\left(\frac{\lambda 1 - \lambda 1_{min}}{\lambda_{bw}} + 1\right)} \right] \cdot \frac{\lambda_{bw}}{2}$$

$$T_{DL2}(\lambda 2) := \left[Z2_{\left(\frac{\lambda 2 - \lambda 2_{min}}{\lambda_{bw}}\right)} + Z2_{\left(\frac{\lambda 2 - \lambda 2_{min}}{\lambda_{bw}} + 1\right)} \right] \cdot \frac{\lambda_{bw}}{2}$$

$$T_{DL3}(\lambda 3) := \left[Z3_{\left(\frac{\lambda 3 - \lambda 3_{min}}{\lambda_{bw}}\right)} + Z3_{\left(\frac{\lambda 3 - \lambda 3_{min}}{\lambda_{bw}} + 1\right)} \right] \cdot \frac{\lambda_{bw}}{2}$$

Calculate total area under product of UVB-313 lamp source spectral irradiance and thesis radiometer absolute response:

$$T_{DL} := \left[\sum_{\lambda 1} T_{DL1}(\lambda 1) \right] + \left[\sum_{\lambda 2} T_{DL2}(\lambda 2) \right] + \left[\sum_{\lambda 3} T_{DL3}(\lambda 3) \right]$$

$$T_{DL} = 32.473 \cdot \frac{watt}{m^2}$$

Set integration ranges for calculating area under UVB-313 lamp source spectral irradiance distribution for UV-B region.

$$\lambda 1 := 280\cdot nm, 280\cdot nm + \lambda_{bw} \,..\, \lambda 1_{max} - \lambda_{bw}$$

$$\lambda 2 := \lambda 2_{min}, \lambda 2_{min} + \lambda_{bw} \,..\, 320\cdot nm - \lambda_{bw}$$

Calculate individual areas for 1-nm bandwidth for the UVB-313 lamp source spectral irradiance distribution for the UV-B region.

$$T_{L1}(\lambda 1) := \left[L1_{\frac{\lambda 1 - \lambda 1_{min}}{\lambda_{bw}}} + L1_{\frac{\lambda 1 - \lambda 1_{min}}{\lambda_{bw}} + 1} \right] \cdot \frac{\lambda_{bw}}{2}$$

$$T_{L2}(\lambda 2) := \left[L2_{\frac{\lambda 2 - \lambda 2_{min}}{\lambda_{bw}}} + L2_{\frac{\lambda 2 - \lambda 2_{min}}{\lambda_{bw}} + 1} \right] \cdot \frac{\lambda_{bw}}{2}$$

Calculate the total area under the UVB-313 lamp spectral irradiance distribution for the UV-B region.

$$T_L := \left[\sum_{\lambda 1} T_{L1}(\lambda 1) \right] + \left[\sum_{\lambda 2} T_{L2}(\lambda 2) \right]$$

$$T_L = 17.93 \cdot \frac{watt}{m^2}$$

Calculate the correction factor for the thesis radiometer when sensing the UVB-313 lamp.

$$UVB\_CAL\_B_{Correction.Factor} := \frac{T_L}{T_{DL}}$$

$$UVB\_CAL\_B_{Correction.Factor} = 0.5521$$

MathCad Program UVX_CALB

This MathCad program performs the necessary integrations to calculate the correction factor of Eq. (4.6) in Sect. 4.1. This will define the portion of the UVX radiometer output that corresponds to the measured UV-B irradiance from 280 to 320 nm from the UVB-313 irradiance lamp source. See the MathCad program ENGRUNIT for definitions of engineering units used in this program.

$\lambda 1_{min} := 270 \cdot nm$ minimum wavelength of first region

$\lambda 1_{max} := 314 \cdot nm$ maximum wavelength of first region

$\lambda 2_{min} := 314 \cdot nm$ minimum wavelength of second region

$\lambda 2_{max} := 358 \cdot nm$ maximum wavelength of second region

$\lambda 3_{min} := 358 \cdot nm$ minimum wavelength of third region

$\lambda 3_{max} := 399 \cdot nm$ maximum wavelength of third region

$\lambda_{bw} := 1 \cdot nm$ nominal integration bandwidth

$\lambda 1 := \lambda 1_{min}, \lambda 1_{min} + \lambda_{bw} .. \lambda 1_{max}$ region 1 variable range

$\lambda 2 := \lambda 2_{min}, \lambda 2_{min} + \lambda_{bw} .. \lambda 2_{max}$ region 2 variable range

$\lambda 3 := \lambda 3_{min}, \lambda 3_{min} + \lambda_{bw} .. \lambda 3_{max}$ region 3 variable range

UVXCAL := 1.09 UVX radiometer absolute response at 310 nm

First array set containing UVB-313 lamp spectral irradiance distribution and absolute response of the UVX radiometer.

$\lambda 1$ / nm	L1 :=	$\cdot \frac{watt}{m^2 \cdot nm}$	UVX1 :=	$\cdot \frac{1}{UVXCAL}$
270	0.0		.05	
271	0.0		.057	
272	0.0		.066	
273	.0012		.075	
274	.0021		.084	
275	.0037		.10	
276	.0062		.115	
277	.0103		.132	
278	.0156		.150	
279	.0235		.178	
280	.0359		.20	
281	.0465		.228	
282	.0614		.252	
283	.0787		.285	
284	.0963		.315	
285	.1149		.355	
286	.1344		.390	
287	.1550		.420	
288	.1767		.455	
289	.2043		.480	
290	.2259		.52	
291	.2515		.560	
292	.2788		.590	
293	.3087		.650	
294	.3364		.680	
295	.3648		.71	
296	.4007		.740	
297	.4467		.770	
298	.4507		.790	
299	.4782		.830	
300	.5076		.85	
301	.5355		.880	
302	.5771		.910	
303	.5895		.940	
304	.5979		.960	
305	.6147		.990	
306	.6271		1.0	
307	.6391		1.02	
308	.6489		1.05	
309	.6566		1.07	
310	.6627		1.09	
311	.6719		1.10	
312	.7497		1.12	
313	.8422		1.14	
314	.7174		1.145	

Second array set containing UVB-313 lamp spectral irradiance distribution and absolute response of the UVX radiometer.

$\lambda 2$ (nm)	L2	UVX2
314	.7174	1.145
315	.6803	1.15
316	.6757	1.17
317	.6705	1.18
318	.6626	1.19
319	.6531	1.16
320	.6417	1.14
321	.6307	1.13
322	.6172	1.12
323	.6015	1.11
324	.5852	1.10
325	.5691	1.09
326	.5531	1.08
327	.5356	1.05
328	.5170	1.02
329	.4959	.99
330	.4751	.950
331	.4551	.890
332	.4338	.820
333	.4159	.760
334	.4093	.710
335	.3798	.650
336	.3565	.590
337	.3371	.540
338	.3175	.490
339	.2989	.440
340	.2792	.38
341	.2607	.335
342	.2431	.295
343	.2250	.255
344	.2104	.20
345	.1966	.170
346	.1830	.140
347	.1706	.120
348	.1582	.106
349	.1469	.092
350	.1360	.079
351	.1253	.067
352	.1164	.057
353	.1079	.050
354	.1006	.0445
355	.0933	.038
356	.0864	.0325
357	.0806	.0290
358	.0746	.0250

$L2 := \begin{bmatrix} .7174 \\ .6803 \\ .6757 \\ .6705 \\ .6626 \\ .6531 \\ .6417 \\ .6307 \\ .6172 \\ .6015 \\ .5852 \\ .5691 \\ .5531 \\ .5356 \\ .5170 \\ .4959 \\ .4751 \\ .4551 \\ .4338 \\ .4159 \\ .4093 \\ .3798 \\ .3565 \\ .3371 \\ .3175 \\ .2989 \\ .2792 \\ .2607 \\ .2431 \\ .2250 \\ .2104 \\ .1966 \\ .1830 \\ .1706 \\ .1582 \\ .1469 \\ .1360 \\ .1253 \\ .1164 \\ .1079 \\ .1006 \\ .0933 \\ .0864 \\ .0806 \\ .0746 \end{bmatrix} \cdot \frac{\text{watt}}{\text{m}^2 \cdot \text{nm}}$

$UVX2 := \begin{bmatrix} 1.145 \\ 1.15 \\ 1.17 \\ 1.18 \\ 1.19 \\ 1.16 \\ 1.14 \\ 1.13 \\ 1.12 \\ 1.11 \\ 1.10 \\ 1.09 \\ 1.08 \\ 1.05 \\ 1.02 \\ .99 \\ .950 \\ .890 \\ .820 \\ .760 \\ .710 \\ .650 \\ .590 \\ .540 \\ .490 \\ .440 \\ .38 \\ .335 \\ .295 \\ .255 \\ .20 \\ .170 \\ .140 \\ .120 \\ .106 \\ .092 \\ .079 \\ .067 \\ .057 \\ .050 \\ .0445 \\ .038 \\ .0325 \\ .0290 \\ .0250 \end{bmatrix} \cdot \frac{1}{\text{UVXCAL}}$

Third array set containing UVB-313 lamp spectral irradiance distribution and absolute response of the UVX radiometer.

$\lambda 3$ (nm)	L3 := (watt / (m^2 · nm))	UVX3 := (1 / UVXCAL)
358	.0746	.0250
359	.0689	.0215
360	.0634	.0175
361	.0585	.016
362	.0535	.0135
363	.0502	.0118
364	.0859	.01
365	.2539	.009
366	.1450	.008
367	.0614	0.0
368	.0336	0.0
369	.0307	0.0
370	.0276	0.0
371	.0255	0.0
372	.0236	0.0
373	.0217	0.0
374	.0197	0.0
375	.0181	0.0
376	.0170	0.0
377	.0159	0.0
378	.0144	0.0
379	.0136	0.0
380	.0125	0.0
381	.0116	0.0
382	.0107	0.0
383	.0098	0.0
384	.0089	0.0
385	.0084	0.0
386	.0081	0.0
387	.0075	0.0
388	.0072	0.0
389	.0068	0.0
390	.0066	0.0
391	.0071	0.0
392	.0055	0.0
393	.0053	0.0
394	.0054	0.0
395	.0051	0.0
396	.0048	0.0
397	.0049	0.0
398	.0046	0.0
399	.0047	0.0

Array containing product of UVB-313 lamp source spectral irradiance and UVX radiometer absolute response for first array.

$$Z1_{\lambda 1-\lambda 1_{min}} := \frac{L1_{\lambda 1-\lambda 1_{min}}}{\lambda_{bw}} \cdot \frac{UVX1_{\lambda 1-\lambda 1_{min}}}{\lambda_{bw}}$$

Array containing product of UVB-313 lamp source spectral irradiance and UVX radiometer absolute response for second array.

$$Z2_{\lambda 2-\lambda 2_{min}} := \frac{L2_{\lambda 2-\lambda 2_{min}}}{\lambda_{bw}} \cdot \frac{UVX2_{\lambda 2-\lambda 2_{min}}}{\lambda_{bw}}$$

Array containing product of UVB-313 lamp source spectral irradiance and UVX radiometer absolute response for third array.

$$Z3_{\lambda 3-\lambda 3_{min}} := \frac{L3_{\lambda 3-\lambda 3_{min}}}{\lambda_{bw}} \cdot \frac{UVX3_{\lambda 3-\lambda 3_{min}}}{\lambda_{bw}}$$

Set integration range variables for calculating the integration of the product of the UVB-313 lamp irradiance and the UVX radiometer absolute response.

$$\lambda 1 := \lambda 1_{min}, \lambda 1_{min} + \lambda_{bw} .. \left\lceil \lambda 1_{max} - \lambda_{bw} \right\rceil$$

$$\lambda 2 := \lambda 2_{min}, \lambda 2_{min} + \lambda_{bw} .. \left\lceil \lambda 2_{max} - \lambda_{bw} \right\rceil$$

$$\lambda 3 := \lambda 3_{min}, \lambda 3_{min} + \lambda_{bw} .. \left\lceil \lambda 3_{max} - \lambda_{bw} \right\rceil$$

Calculate individual areas for 1-nm bandwidths for the product of the UVB-313 lamp source spectral irradiance and the UVX radiometer absolute response for all three regions.

$$T_{DL1}(\lambda 1) := \left[Z1_{\frac{\lambda 1-\lambda 1_{min}}{\lambda_{bw}}} + Z1_{\frac{\lambda 1-\lambda 1_{min}}{\lambda_{bw}}+1} \right] \cdot \frac{\lambda_{bw}}{2}$$

$$T_{DL2}(\lambda 2) := \left[Z2_{\frac{\lambda 2-\lambda 2_{min}}{\lambda_{bw}}} + Z2_{\frac{\lambda 2-\lambda 2_{min}}{\lambda_{bw}}+1} \right] \cdot \frac{\lambda_{bw}}{2}$$

$$T_{DL3}(\lambda 3) := \left[Z3_{\frac{\lambda 3-\lambda 3_{min}}{\lambda_{bw}}} + Z3_{\frac{\lambda 3-\lambda 3_{min}}{\lambda_{bw}}+1} \right] \cdot \frac{\lambda_{bw}}{2}$$

Calculate total area under product of UVB-313 lamp source spectral irradiance and the UVX radiometer absolute response.

$$T_{DL} := \left[\sum_{\lambda 1} T_{DL1}(\lambda 1) \right] + \left[\sum_{\lambda 2} T_{DL2}(\lambda 2) \right] + \left[\sum_{\lambda 3} T_{DL3}(\lambda 3) \right]$$

$$T_{DL} = 24.107 \cdot \frac{watt}{m^2}$$

Set integration ranges for calculating area under UVB-313 lamp source spectral irradiance distribution for UV-B region.

$$\lambda 1 := 280\cdot nm, 280\cdot nm + \lambda_{bw} \;..\; \left[\lambda 1_{max} - \lambda_{bw}\right]$$

$$\lambda 2 := \lambda 2_{min}, \lambda 2_{min} + \lambda_{bw} \;..\; \left[320\cdot nm - \lambda_{bw}\right]$$

Calculate individual areas for 1-nm bandwidth for the UVB-313 lamp source spectral irradiance distribution for the UV-B region.

$$T_{L1}(\lambda 1) := \left[L1_{\frac{\lambda 1 - \lambda 1_{min}}{\lambda_{bw}}} + L1_{\frac{\lambda 1 - \lambda 1_{min}}{\lambda_{bw}} + 1} \right] \cdot \frac{\lambda_{bw}}{2}$$

$$T_{L2}(\lambda 2) := \left[L2_{\frac{\lambda 2 - \lambda 2_{min}}{\lambda_{bw}}} + L2_{\frac{\lambda 2 - \lambda 2_{min}}{\lambda_{bw}} + 1} \right] \cdot \frac{\lambda_{bw}}{2}$$

Calculate the total area under the UVB-313 lamp spectral irradiance distribution for the UV-B region.

$$T_L := \left[\sum_{\lambda 1} T_{L1}(\lambda 1)\right] + \left[\sum_{\lambda 2} T_{L2}(\lambda 2)\right]$$

$$T_L = 17.93\cdot \frac{watt}{m^2}$$

Calculate the correction factor for the UVX radiometer when sensing the UVB-313 Lamp.

$$\text{UVX\_CAL\_B}_{\text{Correction.Factor}} := \frac{T_L}{T_{DL}}$$

$$\text{UVX\_CAL\_B}_{\text{Correction.Factor}} = 0.74374$$

MathCad Program ENGRUNIT

This MathCad program contains the engineering unit definitions used by all of the MathCad programs in this appendix.

UNIT DEFINITIONS

I. Base units

m Þ 1L kg Þ 1M sec Þ 1T coul Þ 1Q

II. Angular measure

rad Þ 1

$$\text{deg} \text{ Þ } \frac{Đ}{180}\cdot \text{rad}$$

III. Derived units:

Time

min Þ 60·sec hr Þ 3600·sec day Þ 24·hr

IV. Derived units: force, energy, power

$$\text{newton} \text{ Þ } \text{kg}\cdot\frac{\text{m}}{\text{sec}^2} \qquad \text{dyne} \text{ Þ } 10^{-5}\cdot\text{newton} \qquad \text{joule} \text{ Þ } \text{newton}\cdot\text{m}$$

$$\text{watt} \text{ Þ } \frac{\text{joule}}{\text{sec}} \qquad \text{kW} \text{ Þ } 1000\cdot\text{watt}$$

V. Derived units: Electrical

$$\text{amp} \text{ Þ } \frac{\text{coul}}{\text{sec}} \qquad \text{volt} \text{ Þ } \frac{\text{watt}}{\text{amp}} \qquad \text{ohm} \text{ Þ } \frac{\text{volt}}{\text{amp}}$$

$$\text{siemens} := \frac{1}{\text{ohm}} \qquad \text{farad} \text{ Þ } \frac{\text{coul}}{\text{volt}} \qquad \text{hz} \text{ Þ } 2\cdot\frac{Đ}{\text{sec}}$$

$$\text{pF} \text{ Þ } 1\cdot 10^{-12}\cdot\text{farad} \qquad \text{ÌF} \text{ Þ } 1\cdot 10^{-6}\cdot\text{farad}$$

VITA

Michael S. Hileman was born January 28, 1958, in Carbondale, Illinois. In 1969, his father became Dean of the College of Communications at The University of Tennessee, and his family moved to Knoxville, Tennessee, where he grew up. He graduated from Central High School, Knoxville, Tennessee, in 1976.

In the fall of 1976, he enrolled in the Electrical Engineering Undergraduate Program at The University of Tennessee in Knoxville. In the spring of 1977, he was accepted into The University of Tennessee Engineering Cooperative Education Program and accepted an engineering trainee position in the Vehicle Engineering–Ground Electrical Division at the National Aeronautics and Space Administration Kennedy Space Center at Cape Canaveral, Florida. After graduating with honors in the summer of 1981 with a BSEE degree, he married the former Catherine L. McCampbell of Knoxville, Tennessee, and accepted employment as a staff engineer with the Product Design Department of Technology for Energy Corporation in Knoxville, Tennessee. In 1983, he accepted employment as a development engineer with the Instrumentation and Controls Division of Oak Ridge National Laboratory in Oak Ridge, Tennessee.

In the fall of 1985, he enrolled as a graduate student at The University of Tennessee in Knoxville in the Electrical and Computer Engineering Department, with this thesis being the culmination of that activity. He is still a staff member of the Instrumentation and Controls Division of Oak Ridge National Laboratory and resides in Lenoir City, Tennessee.